CHAPTER IV

RESULTS AND DISCUSSION

4.1 Physical Properties of the Synthesized Hydrates

Three replications of $ZnHPO_4.H_2O$, $Co(H_2PO_4)_2.2H_2O$, $LiFePO_4.3H_2O$, $LiCoPO_4.3H_2O$, $LiNiPO_4.H_2O$, $LiMnPO_4.H_2O$, and $Li_2Zn(HPO_4)_2.H_2O$ were prepared as described in Chapter 3. Their physical properties are shown in Table 4.1.

Table 4.1 Physical properties of synthesized hydrates

Hydrates	Color	State
$ZnHPO_4.H_2O$	White	Solid
$Co(H_2PO_4)_2.2H_2O$	Violet	Solid
$LiFePO_4.3H_2O$	Green	Solid
$LiCoPO_4.3H_2O$	Pink	Solid
$LiNiPO_4.H_2O$	Pale Green	Solid
$LiMnPO_4.H_2O$	Pale Pink	Solid
$Li_2Zn(HPO_4)_2.H_2O$	White	Solid

4.2 Determination of Water of Crystallization of Synthesized Hydrates

The water of crystallization of $ZnHPO_4.H_2O$, $Co(H_2PO_4)_2.2H_2O$, $LiFePO_4.3H_2O$, $LiCoPO_4.3H_2O$, $LiNiPO_4.H_2O$, $LiMnPO_4.H_2O$ and $Li_2Zn(HPO_4)_2.H_2O$ were determined by using TG and Karl Fischer techniques. The results confirm the required formula of each hydrates.

4.2.1 Thermogravimetric (TG) Analysis Method

The results from the thermogravimetric (TG) method for $LiFePO_4.3H_2O$, $LiCoPO_4.3H_2O$, $LiNiPO_4.H_2O$, $LiMnPO_4.H_2O$ and $Li_2Zn(HPO_4)_2.H_2O$ under nitrogen atmosphere are shown in Figures 4.1-4.5, respectively. The TG curves of $LiFePO_4 \cdot 3H_2O$ (Figure 4.1) and $LiCoPO_4 \cdot 3H_2O$ (Figure 4.2) show the total mass

losses over the range of 80-350 °C of 24.68 and 23.06%, respectively, which correspond to the elimination of water of crystallization. Calculated mole numbers of water in these hydrates were found to be 2.87 and 2.81, respectively. Thermal analysis of $LiNiPO_4 \cdot H_2O$ (Figure 4.3) and $LiMnPO_4 \cdot H_2O$ (Figure 4.4) showed the total mass losses of 11.38 and 9.41%, respectively. The calculated mole number of water of crystallization were 1.14 and 0.90, respectively. The TG curve of $Li_2Zn(HPO_4)_2.H_2O$ (Figure 4.5) under nitrogen atmosphere over the range of 80 – 350 °C illustrates two steps in the temperature range from 150 to 350 °C. The total mass loss of 7.44 % confirms 1.21 mole of water in $Li_2Zn(HPO_4)_2 \cdot H_2O$. The final products at the temperature higher than 280 °C are suggested to be $Li_4P_2O_7$ and $Zn_2P_2O_7$.

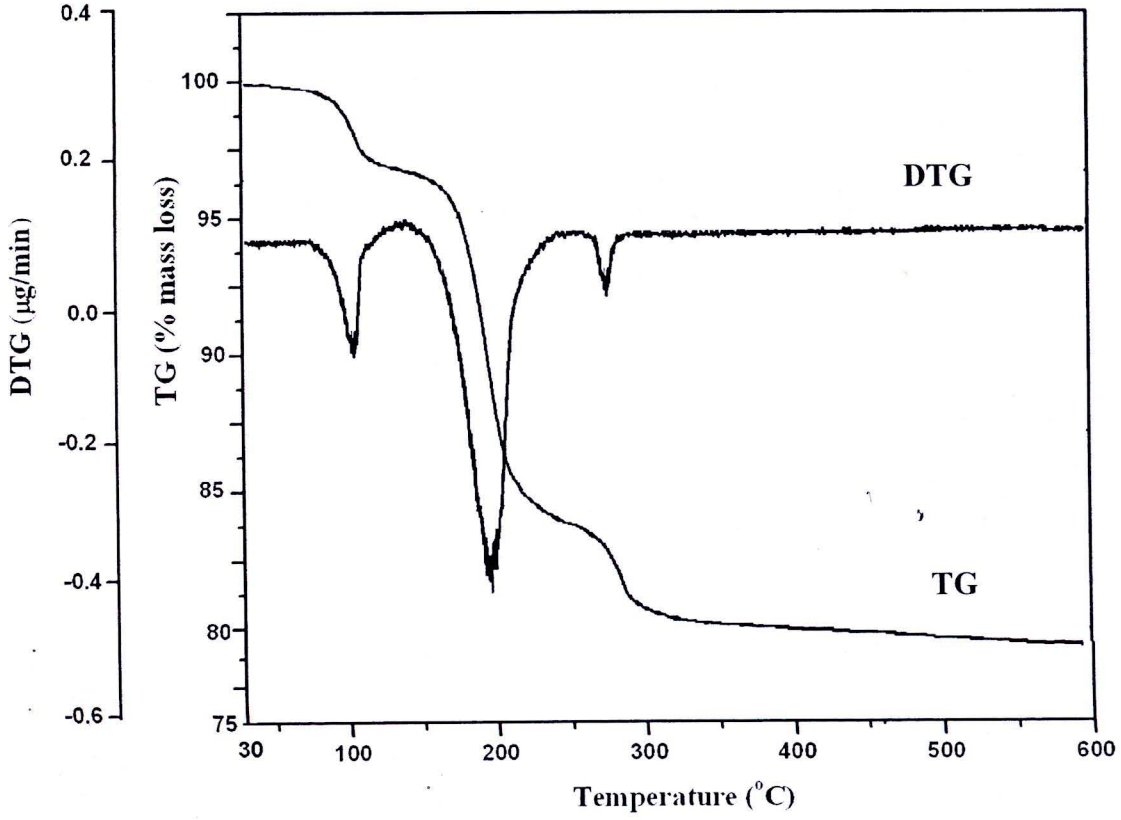

Figure 4.1 TG/DTG curves of $LiFePO_4 \cdot 3H_2O$ at the heating rate 10 °C min^{-1} in N_2 atmosphere

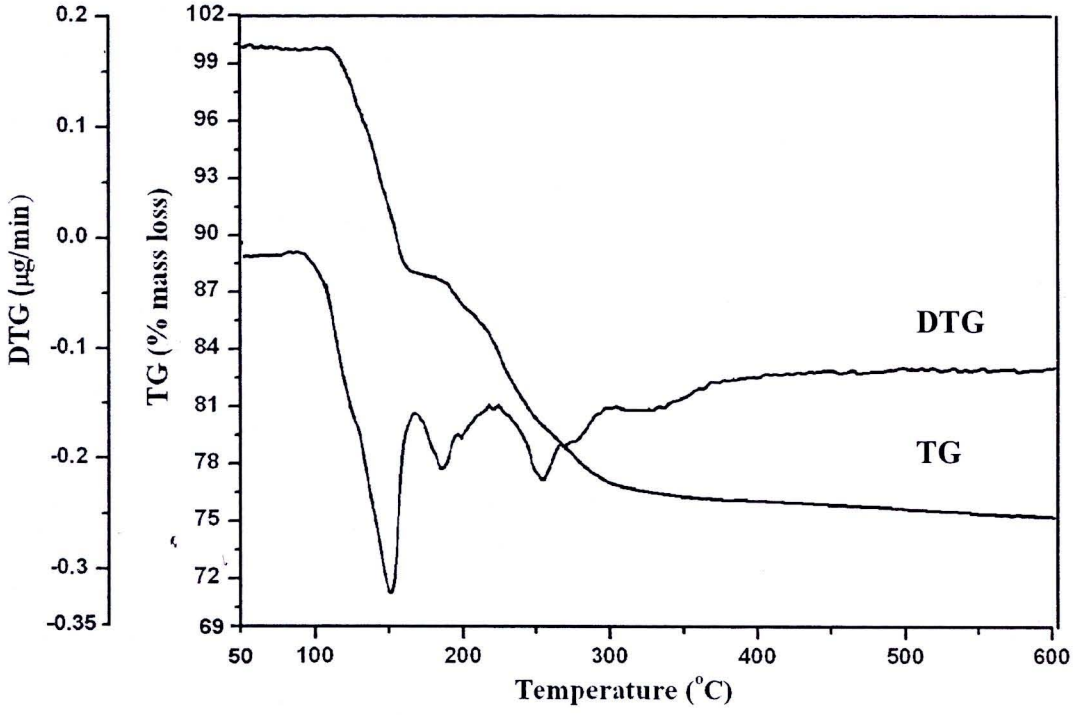

Figure 4.2 TG/DTG curves of $LiCoPO_4 \cdot 3H_2O$ at the heating rate 10 °C min^{-1} in N_2 atmosphere

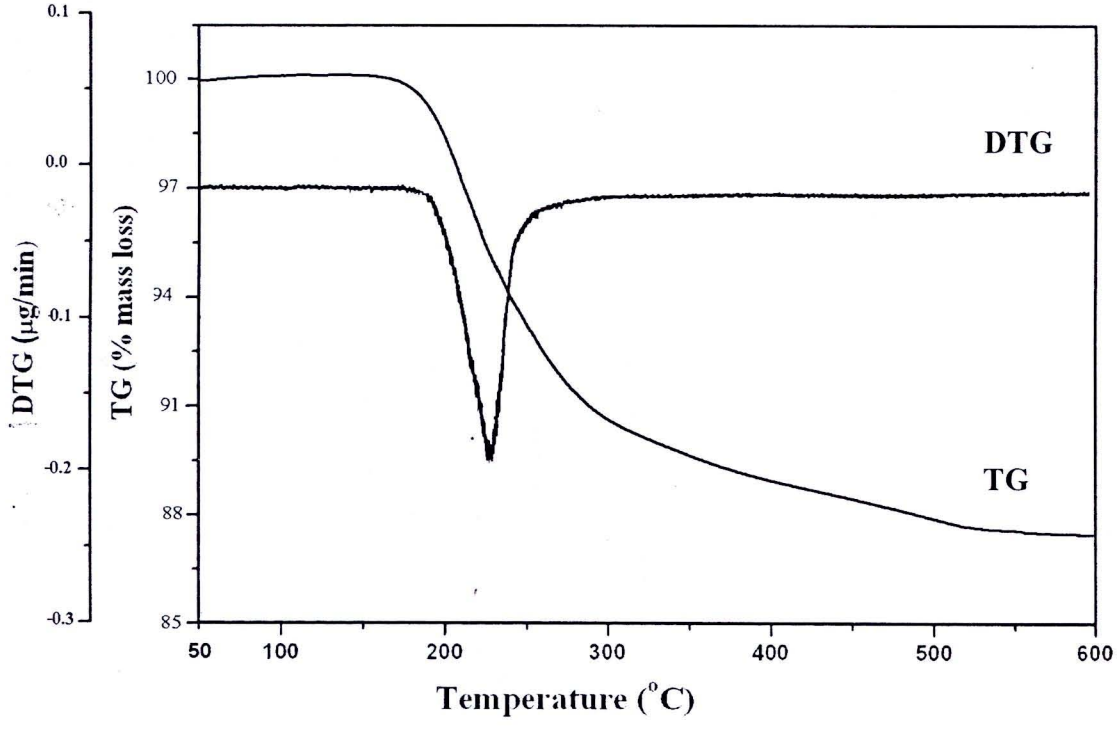

Figure 4.3 TG/DTG curves of $LiNiPO_4 \cdot H_2O$ at the heating rate 10 °C min^{-1} in N_2 atmosphere

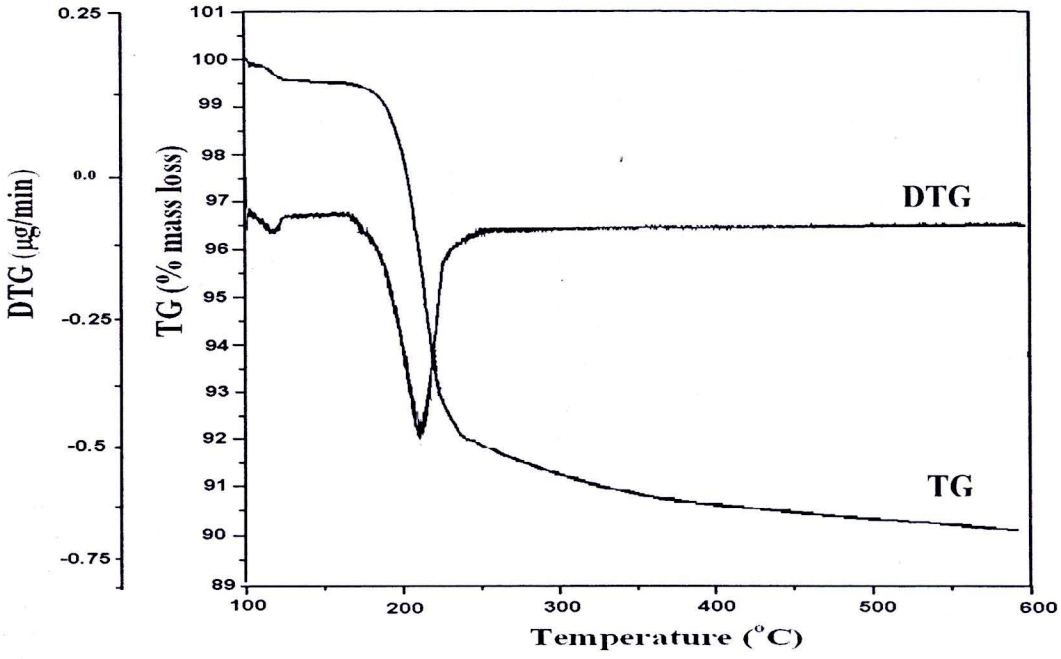

Figure 4.4 TG/DTG curves of $LiMnPO_4 \cdot 3H_2O$ at the heating rate 10 °C min^{-1} in N_2 atmosphere

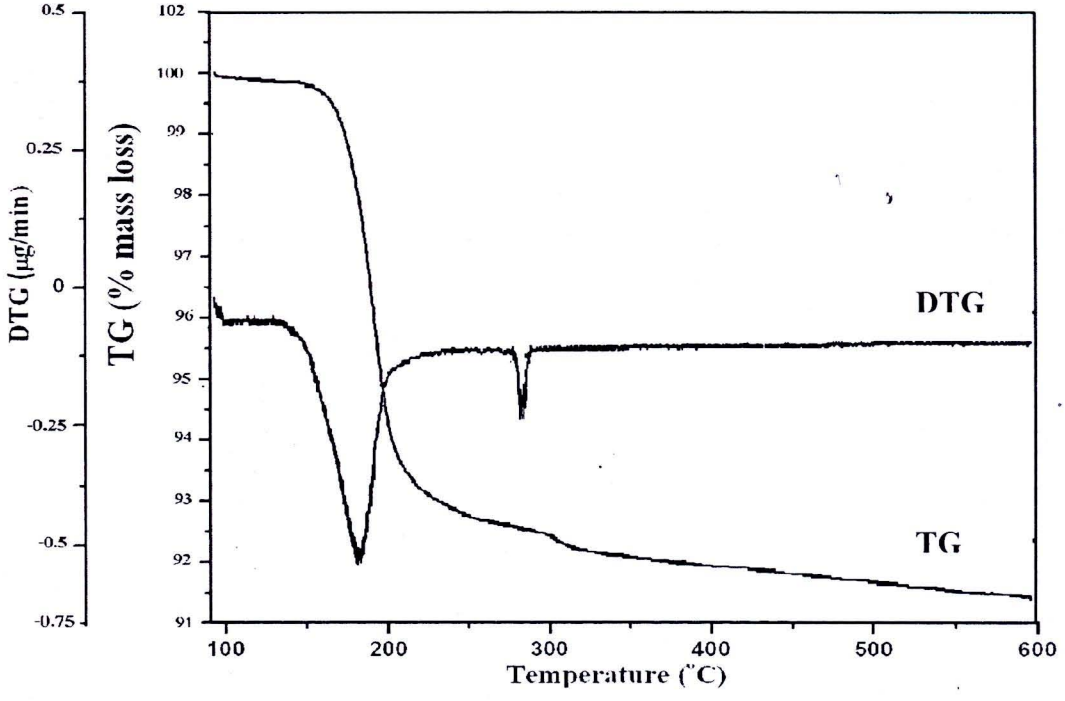

Figure 4.5 TG/DTG curves of $Li_2Zn(HPO_4)_2 \cdot H_2O$ at the heating rate 10 °C min^{-1} in N_2 atmosphere

4.2.1.1 Calculation of the Mole Number of Water of Crystallization from TGA/DTG/DTA Data

$LiMnPO_4.H_2O$

The dehydration of $LiMnPO_4 \cdot H_2O$ according to the thermogram in Figure. 4.4 can be calculated as follow.

The weight of $LiMnPO_4 \cdot H_2O = 5.5000 \times 10^{-3}$ g

The total weight loss from TG data of $LiMnPO_4 \cdot H_2O = 9.41\%$

Calculation of the mole number of crystallization water in step 1

The total mass loss = 9.41 %

100 g of $LiMnPO_4 \cdot H_2O$, the mass loss = 9.41 g

5.50×10^{-3} g of $LiMnPO_4.H_2O$, the mass loss $= \dfrac{(5.5000 \times 10^{-3}) \times 9.41}{100}$ g

$= 5.1755 \times 10^{-4}$ g

Mole equivalent of water $= \dfrac{5.1755 \times 10^{-4}}{18}$ mol

$= 2.8752 \times 10^{-5}$ mol

Mass of anhydrous $LiMnPO_4$ $= (5.5000 \times 10^{-3}) - (5.1755 \times 0^{-4})$ g

$= 4.9824 \times 10^{-3}$ g

Mole of anhydrous $LiMnPO_4$ $= \dfrac{4.9824 \times 10^{-3}}{156.88}$ mol

$= 3.1759 \times 10^{-5}$ mol

3.1759×10^{-5} mol of anhydrous $LiMnPO_4$, consists of water $= 2.8752 \times 10^{-5}$ mol

1.0 mol of $LiMnPO_4$.anhydrous, water content $= \dfrac{2.8752 \times 10^{-5}}{3.1759 \times 10^{-5}}$ mol

$= 0.90$ mole ≈ 1 mol

Similar calculations were carried out for all cases and the data are available in Appendix I. The results were tabulated in Table 4.2.

Table 4.2 The percentage of weight loss, transition temperatures, and calculated mole number of crystallization water per mole of anhydrous salt (n) in synthesized hydrates

Hydrates	Total Percent Mass Loss(%)	Transition Temp.(°C)		n (mol)
		Endothermic	Exothermic	
$LiFePO_4.3H_2O$	24.68	116, 190, 290	-	2.87
$LiCoPO_4.3H_2O$	23.06	179, 198, 215	-	2.81
$LiNiPO_4.H_2O$	11.38	226	-	1.14
$LiMnPO_4.H_2O$	9.41	205	-	0.90
$Li_2Zn(HPO_4)_2.H_2O$	7.44	187, 286	-	1.21

4.2.2 Karl Fischer Method

Karl Fischer method is one of the standard methods for determining the water content in hydrates. The mole numbers of water of crystallization were calculated from the percentage of water and are tabulated in Table 4.3. The average calculated mole number of water by Karl Fischer method of $ZnHPO_4.H_2O$, $Co(H_2PO_4)_2.2H_2O$, $LiFePO_4.3H_2O$, $LiCoPO_4.3H_2O$, $LiNiPO_4.H_2O$, $LiMnPO_4.H_2O$ and $Li_2Zn(HPO_4)_2.H_2O$ are 1.05, 1.92, 3.08, 3.16, 1.17, 0.80 and 1.16 mol, respectively, as illustrated in Table 4.3. The results agree well with the formula of each hydrate.

Table 4.3 The percentage of water and blank solution (CH_3OH : HNO_3) and sample the mole number of water of crystallization per mole of anhydrous salt (n) determined by Karl Fischer method

Hydrates	Percentage of water		Total % water in hydrate	n (mol)	S.D.
	Blank	Sample			
$ZnHPO_4.H_2O$	10.43	10.53	0.10	0.92	0.12
		10.50	0.13	1.21	
		10.55	0.12	1.01	
Average				1.05	
$Co(H_2PO_4)_2.2H_2O$	12.69	12.79	0.10	1.96	0.03
		12.77	0.08	1.93	
		12.79	0.10	1.88	
Average				1.92	
$LiFePO_4.3H_2O$	9.48	9.67	0.19	3.00	0.26
		9.61	0.13	2.80	
		9.66	0.29	3.44	
Average				3.08	
$LiCoPO_4.3H_2O$	16.92	17.40	0.48	2.75	0.23
		17.56	0.64	3.14	
		17.46	0.54	3.59	
Average				3.16	
$LiNiPO_4.H_2O$	8.02	8.19	0.17	1.31	0.11
		8.08	0.06	1.04	
		8.22	0.20	1.26	
Average				1.20	

Table 4.3 The percentage of water and blank solution (CH_3OH : HNO_3) and sample the mole number of water of crystallization per mole of anhydrous salt (n) determined by Karl Fischer method (Cont.)

Hydrates	Percentage of water		Total % water in hydrate	n (mole)	S.D.
	Blank	Sample			
$LiMnPO_4.H_2O$	6.90	7.02	0.12	0.86	0.08
		7.00	0.10	0.75	
		6.99	0.06	0.94	
Average				0.85	
$Li_2Zn(HPO_4)_2.H_2O$	7.45	7.50	0.05	0.98	0.07
		7.53	0.08	1.34	
		7.52	0.07	1.50	
Average				1.16	

4.3 Determination of Metal Content in the Synthesized Hydrates

Iron, cobalt, nickel and manganese content in the synthesized hydrates were determined by AAS technique, while lithium content was determined by AES technique. The stoichiometry of metal in hydrates was determined to confirm the formula of hydrates. The calibration curves for the determination of zinc, iron, cobalt, nickel, manganese and lithium contents are illustrated in Appendix II.

4.3.1 Determination of the Metal Content in the Synthesized Hydrates

Ex. $LiFePO_4.3H_2O$

The preparation of $LiFePO_4.3H_2O$ sample for the determination the iron content in hydrates was carried out as the following steps.

Step 1: Preparation of 100.00 cm^3 solution containing 0.0216 gram of $LiFePO_4.3H_2O$ in 0.15 M HNO_3

Step 2: Preparation of 100.00 cm^3 of the solution containing 5.00 cm^3 of solution from step 1 and adjust to the mark by 0.15 M HNO_3

The concentration of iron from AAS (Table 4.3) in the first sample was 2.759 mg/L. That means,

1 cm^3 of $LiFePO_4.3H_2O$ solution contain Fe = 2.759×10^{-6} g

100 cm^3 of $LiFePO_4.3H_2O$ solution contain Fe = $[(2.759 \times 10^{-6}\ g) \times 100 cm^3]/1 cm^3$

= 2.759×10^{-4} g

Hence,

2.759×10^{-4} gram was obtained from 5.00 cm^3 of $LiFePO_4.3H_2O$ solution

Then, 5.00 cm^3 of $LiFePO_4.3H_2O$ solution contain Fe = 2.759×10^{-4} g

100 cm^3 of $LiFePO_4.3H_2O$ solution contain Fe = $\frac{(2.759 \times 10^{-4})}{5} \times 100$

= 5.51×10^{-3} g

100 cm^3 of $LiFePO_4.3H_2O$ solution are obtained from dissolving 0.0216 g of $LiFePO_4.3H_2O$. Therefore,

0.0216 gram of $LiFePO_4.3H_2O$ contain Fe = 5.51×10^{-3} g

The molecular weight of $LiFePO_4.3H_2O$ = 211.80 g/mol, that means

211.80 gram of $LiFePO_4.3H_2O$ contain Fe = $\frac{(5.51 \times 10^{-3} g) \times 211.80 g}{0.0216\ g}$

= 54.10 g

= 54.10 g / 55.8 g/mol

= 0.96 mol

Similar calculations were carried out for all cases and the details are presented in Appendix I. The results are tabulated in Table 4.4.

Table 4.4 The metal contents in prepared hydrates from AAS and AES techniques

Hydrates	Metal content (mol)					
	Fe	Co	Ni	Mn	Zn	Li
$ZnHPO_4.H_2O$	-	-	-	-	0.86 0.93 0.96	-
Average					0.92 (SD=0.05)	
$Co(H_2PO_4)_2.2H_2O$	-	0.90 0.94 0.93	-	-	-	-
Average		0.92 (SD=0.02)				
$LiFePO_4.3H_2O$	0.96 0.99 1.17	-		-	-	1.28 0.92 1.05
Average	1.04 (SD=0.06)					1.08 (SD=0.15)
$LiCoPO_4.3H_2O$	-	1.00 0.96 1.05	-		-	0.94 0.96 0.96
Average		1.01 (SD=0.04)				0.95 (SD=0.01)
$LiNiPO_4.H_2O$	-	-	1.10 1.05 1.07	-		1. 06 1.03 1.05
Average			1.07 (SD=0.02)			1.04 (SD=0.01)
$LiMnPO_4.H_2O$	-	-	-	1.09 0.97 0.97		0.96 0.98 0.98
Average				1.01 (SD=0.06)		0.97 (SD=0.01)
$Li_2Zn(HPO_4)_2.H_2O$	-		-	-	1.06 1.03 1.08	2.12 1.99 2.19
Average					1.05 (SD=0.02)	2.09 (SD=0.08)

4.4 Thermal Decomposition of Some Selected Hydrated

The thermal decomposition of $ZnHPO_4.H_2O$, $Co(H_2PO_4)_2.H_2O$, $LiFePO_4.3H_2O$, $LiCoPO_4.3H_2O$, $LiNiPO_4.H_2O$, $LiMnPO_4.H_2O$, $Li_2Zn(HPO_4)_2.H_2O$ and $ZnHPO_4.H_2O$ were investigated by DSC technique. The DSC thermograms of these prepared hydrates are shown in Figures 4.6-4.12, respectively.

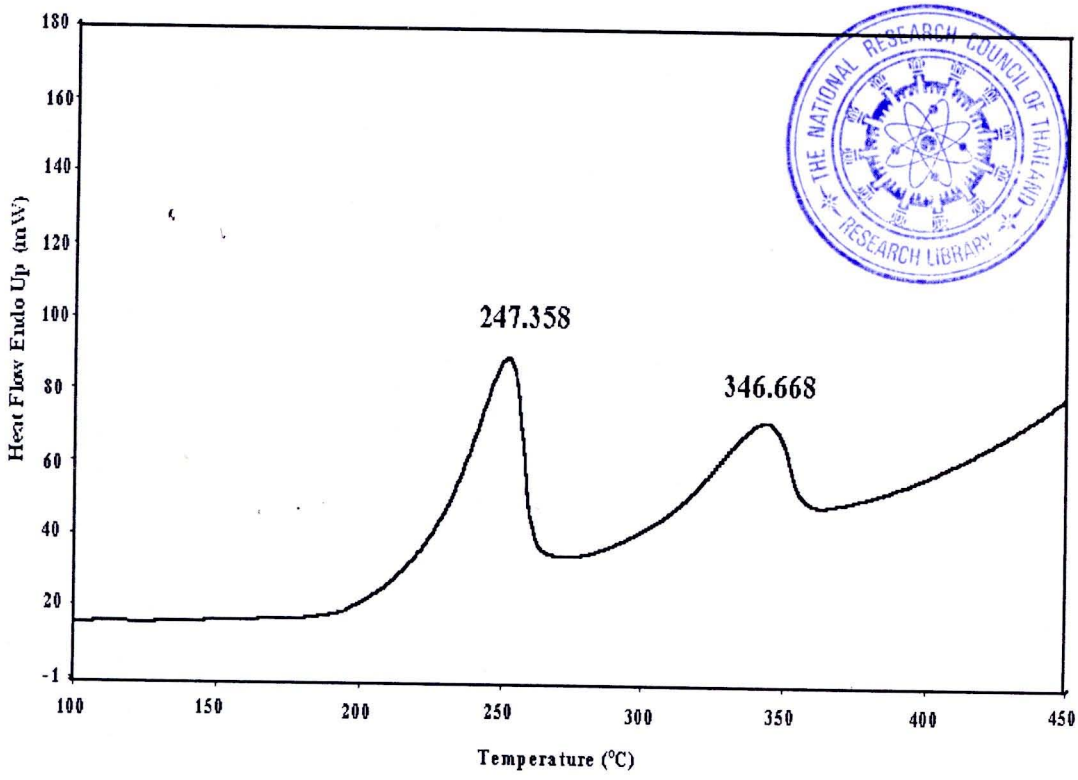

Figure 4.6 DSC curve of $ZnHPO_4.H_2O$ at the heating rate 10 °C min^{-1}

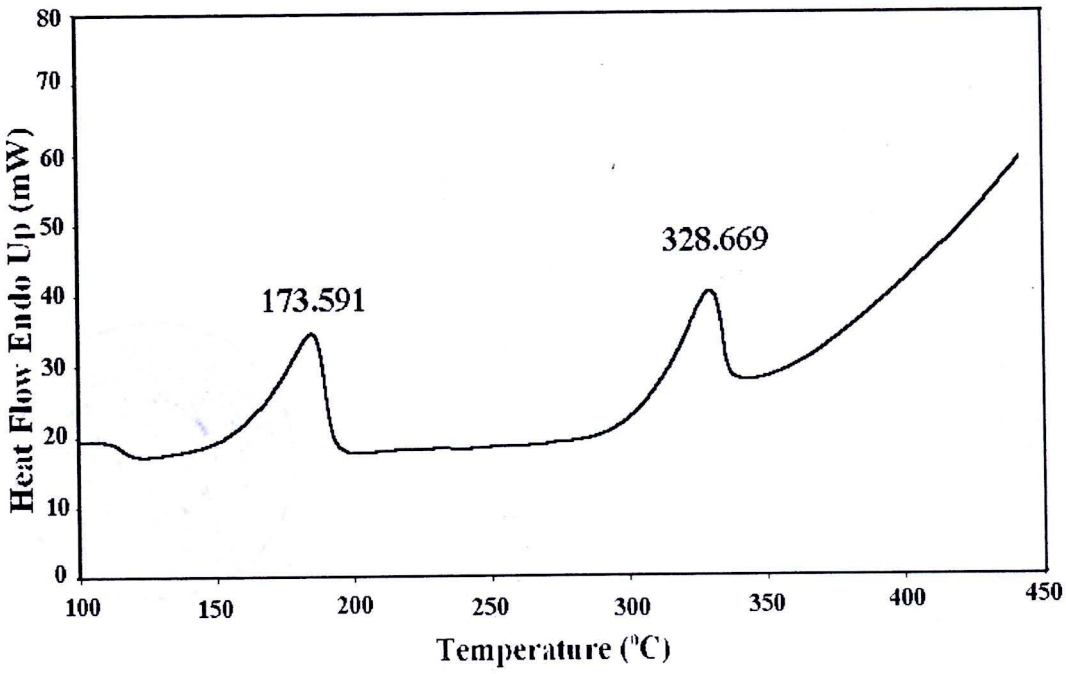

Figure 4.7 DSC curve of $Co(H_2PO_4)_2.2H_2O$ at the heating rate 10 °C min^{-1}

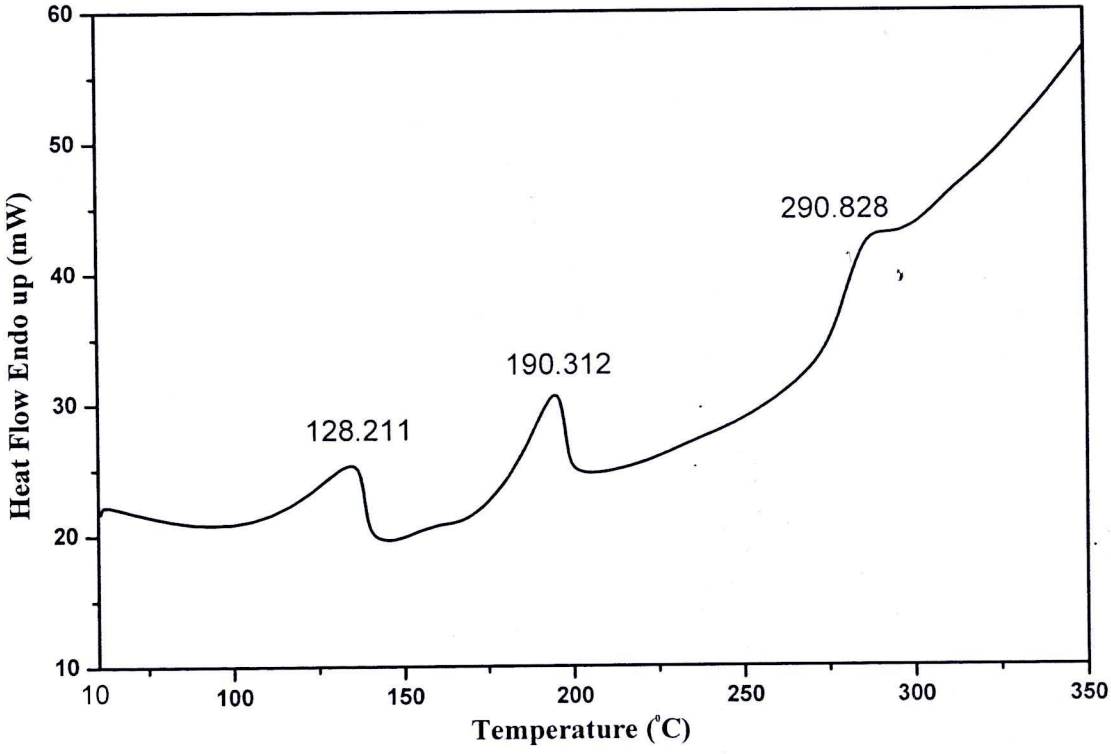

Figure 4.8 DSC curve of $LiFePO_4.3H_2O$ at the heating rate 10 °C min^{-1}

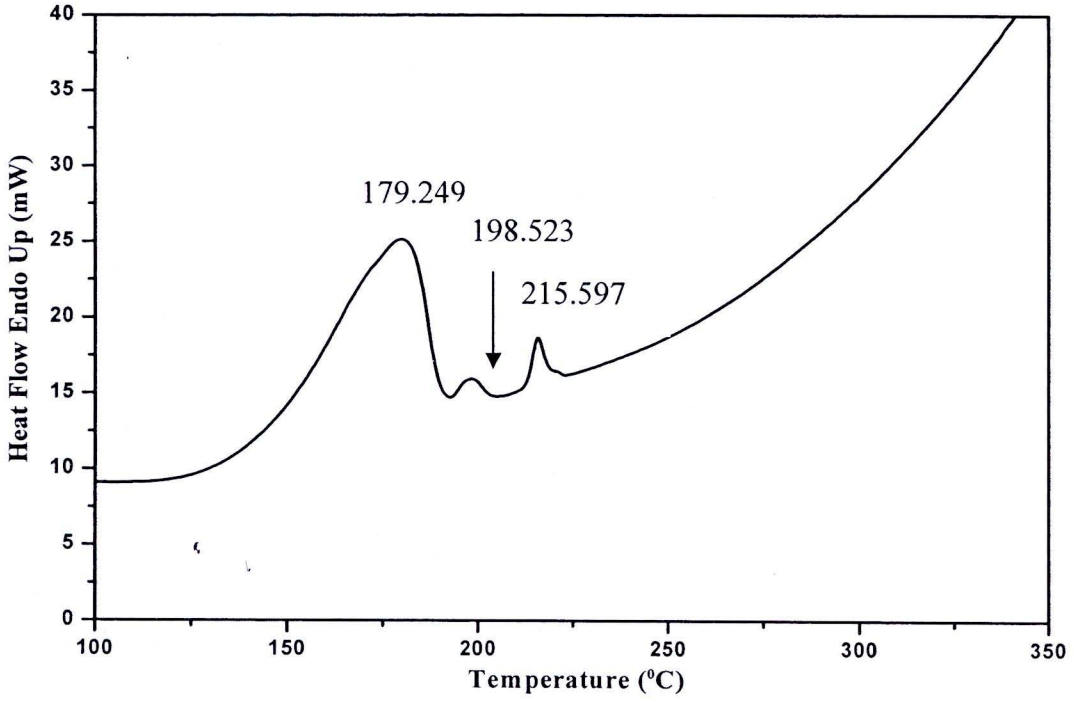

Figure 4.9 DSC curve of $LiCoPO_4.3H_2O$ at the heating rate 10 °C min^{-1}

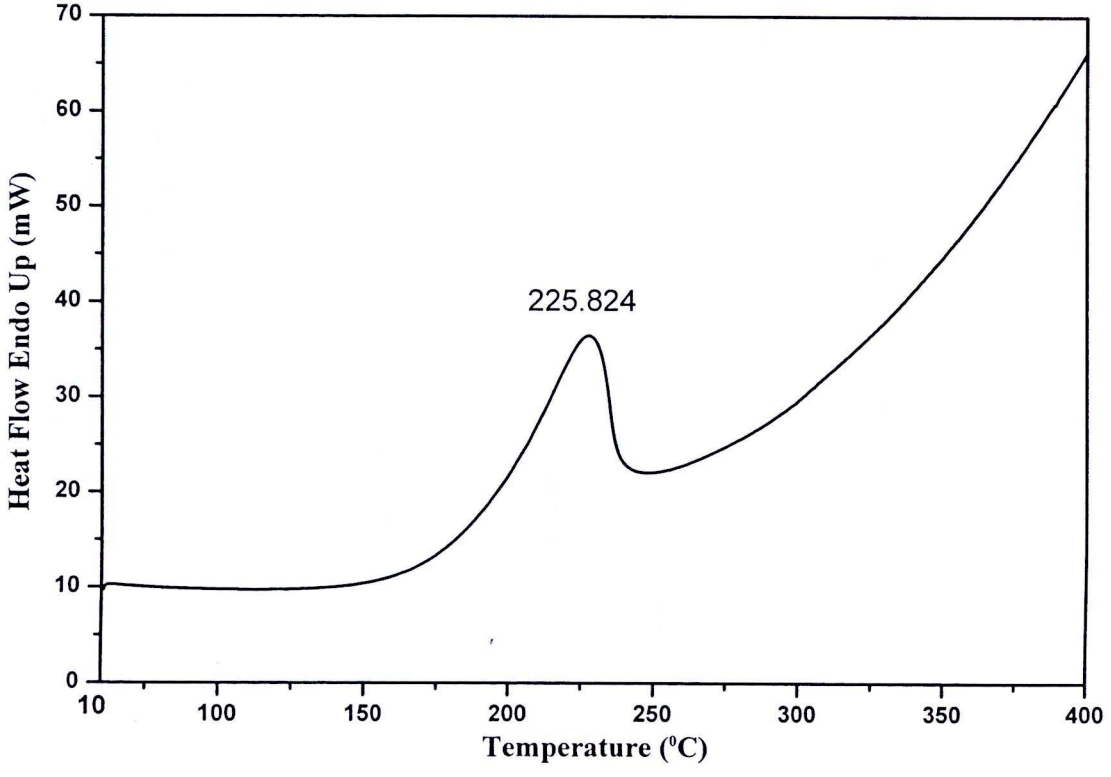

Figure 4.10 DSC curve of $LiNiPO_4.H_2O$ at the heating rate 10 °C min^{-1}

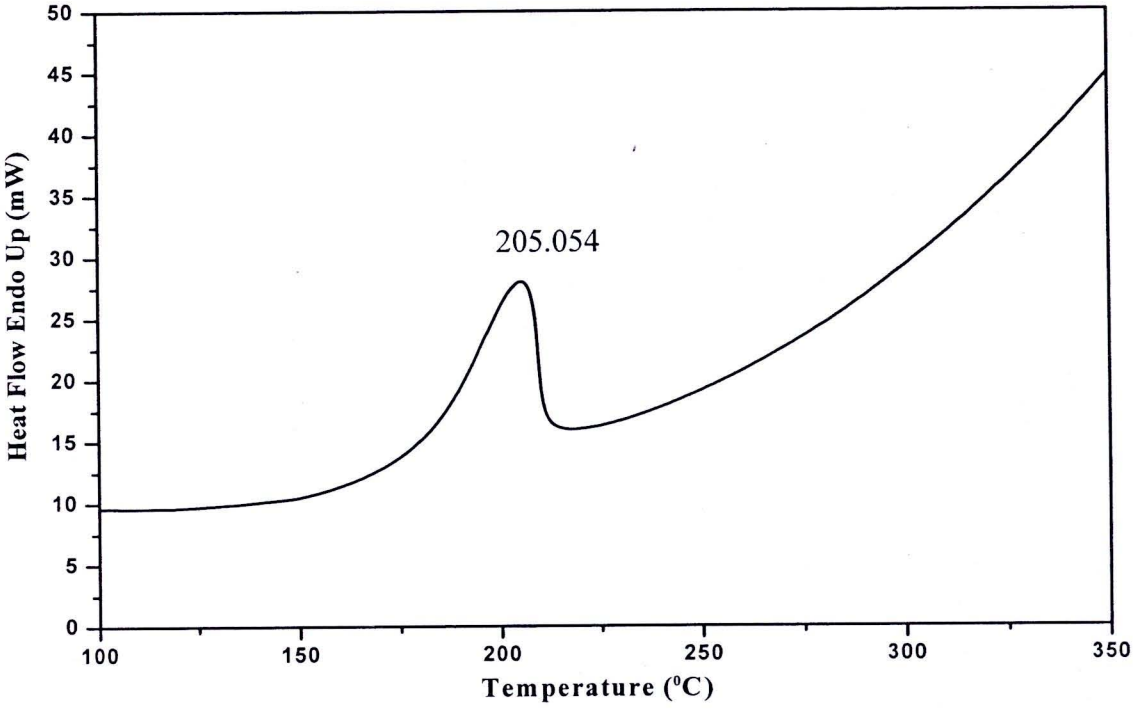

Figure 4.11 DSC curve of $LiMnPO_4.H_2O$ at the heating rate 10 °C min^{-1}

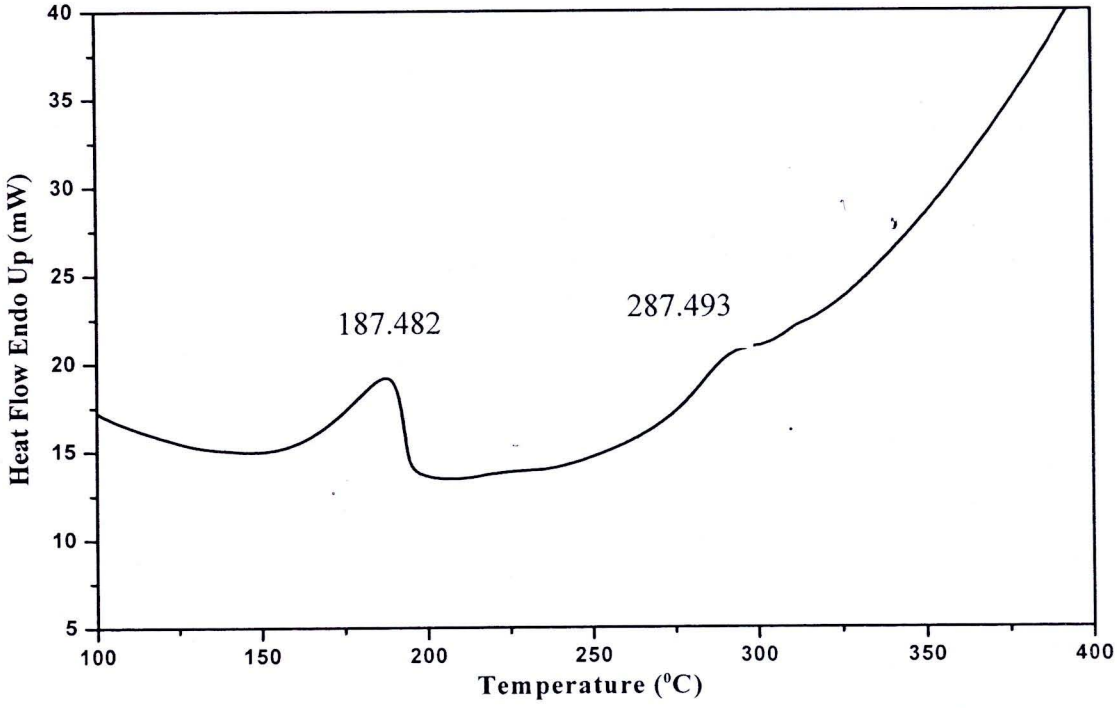

Figure 4.12 DSC curve of $Li_2Zn(HPO_4)_2.H_2O$ at the heating rate 10 °C min^{-1}

The thermal decomposition of $ZnHPO_4.H_2O$ (see Figure 4.6) exhibits two endothermic peaks, hence the thermal decomposition can be suggested to be:

Step 1 (in the range of 198-260 °C)

$$ZnHPO_4.H_2O \rightarrow ZnHPO_4 + H_2O\uparrow \qquad \Delta H_1 = 391.823 \text{ J/g} \qquad (1)$$

Step 2 (in the range of 312-388 °C)

$$ZnHPO_4 \rightarrow \frac{1}{2}Zn_2P_2O_7 + \frac{1}{2}H_2O\uparrow \qquad \Delta H_2 = 316.188 \text{ J/g} \qquad (2)$$

The DSC curve in Figure 4.7 ilustrates two steps of endothermic thermal decomposition of $Co(H_2PO_4)_2.2H_2O$. The changes are sugested to be:

Step 1 (in the range of 153-192 °C)

$$Co(H_2PO_4)_2.2H_2O \rightarrow Co(H_2PO_4)_2 + 2H_2O\uparrow \quad \Delta H_1 = 293.728 \text{ J/g} \qquad (3)$$

Step 2 (in tne range of 306-340 °C)

$$Co(H_2PO_4)_2 \rightarrow \frac{1}{2}Co_2P_4O_{12} + 2H_2O\uparrow \quad \Delta H_2 = 290.566 \text{ J/g} \qquad (4)$$

The DSC curve in Figure 4.8 illustrates three steps of endothermic thermal decomposition of $LiFePO_4{\cdot}3H_2O$. The mechanism is suggested to be three consecutive dehydration as follow:

Step 1 (in the range of 104-135 °C)

$$LiFePO_4{\cdot}3H_2O \rightarrow LiFePO_4{\cdot}aH_2O + xH_2O\uparrow \quad \Delta H_1 = 404.136 \text{ J/g} \qquad (5)$$

Step 2 (in the range of 171-195 °C)

$$LiFePO_4{\cdot}aH_2O \rightarrow LiFePO_4.bH_2O + yH_2O\uparrow \quad \Delta H_2 = 466.034 \text{ J/g} \qquad (6)$$

Step 3 (in the range of 275-308 °C)

$$LiFePO_4.bH_2O \rightarrow LiFePO_4 + zH_2O\uparrow \qquad \Delta H_3 = 250.997 \text{ J/g} \qquad (7)$$

where $x + y + z = 3$. The results can be interpreted in terms of different strengths of hydrogen bonding interactions. This hydrate should contain at least three district strengths of hydrogen bonds.

The thermal decomposition of $LiCoPO_4{\cdot}3H_2O$ (see Figure 4.9) exhibits three endothermic peaks of thermal decomposition. The consecutive dehydration are suggested to be as follow:

Step 1(in the range of 145-189 °C)

$$LiCoPO_4{\cdot}3H_2O \rightarrow LiCoPO_4{\cdot}aH_2O + xH_2O\uparrow \quad \Delta H_1 = 441.092 \text{ J/g} \qquad (8)$$

Step 2 (in the range of 193-202 °C)

$$LiCoPO_4 \cdot aH_2O \rightarrow LiCoPO_4.bH_2O + yH_2O\uparrow \quad \Delta H_2 = 9.704 \text{ J/g} \quad (9)$$

Step 3 (in the range 212-218 °C)

$$LiCoPO_4 \cdot bH_2O \rightarrow LiCoPO_4 + zH_2O\uparrow \quad \Delta H_3 = 12.861 \text{ J/g} \quad (10)$$

where x + y + z = 3 mol.

In contrast, the thermal decomposition of $LiNiPO_4 \cdot H_2O$ (see Figure 4.10) shows one endothermic peak in the rage of 191-237 °C, which can be simply suggested the following dehydration:

$$LiNiPO_4 \cdot H_2O \rightarrow LiNiPO_4 + H_2O\uparrow \quad \Delta H_1 = 306.938 \text{ J/g} \quad (11)$$

Similary thermal decomposition of $LiMnPO_4 \cdot H_2O$ (see Figure 4.11) also exhibits one endothermic peak in the range of 181-210 °C. The following dehydration is suggested:

$$LiMnPO_4 \cdot H_2O \rightarrow LiMnPO_4 + H_2O\uparrow \quad \Delta H_1 = 200.640 \text{ J/g} \quad (12)$$

For the case of $Li_2Zn(HPO_4)_2 \cdot H_2O$ (see Figure 4.12), two endothermic peaks are observed. Thermal decomposition of this compound can be suggested as follow:

Step 1(in the range of 161-194 °C)

$$Li_2Zn(HPO_4)_2 \cdot H_2O \rightarrow Li_2Zn(HPO_4)_2 + H_2O\uparrow \quad \Delta H_1 = 443.635 \text{ J/g} \quad (13)$$

Step 2(in the range of 278-302 °C)

$$Li_2Zn(HPO_4)_2 \rightarrow \frac{1}{2}(Li_4P_2O_7) + \frac{1}{2}(Zn_2P_2O_7) + H_2O\uparrow \quad \Delta H_2 = 269.264 \text{ J/g} \quad (14)$$

4.5 X-Ray Powder Diffraction (XRD) Results

The structure of the synthesized hydrates and their decomposition products were characterized by X-ray powder diffraction. The XRD patterns of the synthesized samples and the decomposition products are shown in the Figurs 4.13-4.19. All detectable peaks of the synthesized samples and their decomposition products are indexed based on the structure in standard data as PDF files and the literature. The XRD patterns of synthetic $ZnHPO_4.H_2O$ (PDF # 350373) and its decomposition product are shown in the Figure 4.13 indicating that both crystal structures are monoclinic with the space group of $P2_{1/c}$ and the lattice is primitive. The XRD patterns of synthetic $Co(H_2PO_4)_2.2H_2O$ (PDF # 792239) and its decomposition products shown in the Figure 4.14 indicate that both crystal structure is monoclinic system with the space group of $P2_{1/n}$ and the lattice is primitive. The XRD pattern of

synthetic $LiFePO_4.3H_2O$ and its dehydration product (anhydrous $LiFePO_4$) are shown in Figure 4.15. The XRD pattern of synthetic $LiFePO_4.3H_2O$ and anhydrous $LiFePO_4$ (PDF # 832092) indicate that both crystal structures are orthorhombic with the space group Pnma with primitive lattice. The XRD patterns of synthetic $LiCoPO_4.3H_2O$ and its dehydration product (anhydrous $LiCoPO_4$) are shown in Figure 4.16. The XRD patterns of synthetic $LiCoPO_4.3H_2O$ and anhydrous $LiCoPO_4$ (PDF # 850002) indicate that both crystal structures are orthorhombic with the space group Pnma and the lattice is primitive. The XRD patterns of synthetic $LiNiPO_4.H_2O$ and its dehydration product (anhydrous $LiNiPO_4$) are shown in Figure 4.17. The XRD patterns of synthetic $LiNiPO_4.H_2O$ and anhydrous $LiNiPO_4$ (PDF # 320578) indicate that both crystal structures are orthorhombic with the space group Pmna and primitive lattice. The XRD patterns of synthetic $LiMnPO_4.H_2O$ and its dehydration product (anhydrous $LiMnPO_4$) are shown in Figure 4.18. The XRD patterns of synthetic $LiMnPO_4.H_2O$ and anhydrous $LiMnPO_4$ (PDF # 740375) indicate that both crystal structures are orthorhombic with the space group Pmna and primitive lattice. The XRD patterns of synthetic $Li_2Zn(HPO_4)_2.H_2O$, anhydrous $Li_2Zn(HPO_4)_2$ and its final decomposition products ($Li_4P_2O_7$ and $Zn_2P_2O_7$) are shown in the Figure 4.19. The standard XRD patterns of $Li_2Zn(HPO_4)_2.H_2O$ and anhydrous $Li_2Zn(HPO_4)_2$ reported in the literature [4-6] indicate that both crystal structures are in monoclinic system.

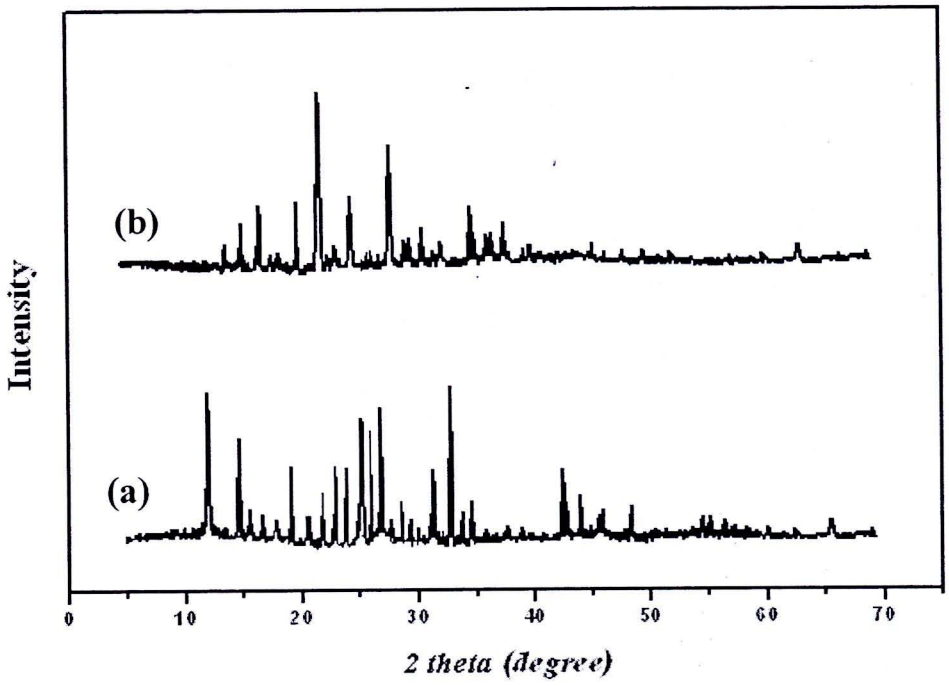

Figure 4.13 The XRD patterns of $ZnHPO_4.H_2O$ (a) and calcined product at 450°C (b)

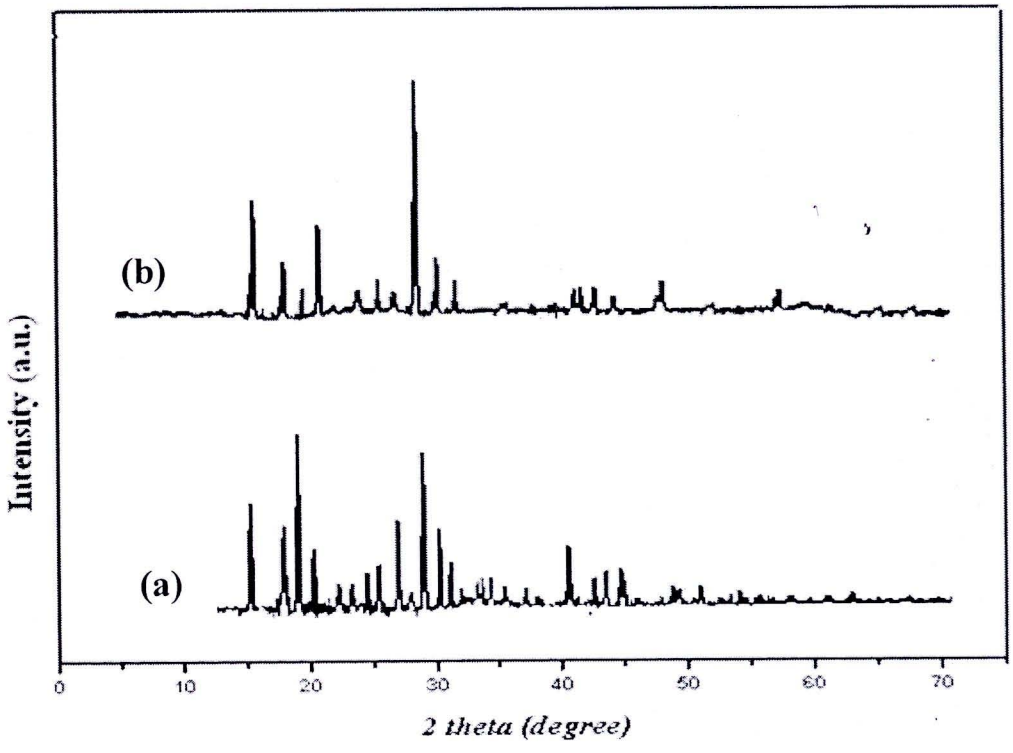

Figure 4.14 The XRD patterns of $Co(H_2PO_4)_2.2H_2O$ (a) and calcined product at 450°C (b)

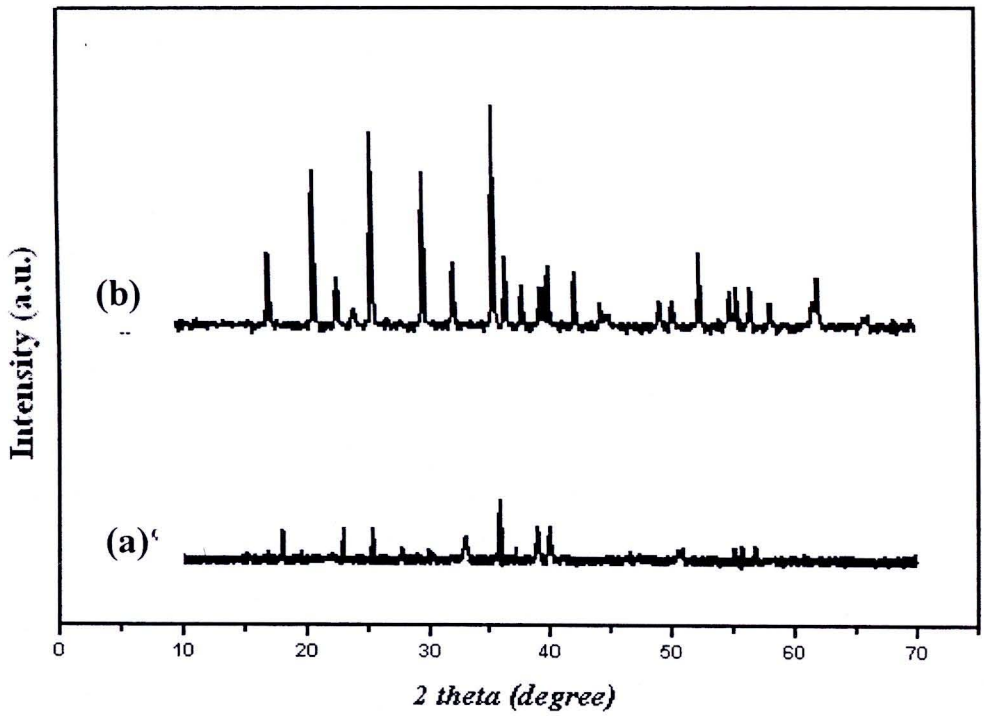

Figure 4.15 The XRD patterns of $LiFePO_4.3H_2O$ (a) and calcined product at 450°C (b)

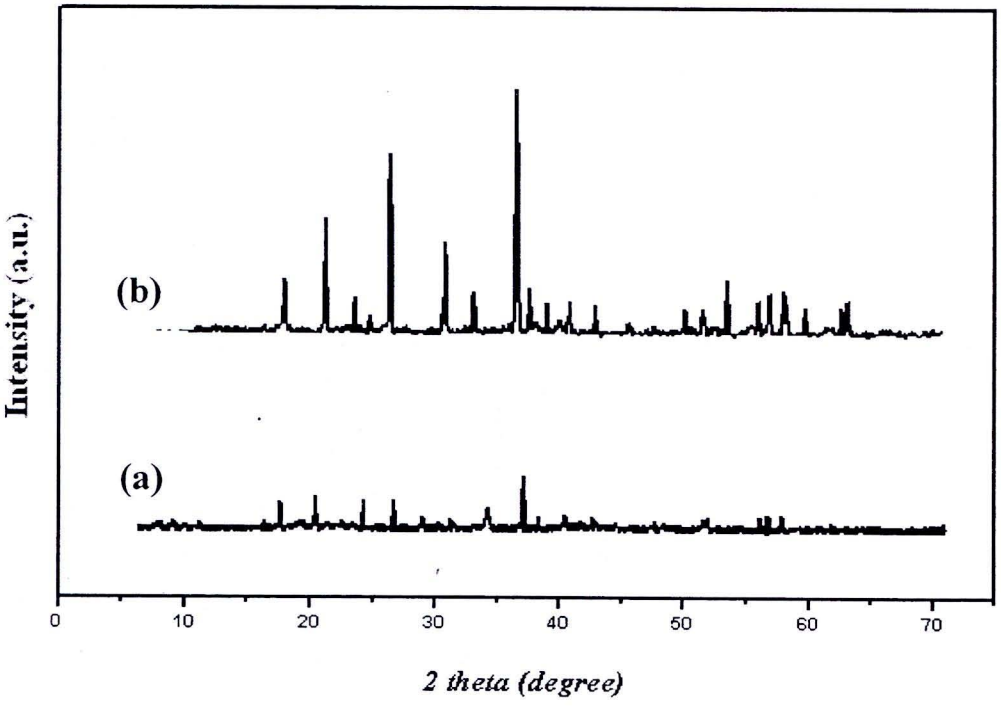

Figure 4.16 The XRD patterns of $LiCoPO_4.3H_2O$ (a) and calcined product at 450°C (b)

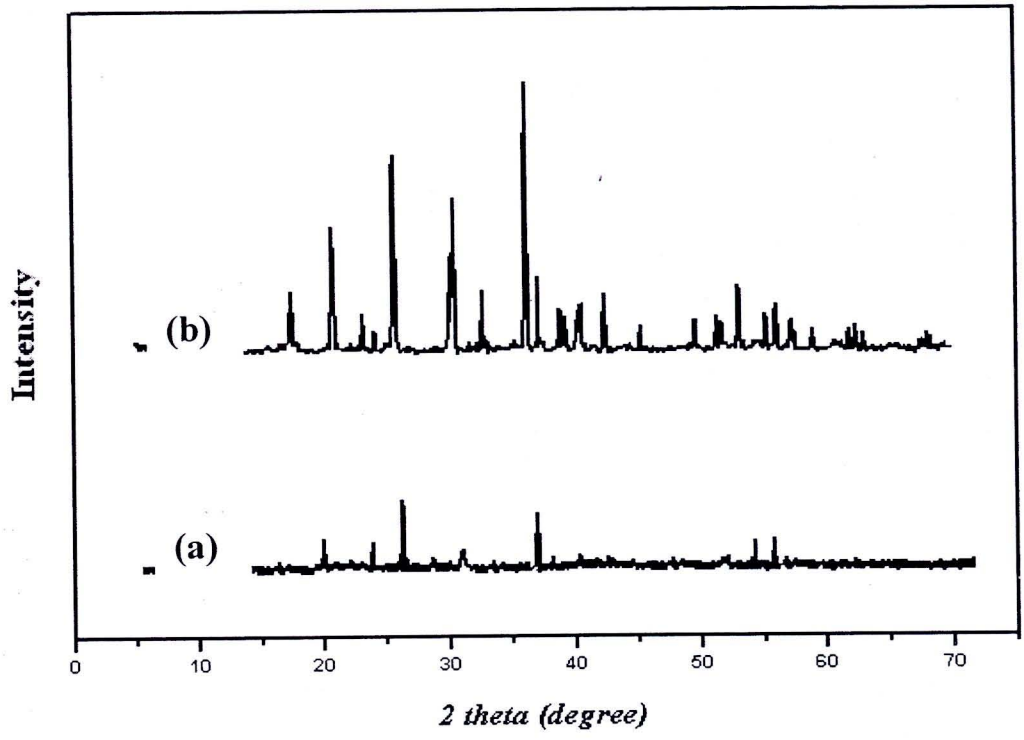

Figure 4.17 The XRD patterns of $LiNiPO_4.H_2O$ (a) and calcined product at 450°C (b)

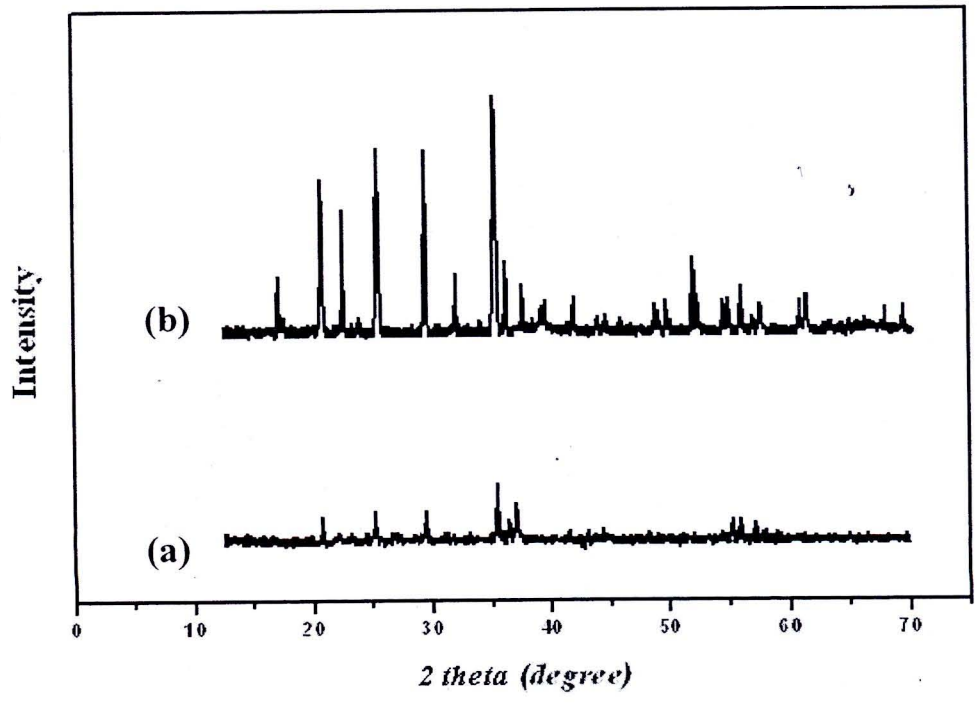

Figure 4.18 The XRD patterns of $LiMnPO_4.H_2O$ (a) and calcined product at 450°C (b)

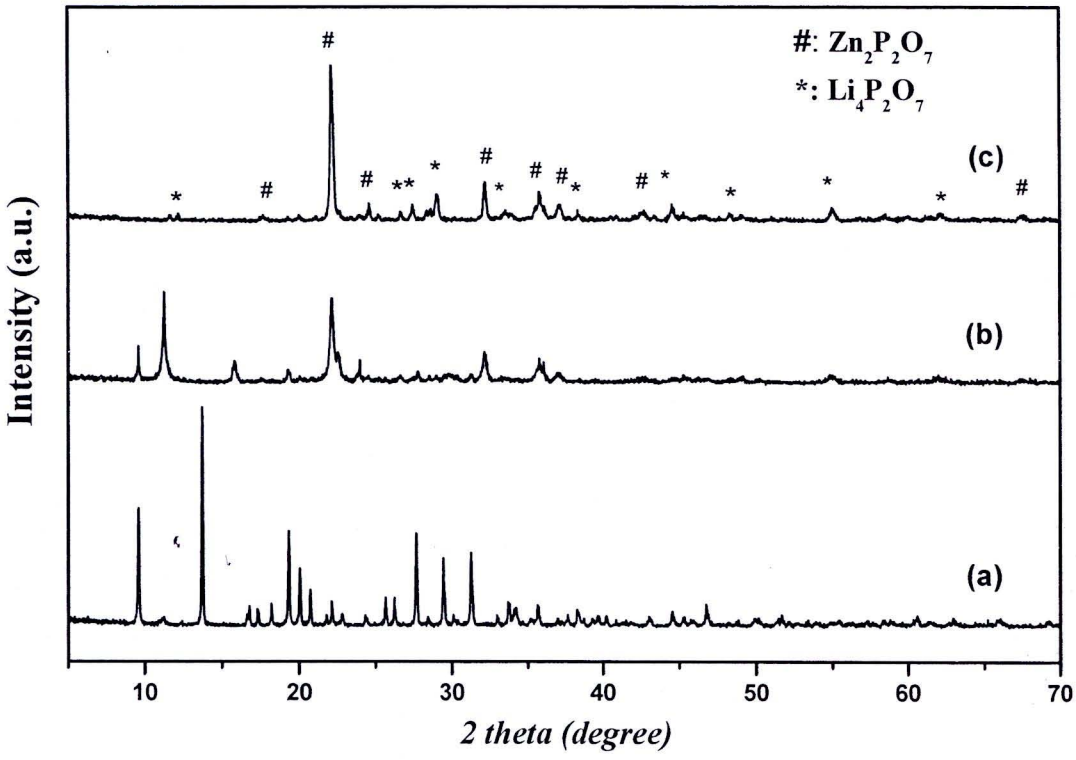

Figure 4.19 The XRD patterns of $Li_2Zn(HPO_4)_2.H_2O$ (a), calcined product at 200°C (b) and calcined product at 450 °C (c)

4.6 Vibrational Spectroscopic Study of Synthesized Hydrates

Middle infrared spectra of the synthesized hydrates were measured on an FTIR/FT Raman spectrophotometer with a resolution of 4.0 cm^{-1} in the range of 4000 – 370 cm^{-1} by KBr die technique. The FT Raman spectra of these hydrates were recorded on the same instrument with the same resolution and in the same range.

The FTIR spectra of $ZnHPO_4.H_2O$, $Co(H_2PO_4)_2.2H_2O$, $LiFePO_4.3H_2O$, $LiCoPO_4.3H_2O$, $LiNiPO_4.H_2O$, $LiMnPO_4.H_2O$ and $Li_2Zn(HPO_4)_2.H_2O$ are shown in Figures 4.20-4.26, respectively. Figures 4.27-4.33 show the extended region to illustrate the $\nu_1(H_2O)$, $\nu_3(H_2O)$ stretching and bending (ν_2) modes, while Figures 4.34-4.40 show the extended region for PO_4^{3-} modes of vibration. The vibrational frequencies and the possible assignments for each case were summarized in Tables 4.5-4.11 for the $ZnHPO_4.H_2O$, $Co(H_2PO_4)_2.2H_2O$, $LiFePO_4.3H_2O$, $LiCoPO_4.3H_2O$, $LiNiPO_4.H_2O$, $LiMnPO_4.H_2O$ and $Li_2Zn(HPO_4)_2.H_2O$, respectively.

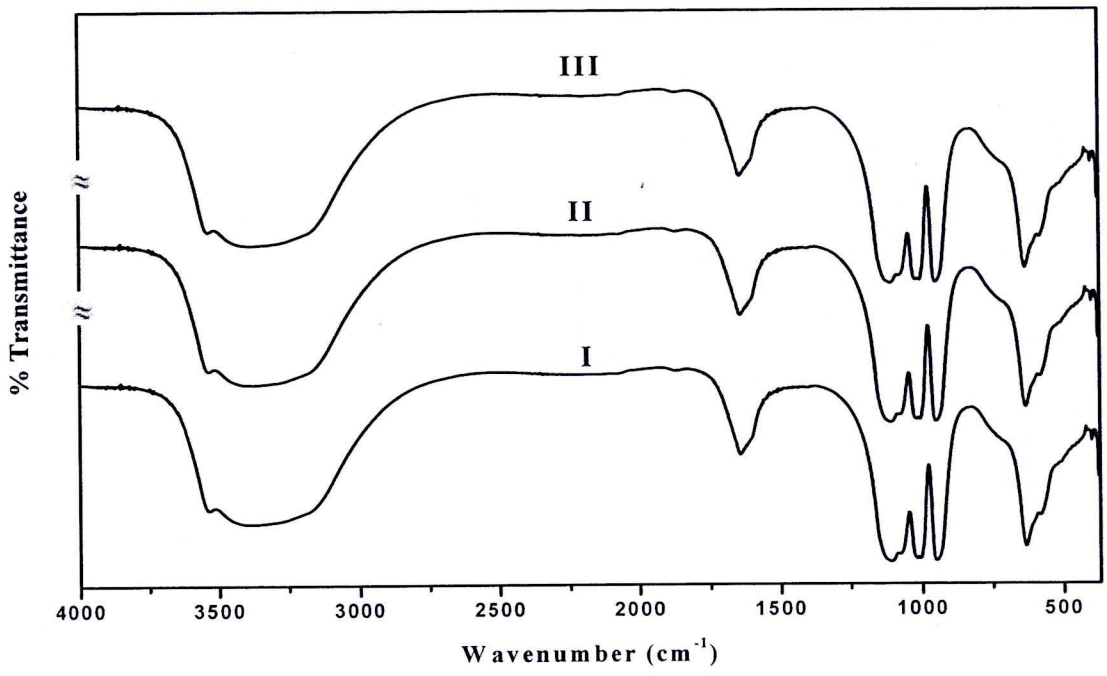

Figure 4.20 FTIR spectra of $ZnHPO_4 \cdot H_2O$ (three replications) in the region of 4000-370 cm^{-1} (KBr)

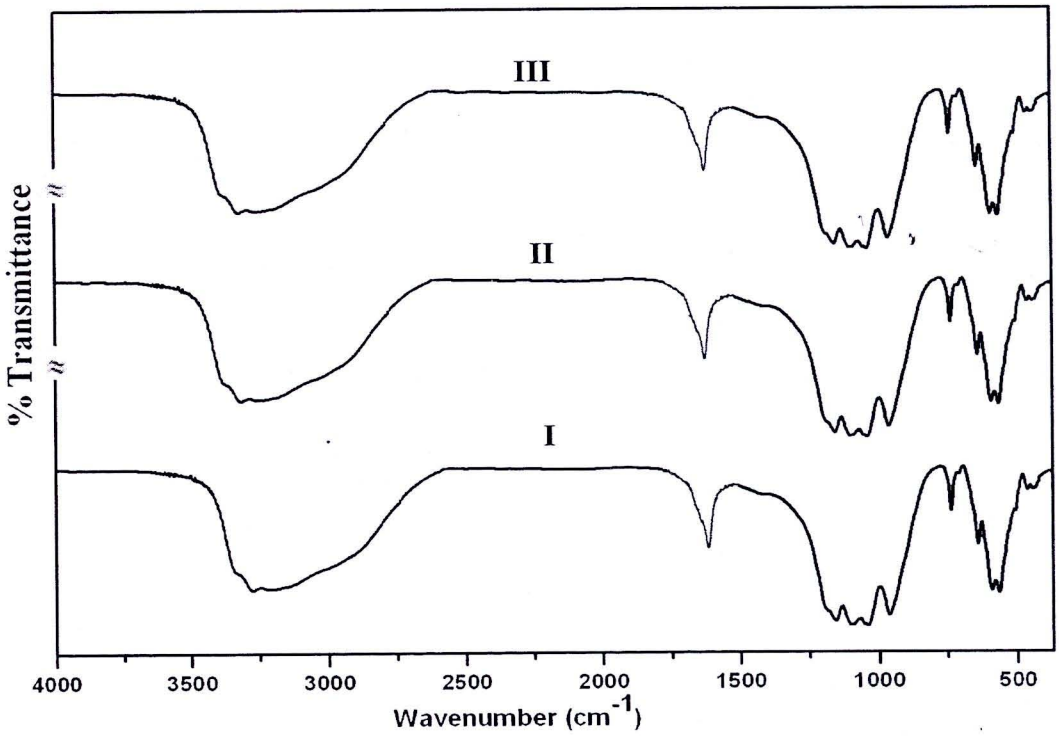

Figure 4.21 FTIR spectra of $Co(H_2PO_4)_2.H_2O$ (three replications) in the region of 4000-370 cm^{-1} (KBr)

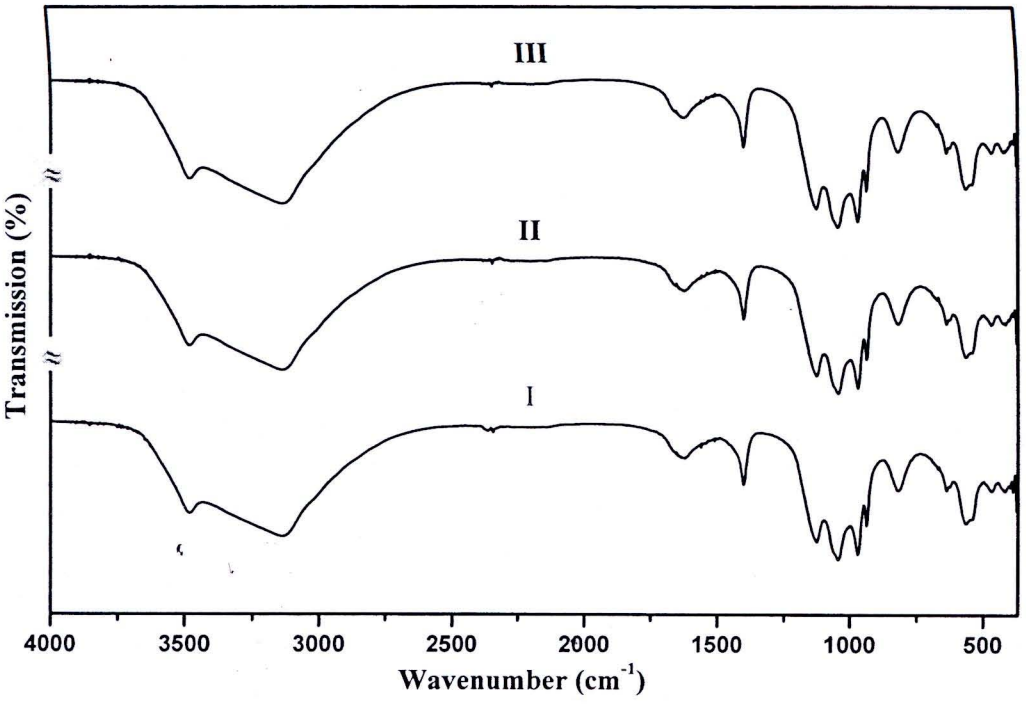

Figure 4.22 FTIR spectra of $LiFePO_4 \cdot 3H_2O$ (three replications) in the region of 4000-370 cm^{-1} (KBr)

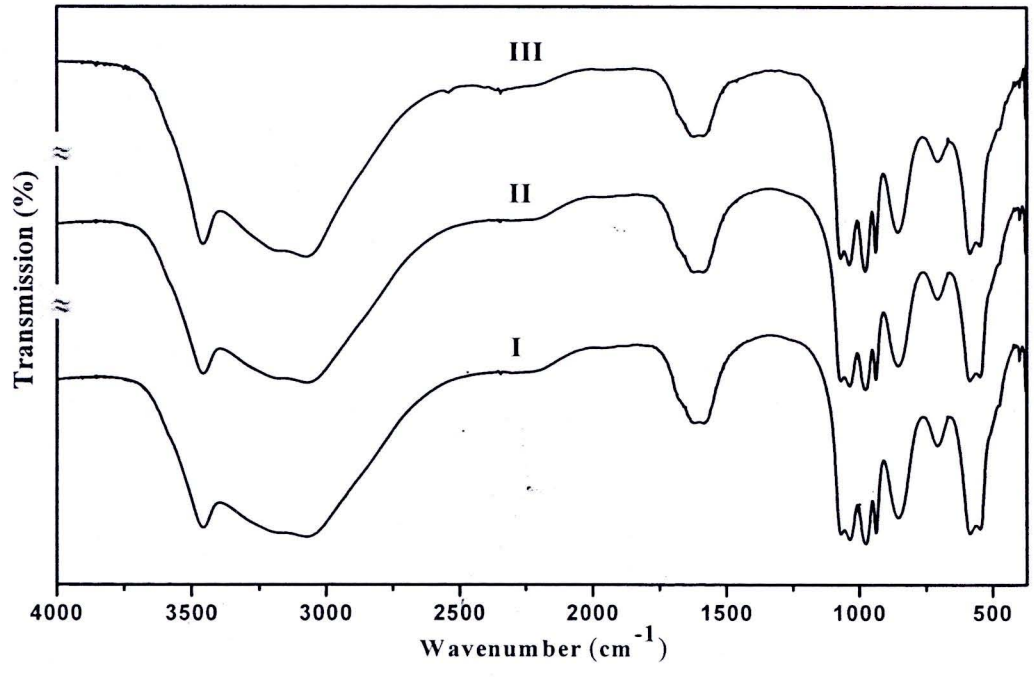

Figure 4.23 FTIR spectra of $LiCoPO_4 \cdot 3H_2O$ (three replications) in the region of 4000-370 cm^{-1} (KBr)

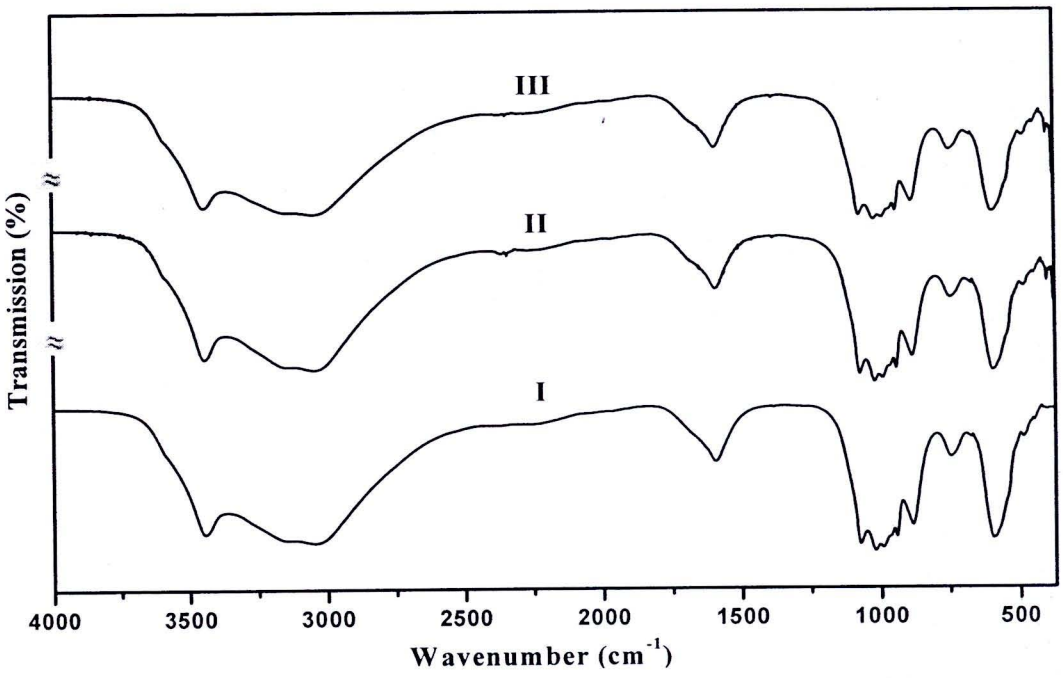

Figure 4.24 FTIR spectra of $LiNiPO_4 \cdot H_2O$ (three replications) in the region of 4000-370 cm^{-1} (KBr)

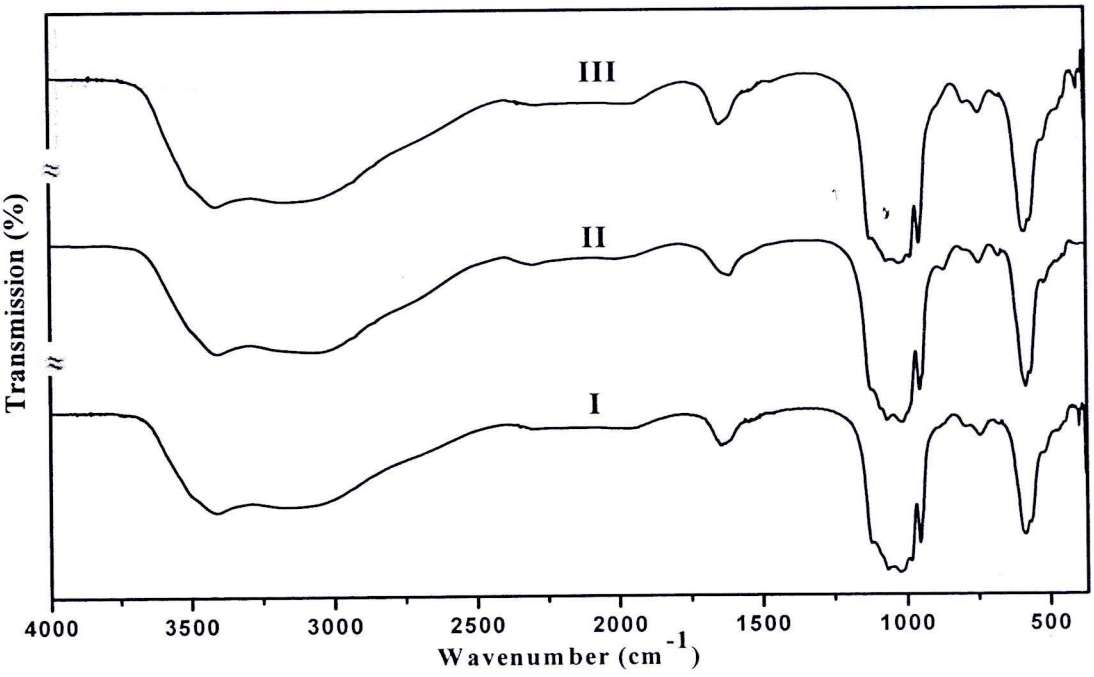

Figure 4.25 FTIR spectra of $LiMnPO_4 \cdot H_2O$ (three replications) in the region of 4000-370cm^{-1} (KBr)

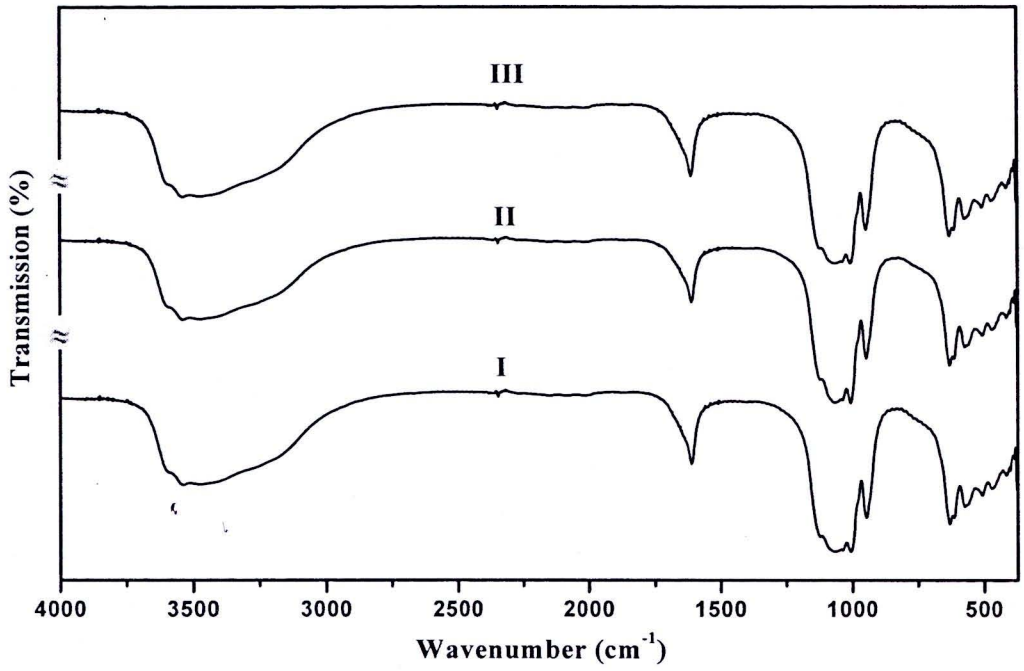

Figure 4.26 FTIR spectra of $Li_2Zn(HPO_4)_2 \cdot H_2O$ (three replications) in the region of 4000-370 cm^{-1} (KBr)

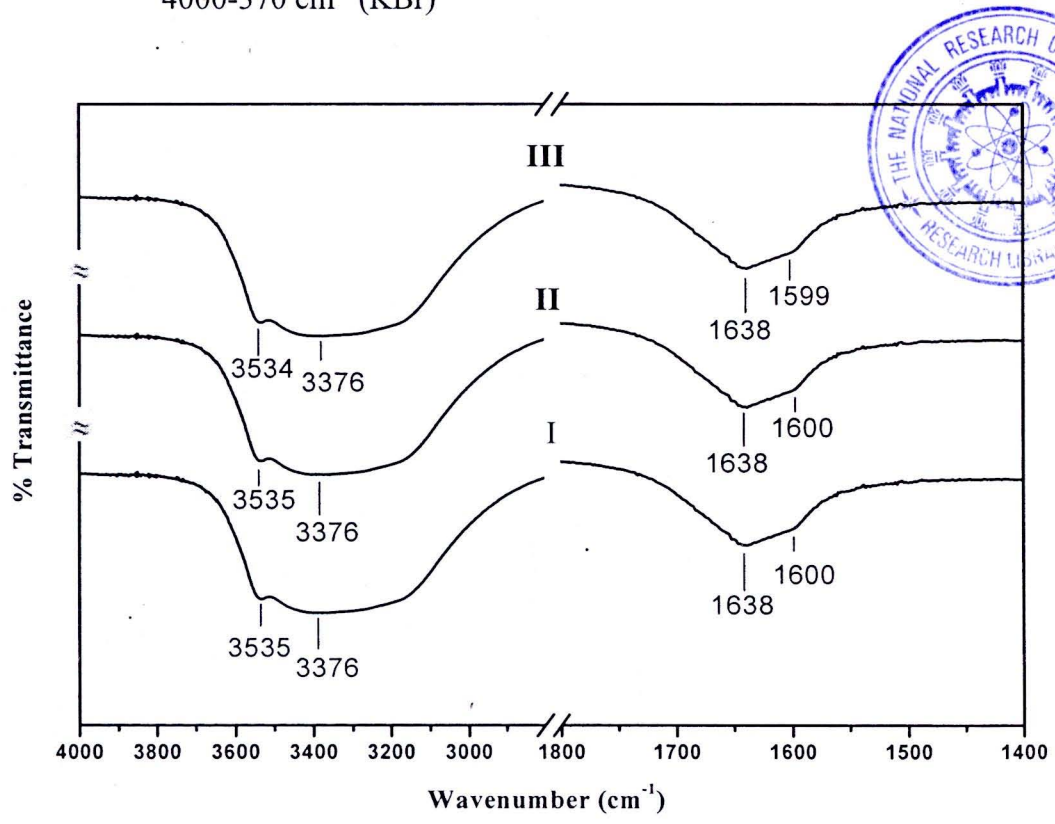

Figure 4.27 FTIR band positions in the OH stretching and bending region of $ZnHPO_4.H_2O$ (three replications, KBr)

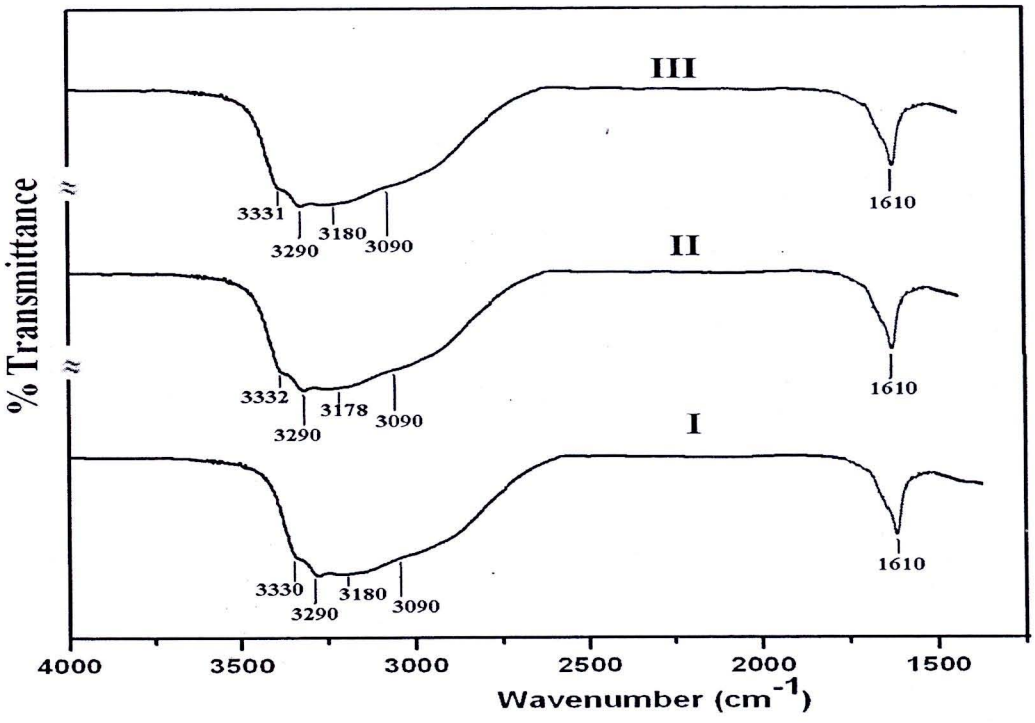

Figure 4.28 FTIR band positions in the OH stretching and bending region of $Co(H_2PO_4)_2.2H_2O$ (three replications, KBr)

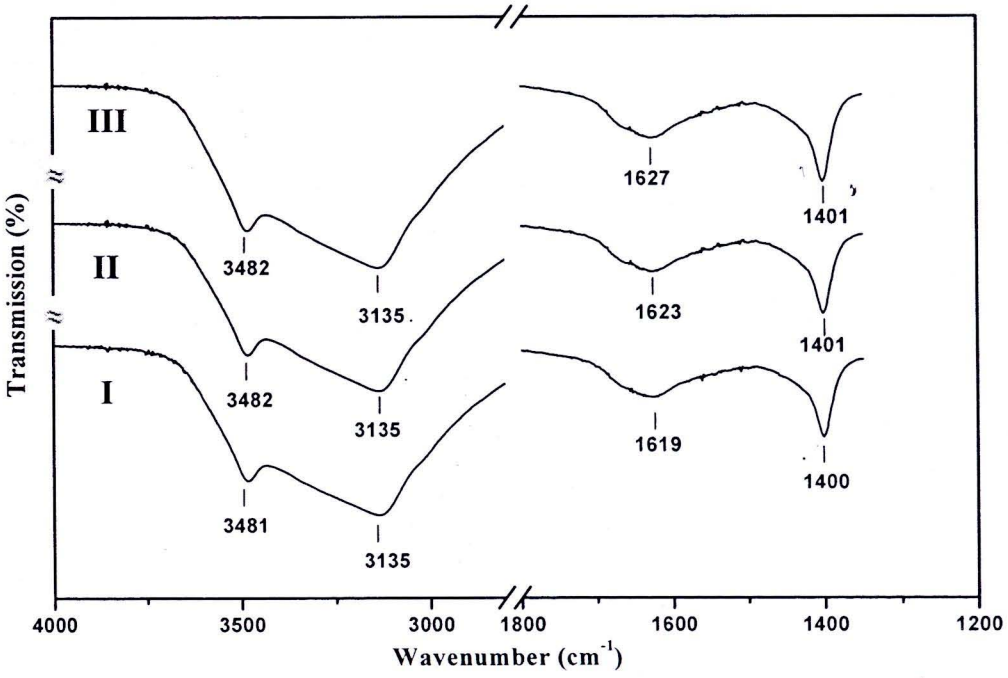

Figure 4.29 FTIR band positions in the OH stretching and bending region of $LiFePO_4.3H_2O$ (three replications, KBr)

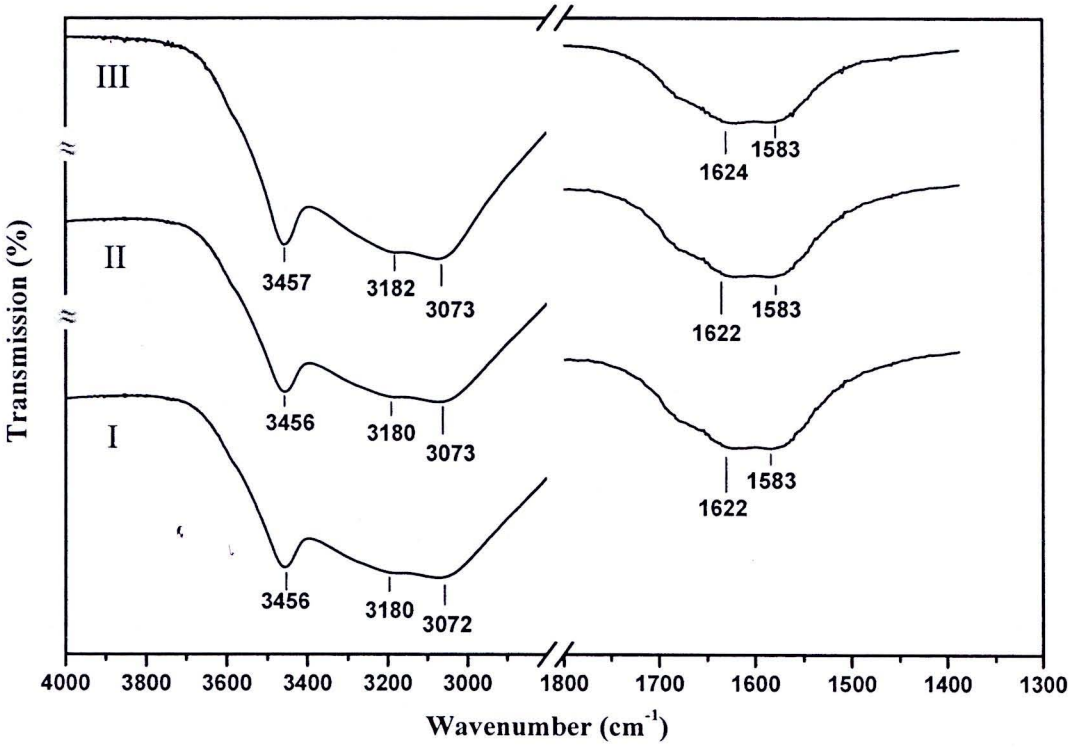

Figure 4.30 FTIR band positions in the OH stretching and bending region of $LiCoPO_4.3H_2O$ (three replications, KBr)

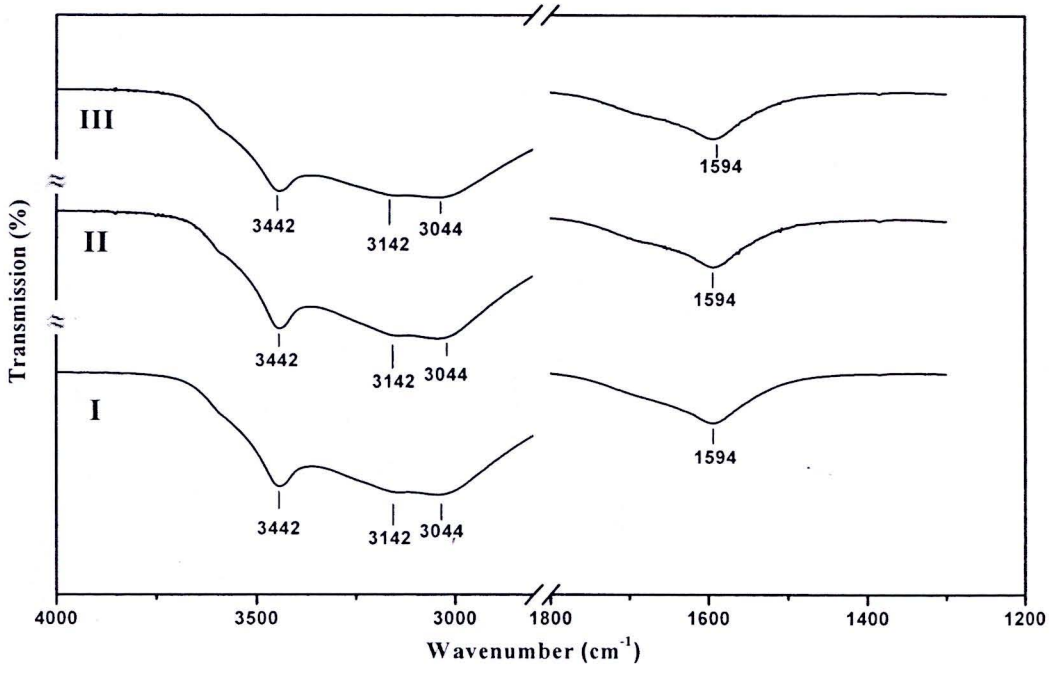

Figure 4.31 FTIR band positions in the OH stretching and bending region of $LiNiPO_4.H_2O$ (tree replications, KBr)

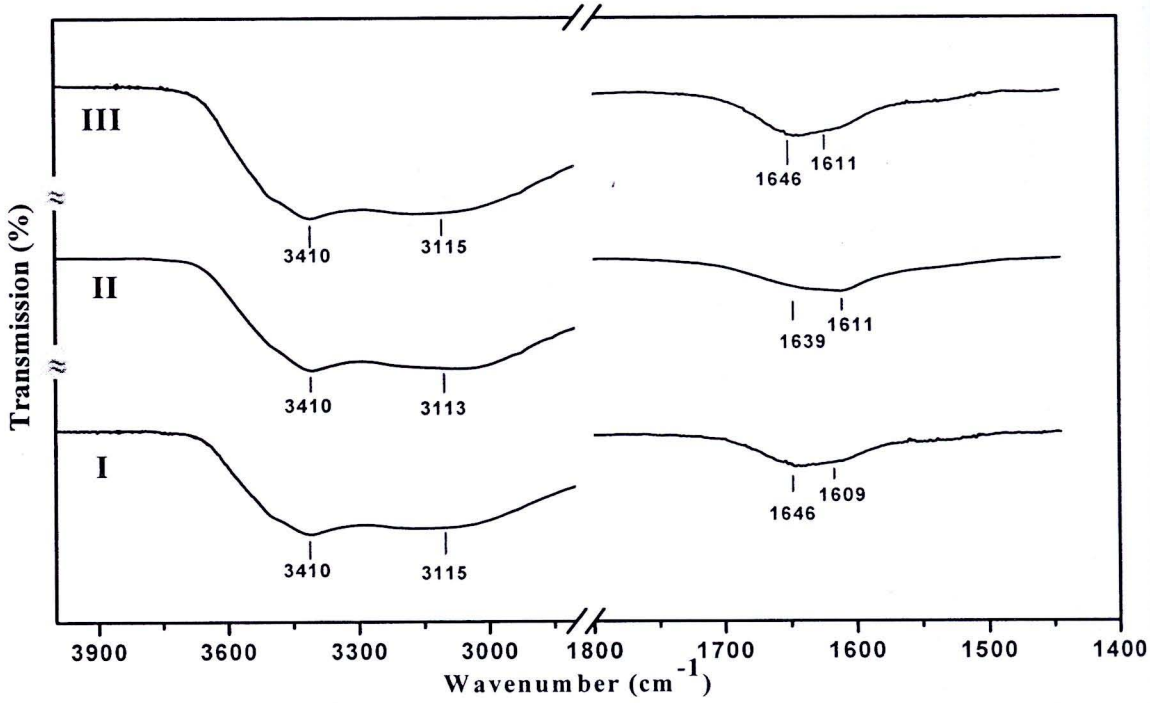

Figure 4.32 FTIR band positions in the OH stretching and bending region of $LiMnPO_4.H_2O$ (three replications, KBr)

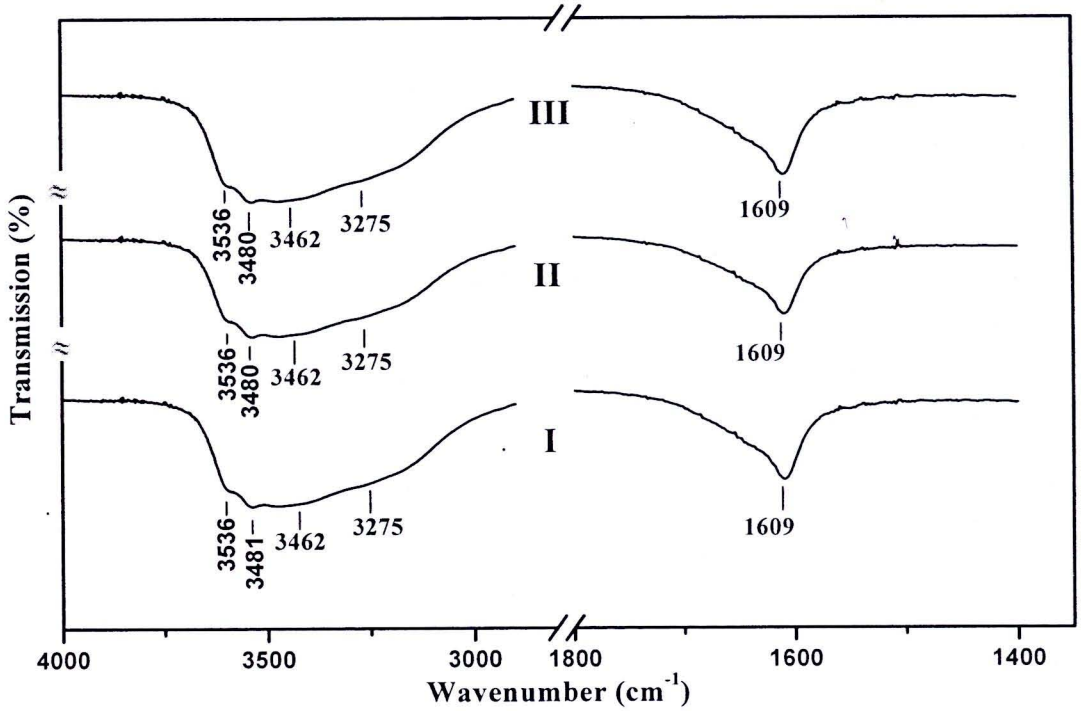

Figure 4.33 FTIR band positions in the OH stretching and bending region of $Li_2Zn(HPO_4)_2.H_2O$ (three replications, KBr)

4.6.1 Water Vibrational Bands

Vibrational modes of water of crystallization in $ZnHPO_4.H_2O$, $Co(H_2PO_4)_2.H_2O$, $LiFePO_4.3H_2O$, $LiCoPO_4.3H_2O$, $LiNiPO_4.H_2O$, $LiMnPO_4.H_2O$ and $Li_2Zn(HPO_4)_2.H_2O$ were observed in the region of 4000-2800 and 1800-1500 cm^{-1}, these are presented in Figures 4.27-4.33, respectively.

Vibrational (FTIR) bands in the range of 3536-3235 cm^{-1} region in all hydrates are assigned to the OH stretching modes, while the bands at the 1627-1401 cm^{-1} region are assigned to the bending mode of water. The lowering of the water bending frequency for the case of $LiFePO_4.3H_2O$ (Figure 4.29) may be effected by the water-cation interactions with a tendency to be more pronounced when the cation size is small and the charge is high as suggested by Falk [113].

4.6.2 Phosphate and Hydrogenphosphate Vibrational Bands

The Vibrational bands of phosphate anion in $ZnHPO_4.H_2O$, $Co(H_2PO_4)_2.2H_2O$, $LiFePO_4.3H_2O$, $LiCoPO_4.3H_2O$, $LiNiPO_4.H_2O$, $LiMnPO_4.H_2O$ and $Li_2Zn(HPO_4)_2.H_2O$ appears in 1154-400 cm^{-1} region and are shown in the Figures 4.34-4.40, respectively. In all compounds, the symmetric $\nu_1(A_1)$ vibrations of phosphate ion are found in the range of 991-930 cm^{-1}, while the asymmetric $\nu_3(F_2)$ vibrations are in the range of 1154-1007 cm^{-1}. The symmetric bending band $\nu_2(E)$ and the asymmetric bending $\nu_4(F_2)$ of PO_4^{3-} in all cases were observed in the range of 497-400 cm^{-1} and 637-500 cm^{-1}, respectively. The region of symmetric stretching $\nu_1(A_1)$ vibration of PO_4^{3-} in $Co(H_2PO_4)_2.2H_2O$, $LiFePO_4.3H_2O$, $LiCoPO_4.3H_2O$, $LiMnPO_4.H_2O$ and $Li_2Zn(HPO_4)_2.H_2O$ compounds appear as two bands at around 982-938 cm^{-1} (Figure. 4.35, 4.36, 4.37, 4.39 and 4.40), while, in $ZnHPO_4.H_2O$ and $LiNiPO_4.H_2O$ compounds exhibits as one band and three bands around 991-944 cm^{-1}, respectively. The splitting of the triply degenerate mode $\nu_3(F_2)$ and the doubly degenerate modes $\nu_2(E)$ are due to the lowering of the symmetry of PO_4^{3-} group and its site symmetry in the lattice. The number of bands and their Mulliken symbols are characterized according to the correlation field splitting for each case as described in Chapter 2 . In the region of the triply degenerate asymmetric bending $\nu_4(F_2)$ vibrations of $LiFePO_4.3H_2O$, $LiCoPO_4.3H_2O$ and $LiNiPO_4.H_2O$ exhibit two band

while for $LiMnPO_4.H_2O$ and $Li_2Zn(HPO_4)_2.H_2O$, exhibit three bands. The two bands around 637 and 624 cm^{-1} regions were observed in the case of the $LiFePO_4 \cdot 3H_2O$, one band around 706 cm^{-1} regions was observed in the case of the $LiCoPO_4 \cdot 3H_2O$, one band around 745 cm^{-1} regions was observed in the case of the $LiNiPO_4 \cdot H_2O$, two bands around 792 and 743 cm^{-1} regions were observed in the case of the $LiMnPO_4 \cdot H_2O$ and two bands around 563 and 507 cm^{-1} regions were observed in the case of the $Li_2Zn(HPO_4)_2 \cdot H_2O$. These bands were assigned to the librational mode of the water molecule. In this region, the different vibrational behavior of the phosphate ion was observed. It is suggested to be influenced by two factors, namely : (i) the repulsion potential of the lattices, and (ii) the weakening of the intramolecular P-O bonds owing to both the interionic M^{2+}-O and M^{+}-O interactions [106].

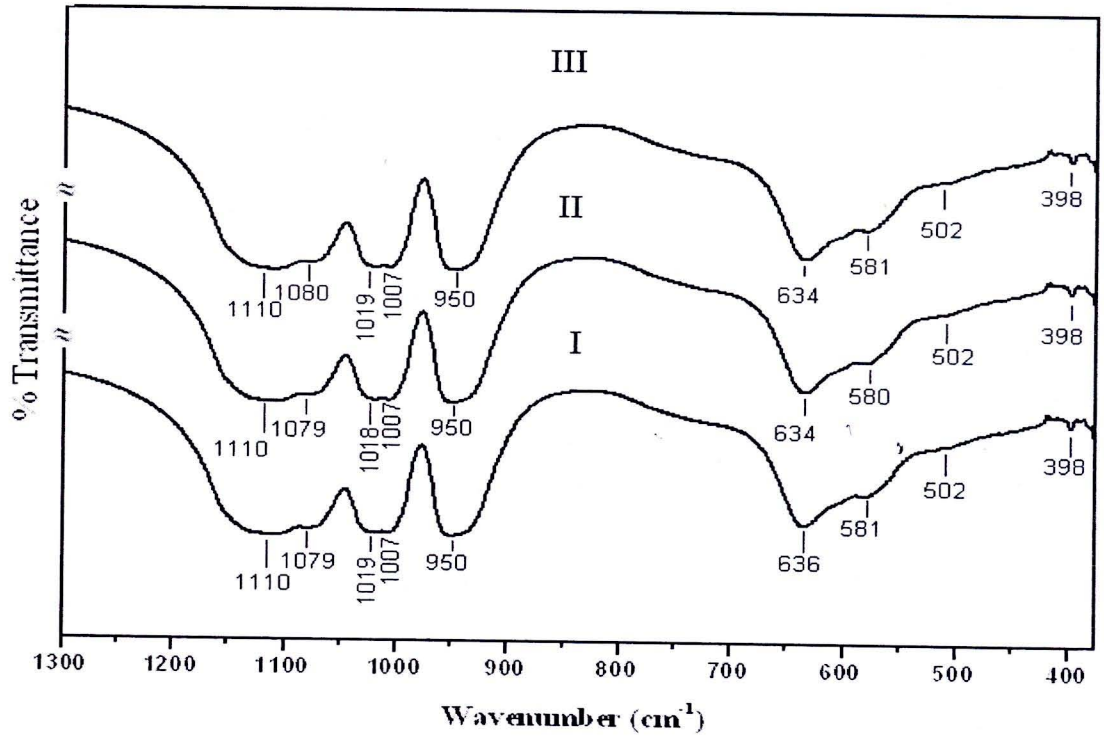

Figure 4.34 FTIR band positions in the region of PO_4^{3-} vibrations of $ZnHPO_4.H_2O$ (three replications, KBr)

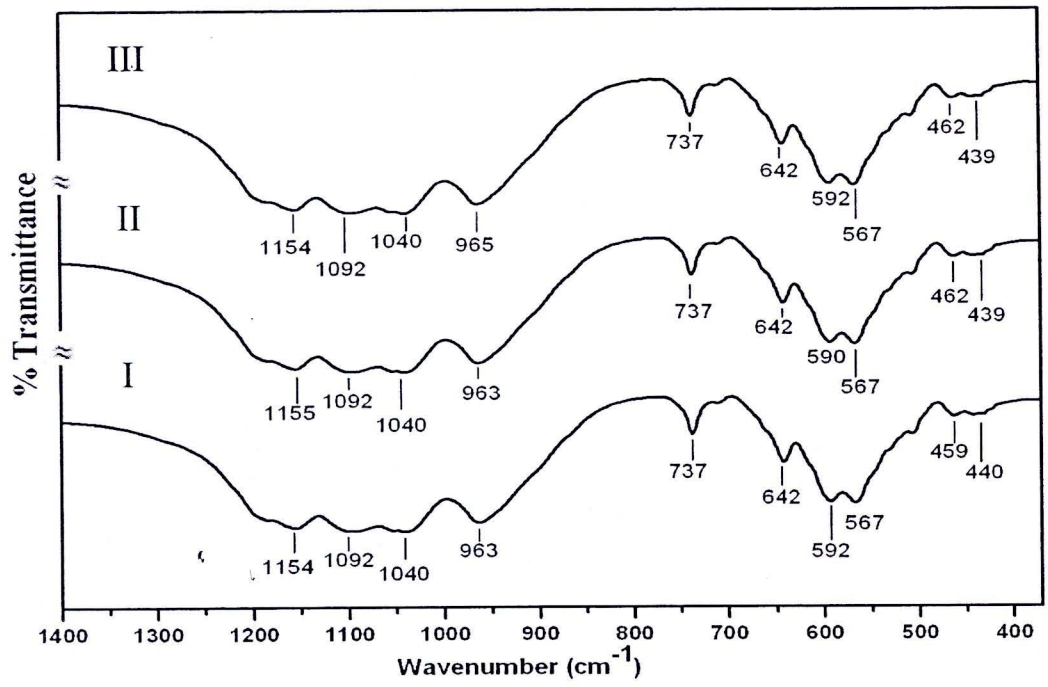

Figure 4.35 FTIR band positions in the region of PO_4^{3-} vibrations of $Co(H_2PO_4)_2.2H_2O$ (three replications, KBr)

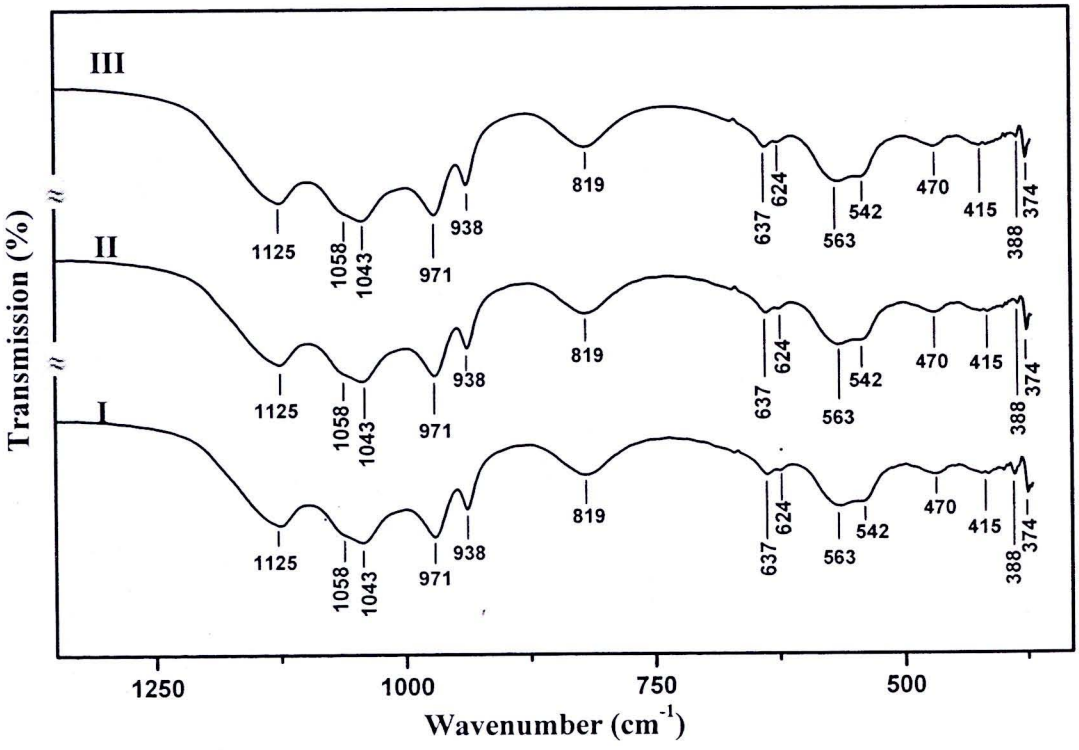

Figure 4.36 FTIR band positions in the region of PO_4^{3-} vibrations of $LiFePO_4.3H_2O$ (three replications, KBr)

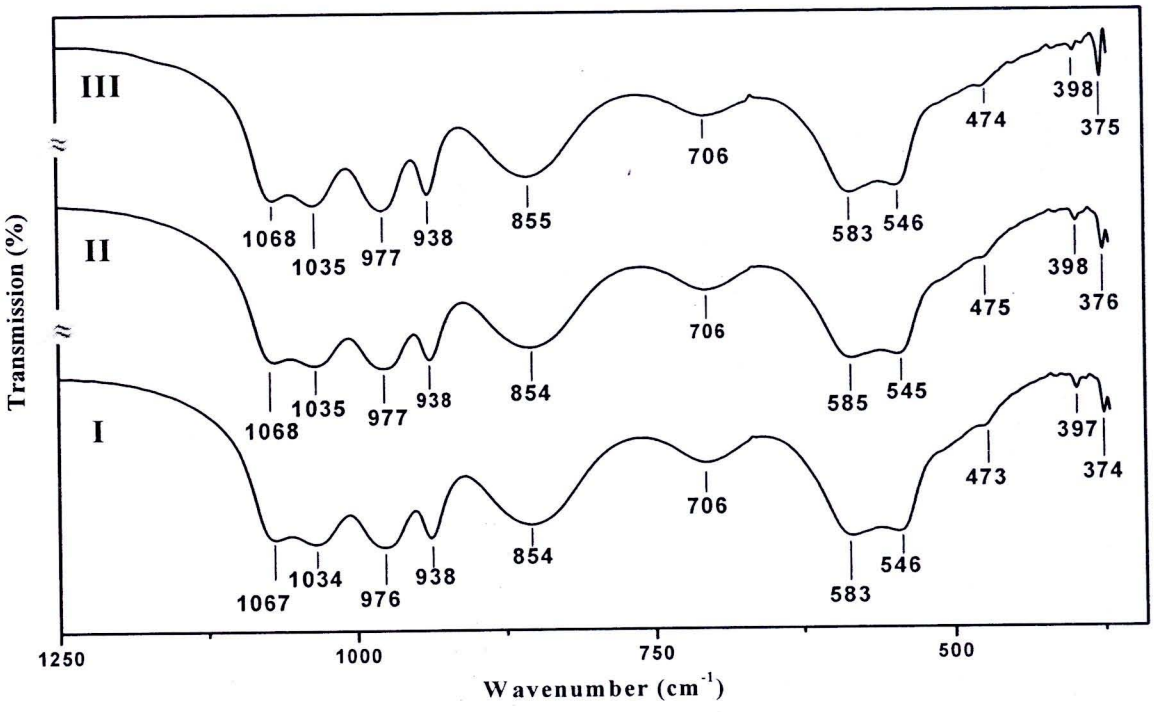

Figure 4.37 FTIR band positions in the region of PO_4^{3-} vibrations of $LiCoPO_4.3H_2O$ (three replications, KBr)

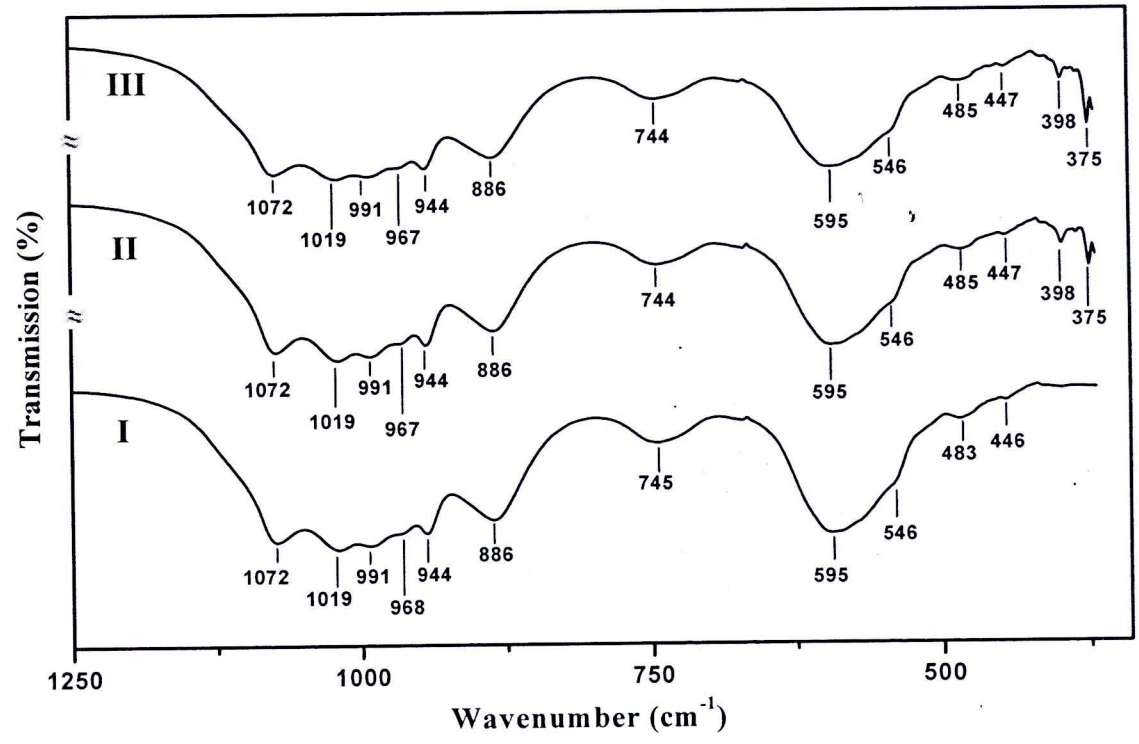

Figure 4.38 FTIR band positions in the region of PO_4^{3-} vibrations of $LiNiPO_4.H_2O$ (three replications, KBr)

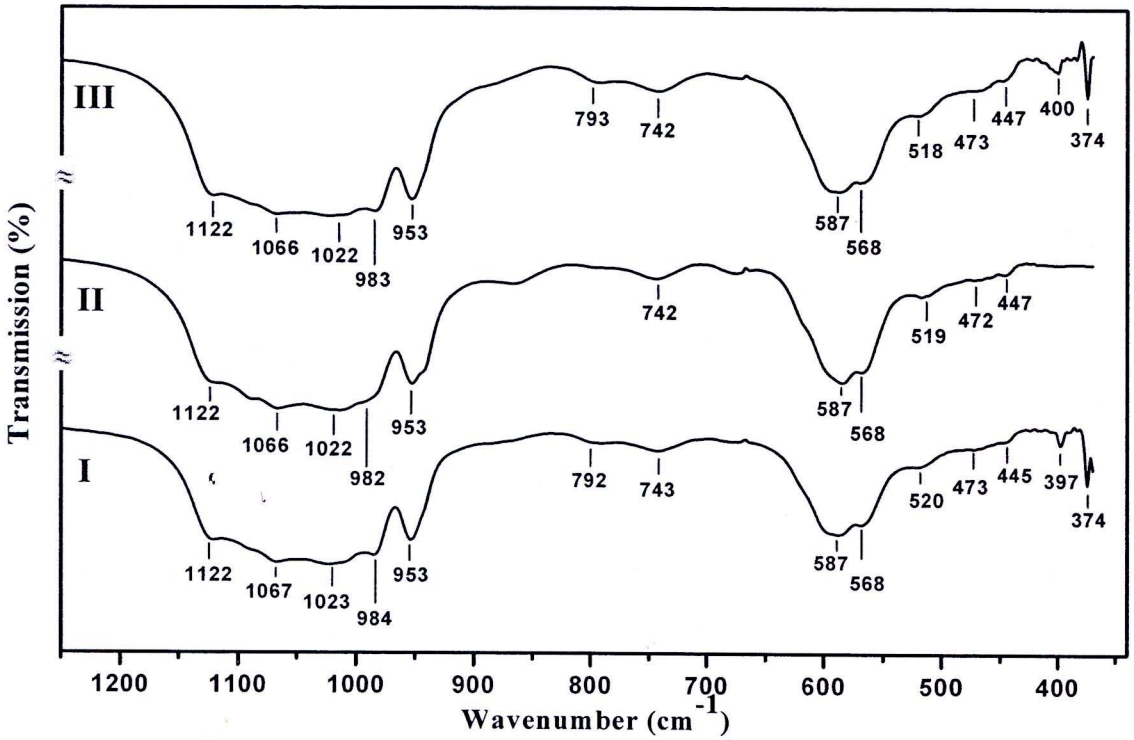

Figure 4.39 FTIR band positions in the region of PO_4^{3-} vibrations of $LiMnPO_4.H_2O$ (three replications, KBr)

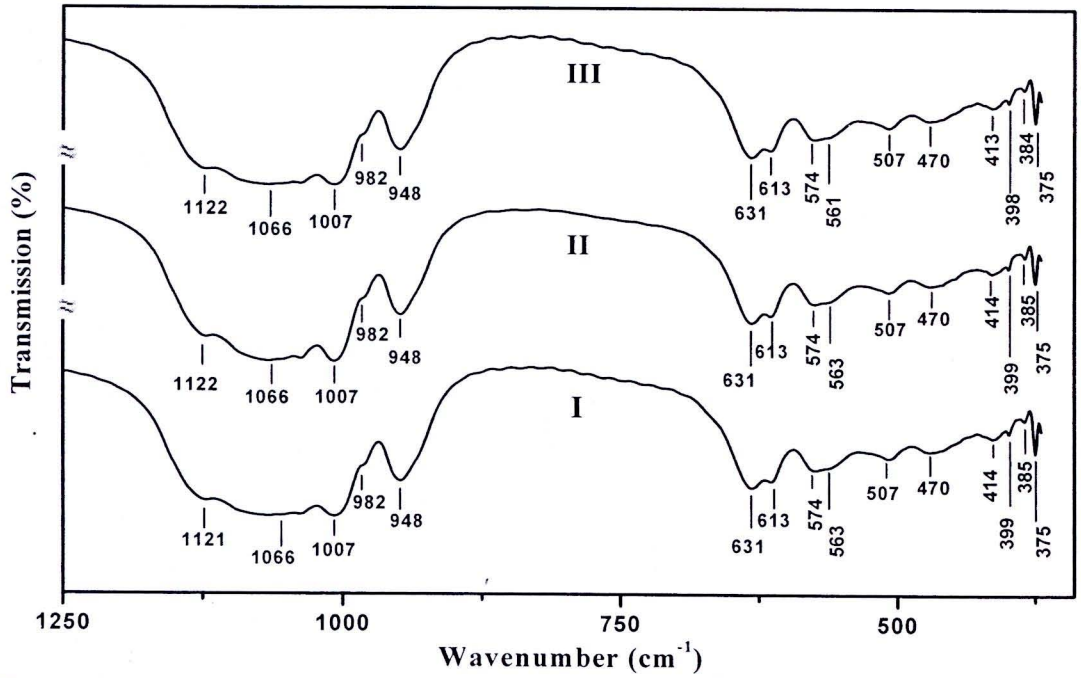

Figure 4.40 FTIR band positions in the region of PO_4^{3-} vibrations of $Li_2Zn(HPO_4)_2.H_2O$ (three replications, KBr)

Table 4.5 Vibrational band positions (cm^{-1}) and the possible assignment in three replications of $ZnHPO_4.H_2O$ using KBr pellet technique

Vibrational Band Positions (cm^{-1})			
Replication Numbers			Possible assignments
I	II	III	
3535 s	3535 s	3534 s	ν_{as}(H-OP)
3376 s	3376 s	3376 s	$\nu_3(B_2)$ H_2O
1638 s	1638 s	1638 s	$\nu_2(A_1)H_2O$
1110 s	1110m	1110 m	$\nu_3(F_2)PO_4^{3-}$
1079 vs	1079 vs	1079 vs	$\nu_3(F_2)PO_4^{3-}$
1019 vs	1019 vs	1019 vs	$\nu_3(F_2)PO_4^{3-}$
950 vs, sh	950 s, sh	950 vs, sh	$\nu_1(A_1)PO_4^{3-}$
636 w	634 m	634 m	$\nu_4(F_2)PO_4^{3-}$
581 m	580 m	581 m	$\nu_4(F_2)PO_4^{3-}$
502 w	502 w	502 w	$\nu_2(E)PO_4^{3-}$
398 w	398 w	398 w	ν (Zn-O)

Table 4.6 Vibrational band positions (cm^{-1}) and the possible assignment in three replications of $Co(H_2PO_4)_2.H_2O$ using KBr pellet technique

Vibrational Band Positions (cm^{-1})			
Replication Numbers			Possible assignments
I	II	III	
3330 s	3332 s	3331 s	ν_{as}(H-OP)
3290 s	3290 s	3290 s	ν_s(H-OP)
3180 s, sh	3178 s, sh	3180 s, sh	$\nu_3(B_2)$ H_2O
3090 s, sh	3090 s, sh	3090 s, sh	$\nu_1(A_1)H_2O$
1610 m	1610 m	1610 m	$\nu_2(A_1)H_2O$
1154 s, sh	1155 m, sh	1154 m, sh	$\nu_3(F_2)PO_4^{3-}$
1092 vs	1092 vs	1092 vs	$\nu_3(F_2)PO_4^{3-}$
1040 vs	1040 vs	1040 vs	$\nu_3(F_2)PO_4^{3-}$
963 s	963 s	965 s	$\nu_1(A_1)PO_4^{3-}$
631 s	632 s	631 s	$\nu_4(F_2)PO_4^{3-}$
737 s	737 s	737 s	$\rho(H_2O)$
642 m	642 m	642 m	$\nu_4(F_2)PO_4^{3-}$
592 m	590 m	592 m	$\nu_4(F_2)PO_4^{3-}$
567 m	567 m	567 m	$\nu_4(F_2)PO_4^{3-}$
459 m	462 m	462 m	$\nu_2(E)PO_4^{3-}$
440 m	439 m	439 m	$\nu_2(E)PO_4^{3-}$
375 w	375	375 w	ν (Zn-O)

Table 4.7 Vibrational band positions (cm^{-1}) and the possible assignment in three replications of $LiFePO_4 \cdot 3H_2O$ using KBr pellet technique

Vibrational Band Positions (cm^{-1})			
Replication Numbers			Possible assignments
I	II	III	
3481 s	3482 s	3482 s	$\nu_3(B_2)\ H_2O$
3135 s	3135 s	3135 s	$\nu_1(A_1)H_2O$
1619 s	1623 s	1627 s	$\nu_2(A_1)H_2O$
1400 s	1401 s	1401 s	$\nu_2(A_1)H_2O$
1125 s	1125 m	1125 m	$\nu_3(F_2)PO_4^{3-}$
1058 vs	1058 vs	1058 vs	$\nu_3(F_2)PO_4^{3-}$
1043 vs	1043 vs	1043 vs	$\nu_3(F_2)PO_4^{3-}$
971 vs, sh	972 s, sh	971 vs, sh	$\nu_1(A_1)PO_4^{3-}$
939 s, sh	938 s, sh	939 m, sh	$\nu_{as}(A_1)$P-OH
819 m, sh	819 w	819 w, sh	$\nu_s(A_1)$P-OH
637 w	637 m	637 m	$\rho(H_2O)$
624 m	624 m	624 m	$\rho\ (H_2O)$
563 m	563 m	563 m	$\nu_4(F_2)PO_4^{3-}$
542 w	542 w	542 w	$\nu_4(F_2)PO_4^{3-}$
470 m	470 m	470 m	$\nu_2(E)PO_4^{3-}$
415 w	415 w	415 w	$\nu_2(E)PO_4^{3-}$
388 w	388 w	388 w	ν (Li-O)
374 m	374 m	374 m	ν (Fe-O)

Table 4.8 Vibrational band positions (cm^{-1}) and the possible assignment in three replications of $LiCoPO_4 \cdot 3H_2O$ using KBr pellet technique

Vibrational Band Positions (cm^{-1})			
Replication Numbers			Possible assignments
I	II	III	
3456 s	3456 s	3457 s	$\nu_3(B_2)\ H_2O$
3180 s, sh	3180 s, sh	3180 s, sh	$\nu_1(A_1)H_2O$
3072 s	3073 s	3073 s	ν(MO-H)
1622 m	1622 m	1624 m	$\nu_2(A_1)H_2O$
1583 w	1583 w	1583 w	$\nu_2(A_1)H_2O$
1067 m	1068 m	1068 m	$\nu_3(F_2)PO_4^{3-}$
1034 m	1035 m	1035 m	$\nu_3(F_2)PO_4^{3-}$
976 s	977 s	977 s	$\nu_1(A_1)PO_4^{3-}$
938 s	938 s	938 s	$\nu_{as}(A_1)$P-OH
854 s	854 s	854 s	$\nu_s(A_1)$P-OH
706 m	706 w	706 w	$\rho_w\ (H_2O)$
583 s	585 m	583 s	$\nu_4(F_2)PO_4^{3-}$
546 m	545 m	546 m	$\nu_4(F_2)PO_4^{3-}$
473 w	475 w	474 w	$\nu_2(E)PO_4^{3-}$
397 m	398 m	398 m	ν (Li-O)
374 m	374 m	374 m	ν (Co-O)

Table 4.9 Vibrational band positions (cm^{-1}) and the possible assignment in three replications of $LiNiPO_4 \cdot H_2O$ using KBr pellet technique

Vibrational Band Positions (cm^{-1})			
Replication Numbers			Possible assignments
I	II	III	
3442 s	3442 s	3442 s	$\nu_3(B_2)$ H_2O
3142 s	3142 s	3142 s	$\nu_1(A_1)H_2O$
3044 s	3044 s	3044 s	ν(MO-H)
1594 m	1594 m	1594 m	$\nu_2(A_1)H_2O$
1072 vs	1072 vs	1072 vs	$\nu_3(F_2)PO_4^{3-}$
1019 vs	1019 vs	1019 vs	$\nu_3(F_2)PO_4^{3-}$
991 m	991 m	991 m	$\nu_1(A_1)PO_4^{3-}$
968 m, sh	967 m, sh	967 m, sh	$\nu_1(A_1)PO_4^{3-}$
944 s, sh	944 s, sh	944 m, sh	$\nu_{as}(A_1)$P-OH
886 s	886 s	886 s	$\nu_s(A_1)$P-OH
745 m	744 m	744 m	ρ_w (H_2O)
595 s	595 s	595 s	$\nu_4(F_2)PO_4^{3-}$
546 m, sh	546 m, sh	546 m, sh	$\nu_4(F_2)PO_4^{3-}$
483 m	485 m	485 w	$\nu_2(E)PO_4^{3-}$
446 m	447 m	447 m	$\nu_2(E)PO_4^{3-}$
-	398 m	398 m	ν (Li-O)
-	375 m	375 m	ν (Ni-O)

Table 4.10 Vibrational band positions (cm^{-1}) and the possible assignment in three replications of $LiMnPO_4 \cdot H_2O$ using KBr pellet technique

Vibrational Band Positions (cm^{-1})			
Replication Numbers			Possible assignments
I	II	III	
3410 s	3410 s	3410 s	$\nu_3(B_2)$ H_2O
3115 s	3113 s	3115 s	$\nu_1(A_1)H_2O$
1646 m	1639 m	1646 m	$\nu_2(A_1)H_2O$
1609 s	1611 m	1611 m	$\nu_2(A_1)H_2O$
1122 s	1122 s	1122 s	$\nu_3(F_2)PO_4^{3-}$
1067 vs	1066 vs	1066 vs	$\nu_3(F_2)PO_4^{3-}$
1023 s	1022vs	1022 s	$\nu_3(F_2)PO_4^{3-}$
984 vs	982 vs	983 vs	$\nu_1(A_1)PO_4^{3-}$
953 vs	953 vs	953 vs	$\nu_1(A_1)PO_4^{3-}$
792 m	-	793 m	$\rho(H_2O)$
743 m	742 w	742 w	$\rho(H_2O)$
587 s	587 s	587 s	$\nu_4(F_2)PO_4^{3-}$
568 s	568 s	568 s	$\nu_4(F_2)PO_4^{3}$
520 s, sh	519 s, sh	518 s, sh	$\nu_4(F_2)PO_4^{3-}$
473 w	472 w	473 w	$\nu_2(E)PO_4^{3-}$
445 m	447 m	447 m	$\nu_2(E)PO_4^{3-}$
397 w	-	400	ν(Li-O)
374 m	-	374 m	ν(Mn-O)

Table 4.11 Vibrational band positions (cm^{-1}) and the possible assignment in three replications of $Li_2Zn(HPO_4)_2 \cdot H_2O$ using KBr pellet technique

Vibrational Band Positions (cm^{-1})			
Replication Numbers			Possible assignments
I	II	III	
3536 s	3536 s	3536 s	ν_{as}(H-OP)
3481 s	3480 s	3480 s	ν_s(H-OP)
3462 s, sh	3462 s, sh	3462 s, sh	$\nu_3(B_2)$ H_2O
3275 s, sh	3275 s, sh	3275 s, sh	$\nu_1(A_1)H_2O$
1609 m	1609 m	1609 m	$\nu_2(A_1)H_2O$
1121 s, sh	1122 m, sh	1122 m, sh	$\nu_3(F_2)PO_4^{3-}$
1066 vs	1066 vs	1066 vs	$\nu_3(F_2)PO_4^{3-}$
1007 vs	1007 vs	1007 vs	$\nu_3(F_2)PO_4^{3-}$
982 w, sh	982 w, sh	982 w, sh	$\nu_1(A_1)PO_4^{3-}$
948 s	948 s	948 s	$\nu_1(A_1)PO_4^{3-}$
631 s	632 s	631 s	$\nu_4(F_2)PO_4^{3-}$
613 m	613 m	613 m	$\nu_4(F_2)PO_4^{3-}$
574 m	574 m	574 m	$\nu_4(F_2)PO_4^{3-}$
563 m	563 m	561 m	$\rho(H_2O)$
507 m	507 m	507 m	$\rho(H_2O)$
470 m	470 m	470 m	$\nu_2(E)PO_4^{3-}$
414 m	414 m	414 m	$\nu_2(E)PO_4^{3-}$
399 m	399 m	398 m	ν (Li-O)
385 w	385 w	385 w	ν (Li-O)
375 w	375	375 w	ν (Zn-O)

4.7 Vibrational Spectra of Deuterated Metal Phosphate Hydrates

Isotopic dilution technique has been applied to the hydrogen bonding study in solid hydrates [72]. FTIR and FT Raman spectra of deuterated samples containing small amount of HOD molecules surrounded by a large amount of D_2O (as in our study) or H_2O exhibit the uncoupled ν_{OH}(HOD) or ν_{OD}(HOD). That means, the intermolecular and intramolecular coupling between water molecules is eliminated. The observed frequency is called the "uncoupled" one. The FTIR band positions of isolated HOD molecule according to the effective symmetry C_s are the stretching vibrations ν_{OD}(A′) at 2727, $\nu_2(\delta)$ at 1402 and ν_{OH}(A″) at 3707 cm^{-1}.

The vibrational spectra of $LiFePO_4.3H_2O$-dx in three replications are shown in the Figure 4.41 and the assigned in the Figure 4.42 and Table 4.12. The uncoupled ν_{OH}(HOD) of $LiFePO_4.3H_2O$ compound was observed around 3382 cm^{-1} region, whereas complicated peaks in this region were observed in the compound. Thus the uncoupled ν_{OH}(HOD) of this compound would not be clearly observed (appear the coupling vibration), because this compound might not undergo partially deuteration in D_2O.

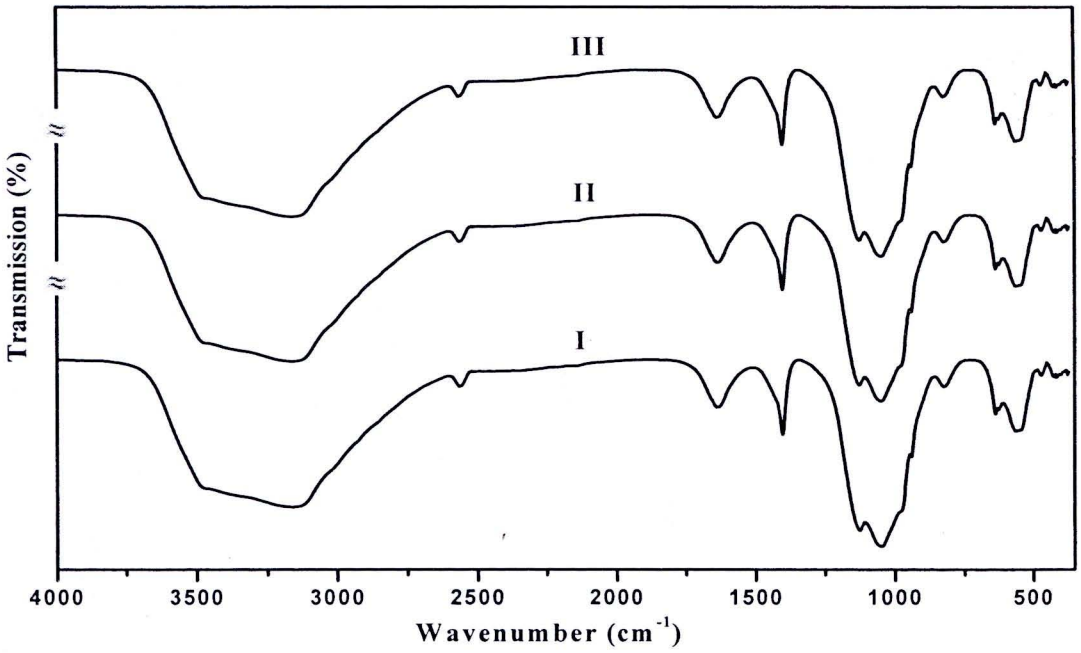

Figure 4.41 FTIR spectra of $LiFePO_4 \cdot 3H_2O$-dx (three replications) in the region of 4000-370 cm^{-1} (KBr)

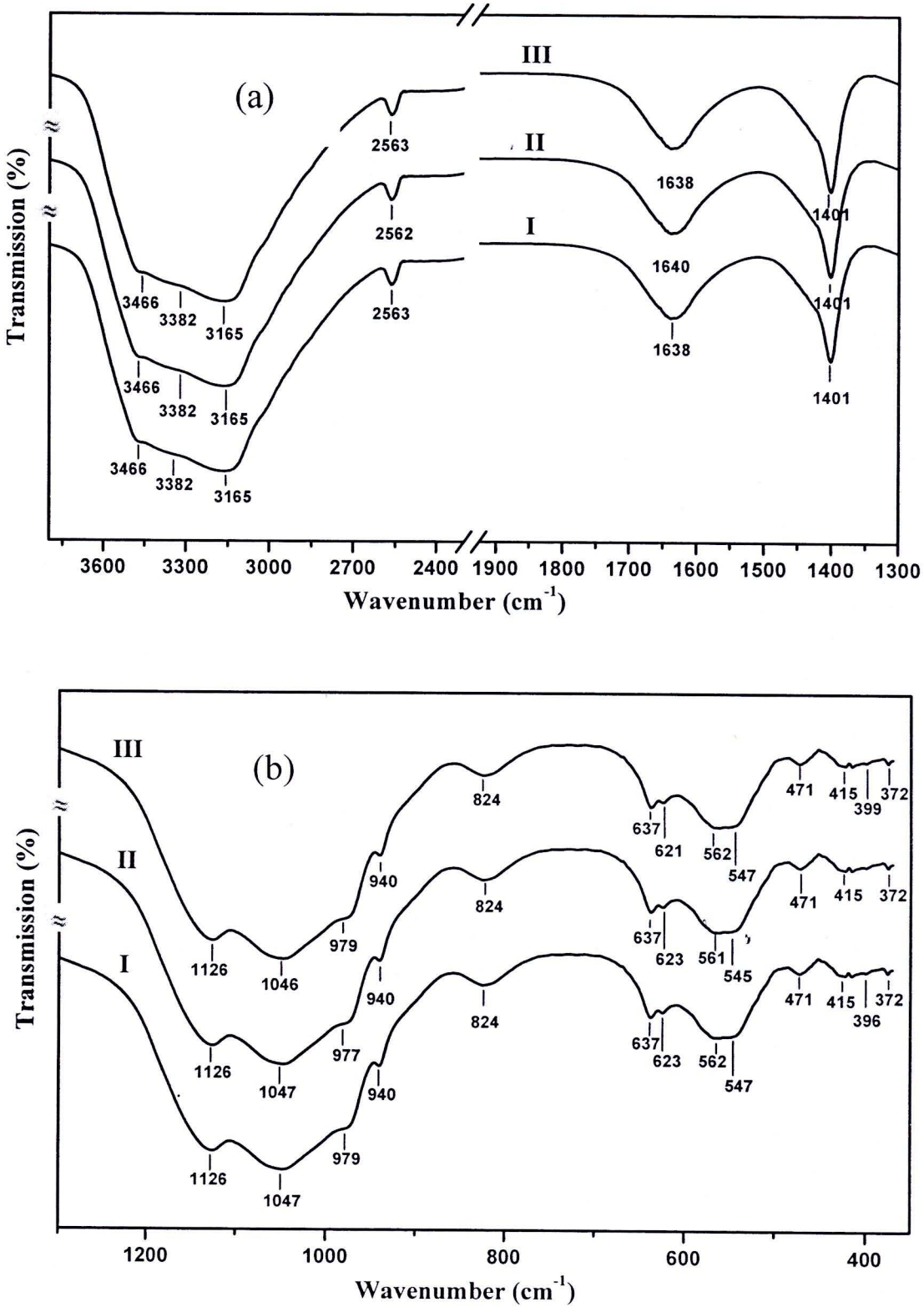

Figure 4.42 FTIR spectra of $LiFePO_4 \cdot 3H_2O$-dx (three replications) in the range of 4000-2400; 1900-1300 cm^{-1} (a) and 1300-370 cm^{-1} (b) regions (KBr)

The vibrational spectra of $LiCoPO_4.3H_2O$-dx in three replications are shown in Figure 4.43 and the assignment of all bands in the Figure 4.44 are presented in Table 4.13. The uncoupled ν_{OH}(HOD) of $LiCoPO_4.3H_2O$ compound was observed around 3372 cm^{-1}, whereas complicated peaks in this region were also observed. Thus the uncoupled ν_{OH}(HOD) of this compound was not be clearly observed. This may be affected by the efficiency of the partial deuteration.

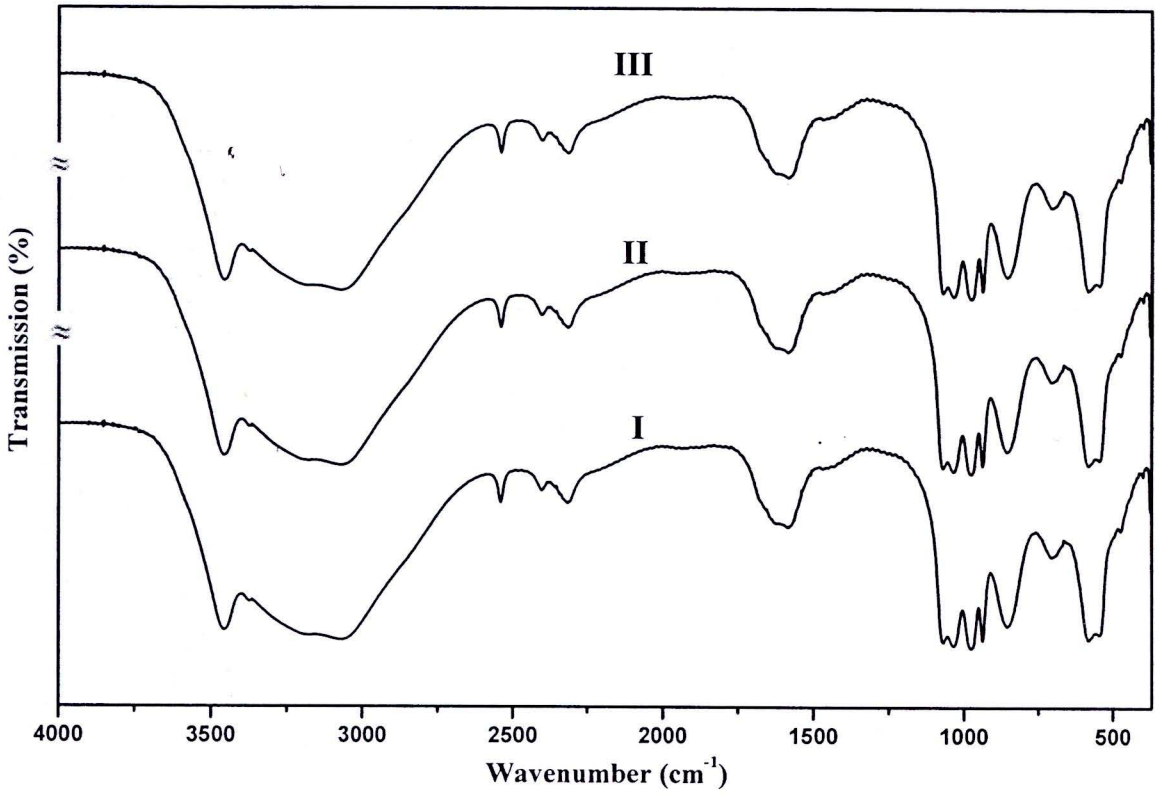

Figure 4.43 FTIR spectra of $LiCoPO_4 \cdot 3H_2O$-dx (three replications) in the region of 4000-370 cm^{-1} (KBr)

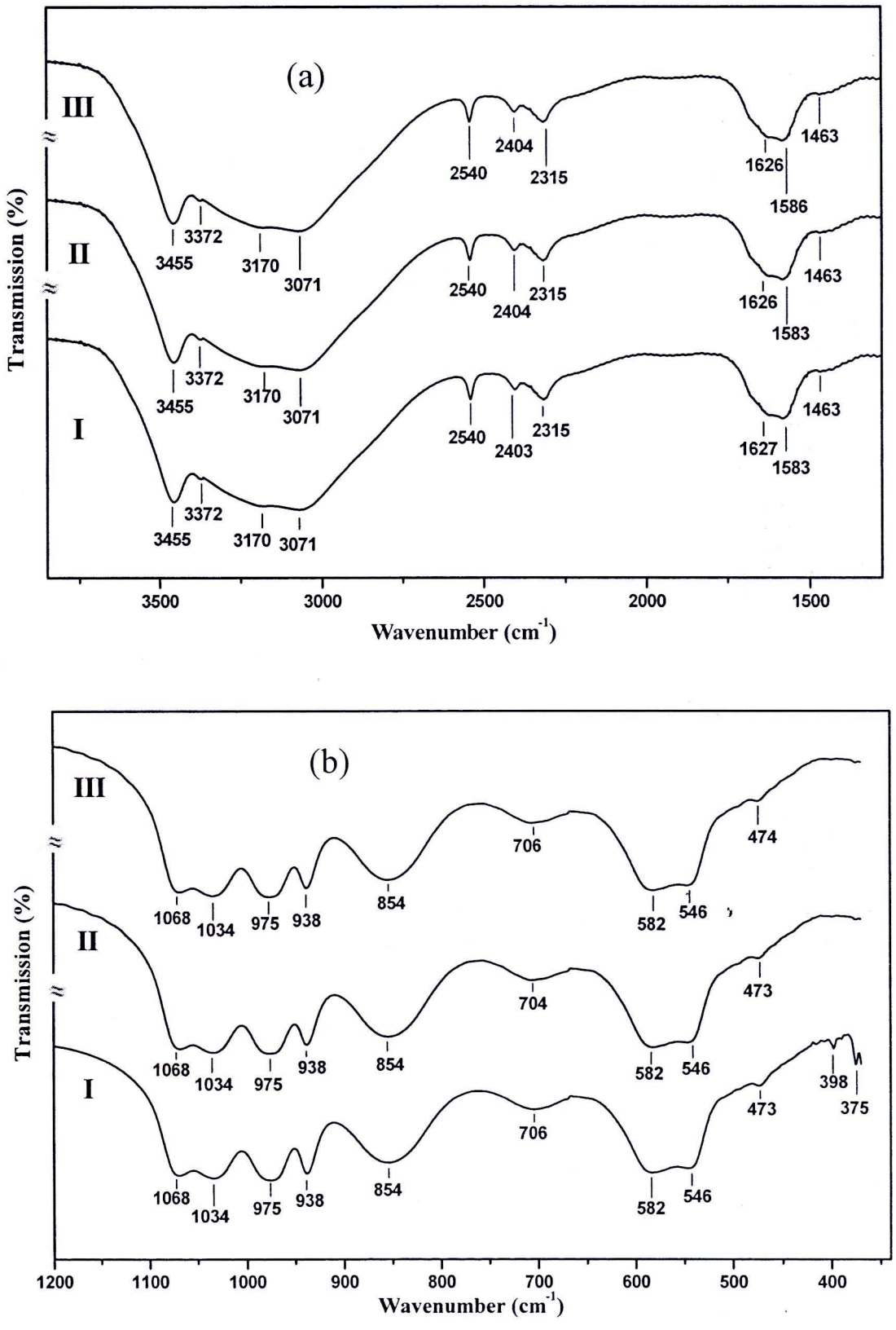

Figure 4.44 FTIR spectra of $LiCoPO_4 \cdot 3H_2O$-dx (three replications) in the range of 4000-1250 (a) and 1200-370 cm^{-1} (b) regions (KBr)

The vibrational spectra of $LiNiPO_4.H_2O$-dx in three replications are shown in the Figure 4.45 and the assignment of the bands in the Figure 4.46 are presented in Table 4.14. The uncoupled ν_{OH}(HOD) of $LiNiPO_4.H_2O$ compound was appeared at 3337 cm^{-1}, whereas complicated peaks in this region were also observed. Thus, the uncoupled ν_{OH}(HOD) of this compound was not be clearly resolved. The effect is suggested to be due to the insufficient dilution of the isotope.

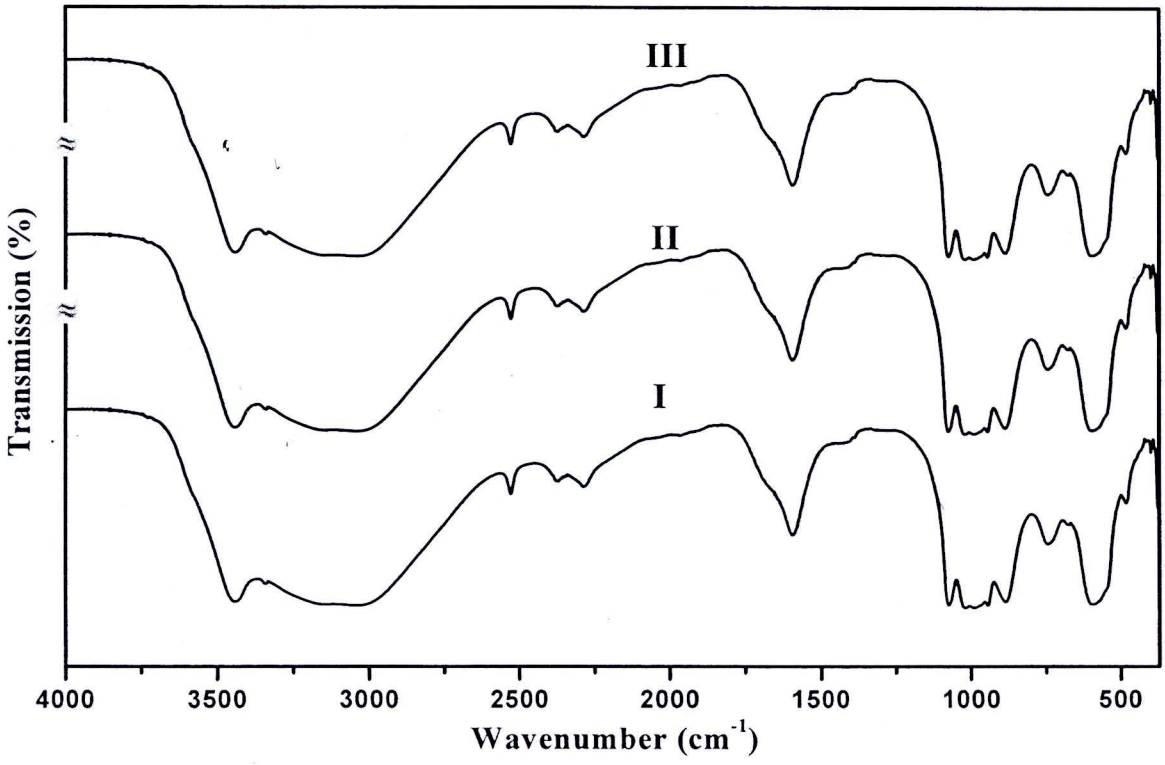

Figure 4.45 FTIR spectra of $LiNiPO_4 \cdot H_2O$-dx (three replications) in the region of 4000-370 cm^{-1} (KBr)

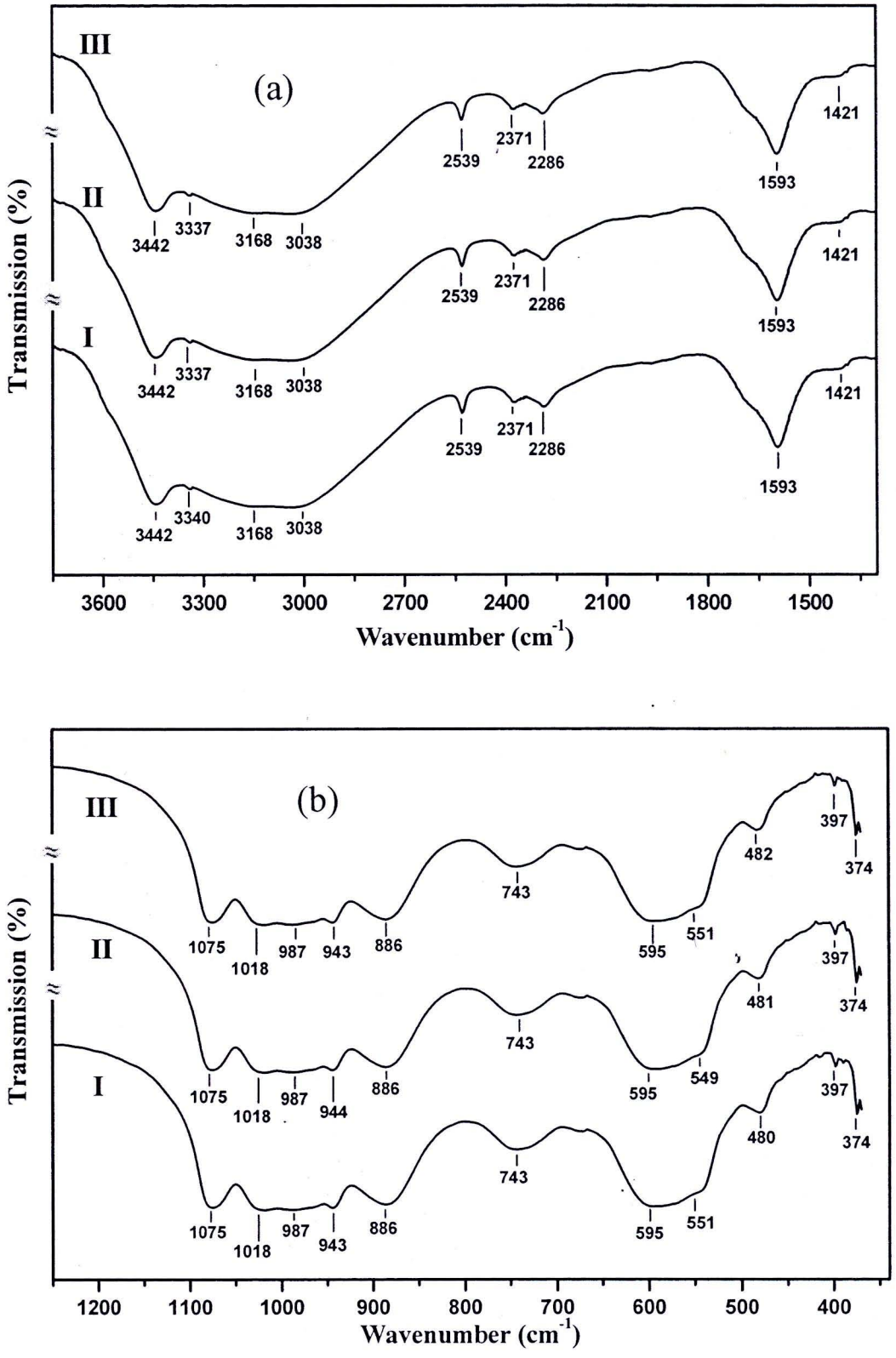

Figure 4.46 FTIR spectra of $LiNiPO_4 \cdot H_2O$-dx (three replications) in the range of 4000-1250 cm^{-1} (a) and 1250-370 cm^{-1} (b) regions (KBr)

The Vibrational spectra of $LiMnPO_4.H_2O$-dx in three replications are shown in the Figure 4.47 and the assigment of the bands in the Figure 4.48 are presented in Table 4.15. The uncoupled ν_{OH}(HOD) of $LiFePO_4.3H_2O$ compound was observed at 3317 cm^{-1}, whereas complicated peaks in this region were also observed. The insufficient isotope dilution is suggested to affect the unresolved uncoupled ν_{OH}(HOD).

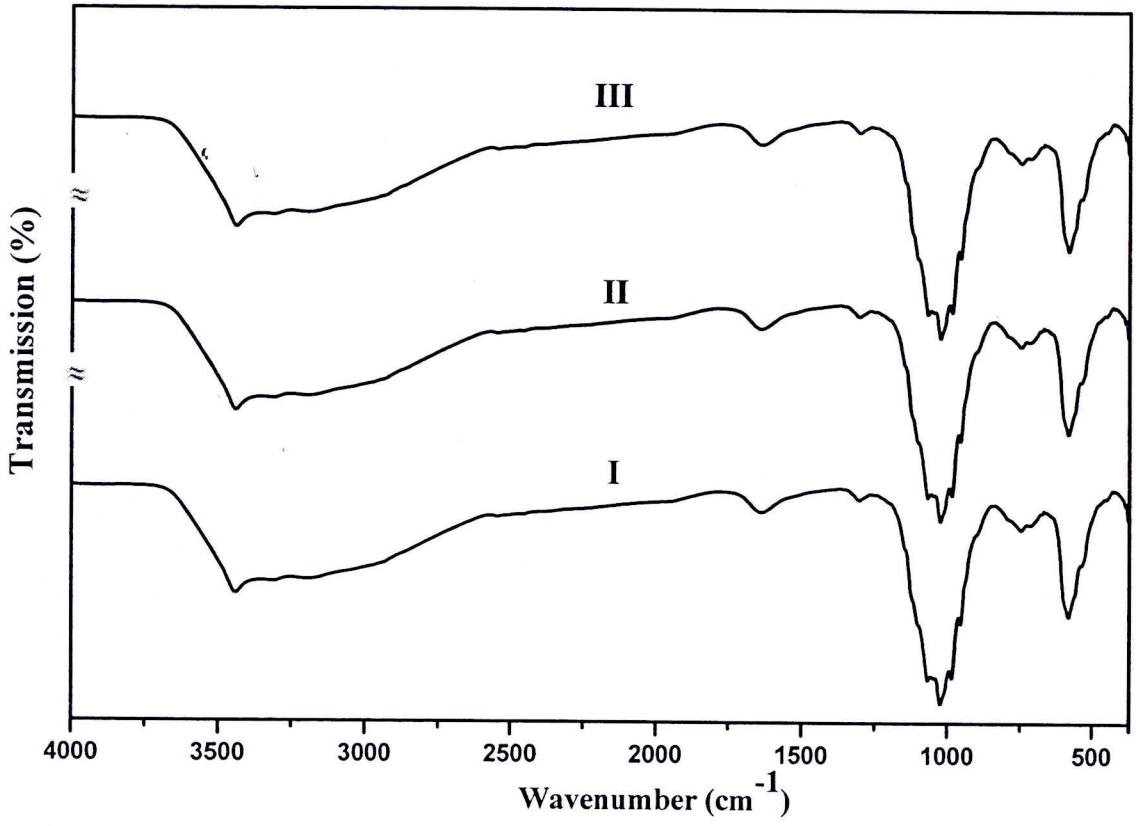

Figure 4.47 FTIR spectra of $LiMnPO_4 \cdot H_2O$-dx (three replications) in the region of 4000-370 cm^{-1} (KBr)

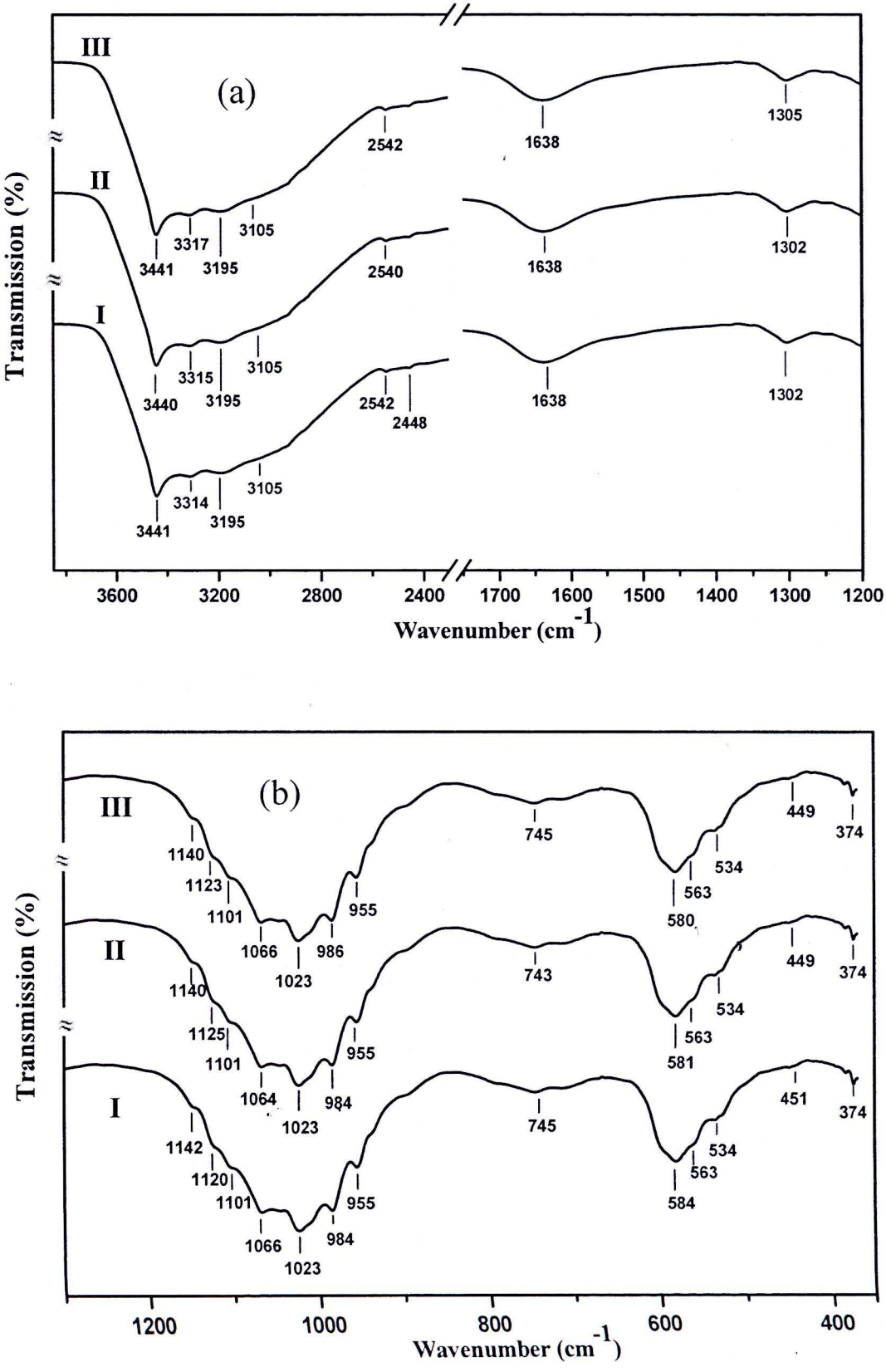

Figure 4.48 FTIR spectra of $LiMnPO_4 \cdot H_2O$-dx (three replications) in the range of 4000-2300;1750-1200 cm^{-1} (a) and 1400-370 cm^{-1} regions (b) (KBr)

The FTIR spectra of $Li_2Zn(HPO_4)_2.H_2O$-dx in three replications are shown in Figure 4.49 and Figure 4.50. Table 4.16 illustrates the corresponding assignments of vibrational band positions. The uncoupled ν_{OH}(HOD) of $LiFePO_4.3H_2O$ compound can not be observed in the expected region.

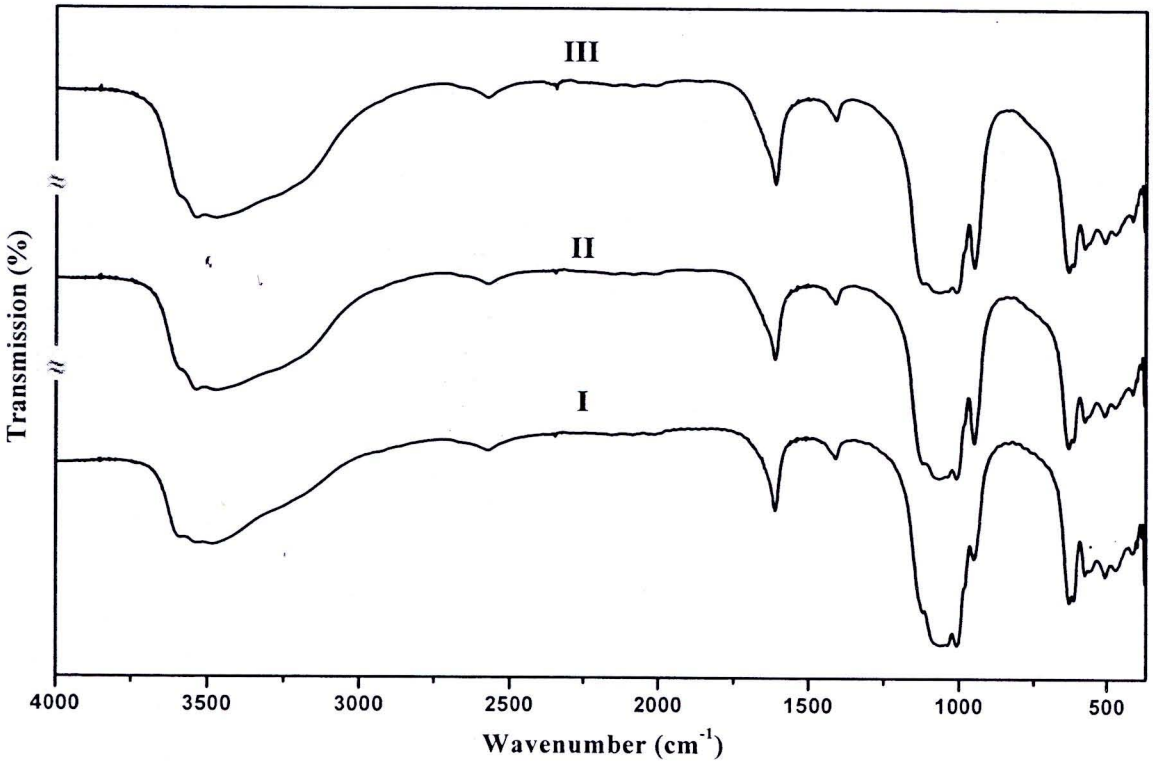

Figure 4.49 FTIR spectra of $Li_2Zn(HPO_4)_2 \cdot H_2O$-dx (three replications) in the region of 4000-370 cm^{-1} (KBr)

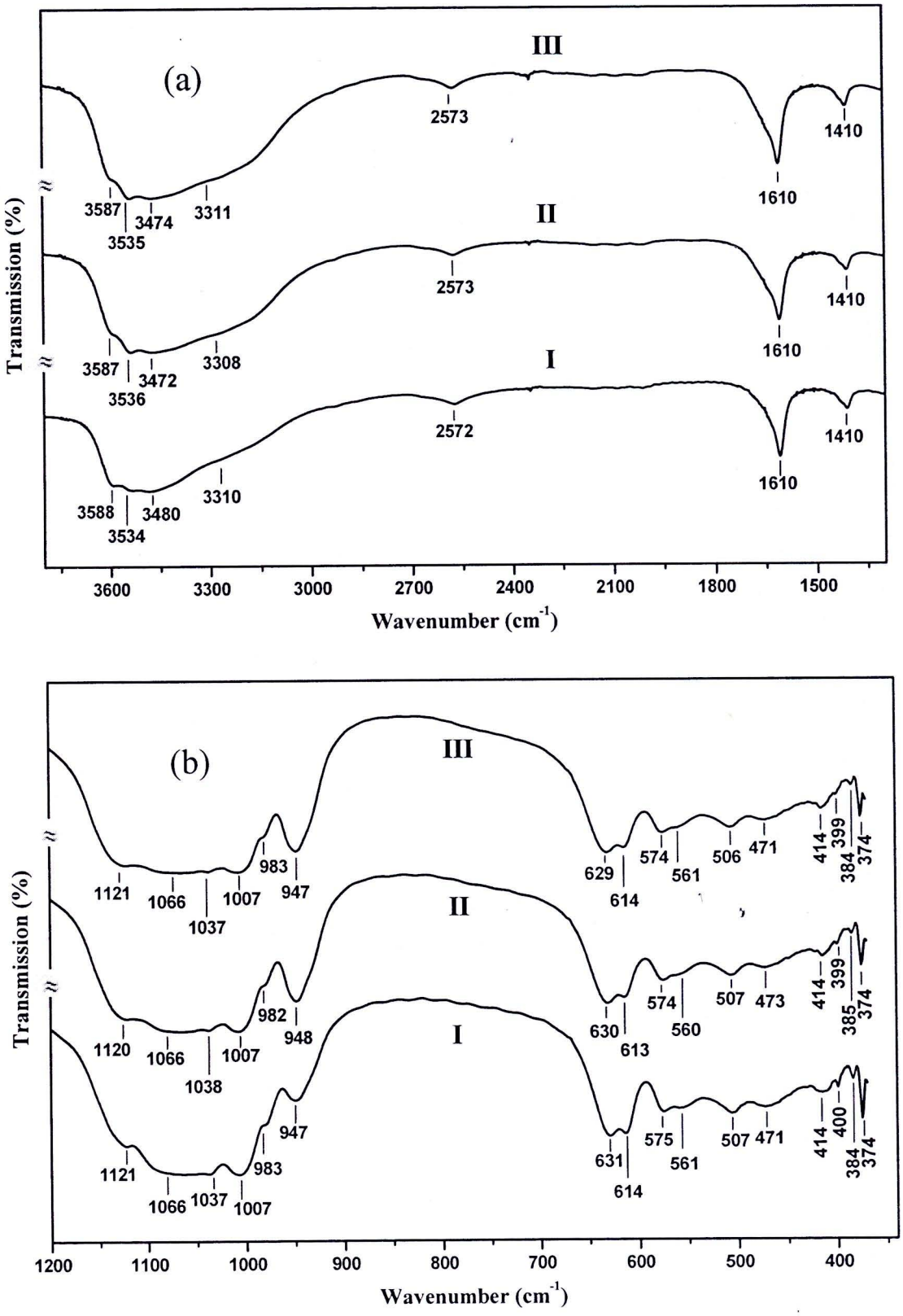

Figure 4.50 FTIR spectra of $Li_2Zn(HPO_4)_2 \cdot H_2O$-dx (three replications) in the range of 4000-1300 cm^{-1} (a) and 1200-370 cm^{-1} (b) regions (KBr)

Table 4.12 FTIR band positions (cm^{-1}) and the possible assignment in three replications of $LiFePO_4 \cdot 3H_2O$-dx using KBr pellet technique

Vibrational Band Positions (cm^{-1})			
Replication Numbers			Possible assignments
I	II	II	
3466 s	3466 s	3466 s	$\nu_3(B_2)\ H_2O$
3382s sh	3382 s, sh	3382 s, sh	$\nu_{OH}(HOD)$
3165 s	3165 s	3165 s	$\nu_1(A_1)H_2O$
2563 m	2562 m	2563 m	$\nu_3(B_2)D_2O$
1638 s	1640 s	1638 s	$\nu_2(A_1)H_2O$
1401 s	1401 s	1401 s	$\nu_2(A_1)H_2O$
1126 s	1126 m	1126 m	$\nu_3(F_2)PO_4^{3-}$
1047 vs	1047 vs	1046 vs	$\nu_3(F_2)PO_4^{3-}$
979 m	977 m	979 m	$\nu_1(A_1)PO_4^{3-}$
940 s, sh	940 s, sh	940 m, sh	$\nu_{as}(A_1)$P-OH
824 m	824 m	824 m	$\nu_s(A_1)$P-OH
637 w	637 m	637 m	$\rho(H_2O)$
623m	623 m	621 m	$\rho\ (H_2O)$
562 m	561 m	562 m	$\nu_4(F_2)PO_4^{3-}$
547 m	545 m	547 m	$\nu_4(F_2)PO_4^{3-}$
471 m	471 m	471 m	$\nu_2(E)PO_4^{3-}$
415 w	415 w	415 w	$\nu_2(E)PO_4^{3-}$
396 w	-	399 w	ν (Li-O)
372 m	372 m	372 m	ν (Fe-O)

Table 4.13 FTIR band positions (cm^{-1}) and the possible assignment in three replications of $LiCoPO_4 \cdot 3H_2O$-dx using KBr pellet technique

Vibrational Band Positions (cm^{-1})			
Replication Numbers			Possible assignments
I	II	III	
3455 s	3455 s	3455 s	$\nu_3(B_2)$ H_2O
3372 m	3372 m	3372 m	ν_{OH}(HOD)
3170 s, sh	3170 s, sh	3170 s, sh	$\nu_1(A_1)H_2O$
3071 s	3070 s	3070 s	ν(MO-H)
2540 m	2540 m	2540 m	$\nu_3(B_2)D_2O$
2403 m	2404 m	2404 m	$\nu_1(A_1)D_2O$ or ν_{OD}(HOD)
2315 m	2315 m	2315 m	$\nu_1(A_1)D_2O$ or ν_{OD}(HOD)
1627 m	1626 m	1626 m	$\nu_2(A_1)H_2O$
1583 w	1583 w	1583 w	$\nu_2(A_1)H_2O$
1463 m	1463 m	1463 m	$\nu_2(A_1)$HOD
1068 m	1068 m	1068 m	$\nu_3(F_2)PO_4^{3-}$
1034 m	1034 m	1034 m	$\nu_3(F_2)PO_4^{3-}$
975 s	975 s	975 s	$\nu_1(A_1)PO_4^{3-}$
938 s	938 s	938 s	$\nu_{as}(A_1)$P-OH
854 s	854 s	854 s	$\nu_s(A_1)$P-OH
706 m	704 w	706 w	ρ_w (H_2O)
582 s	582 m	582 s	$\nu_4(F_2)PO_4^{3-}$
546 m	546 m	546 m	$\nu_4(F_2)PO_4^{3-}$
473 w	475 w	474 w	$\nu_4(F_2)PO_4^{3-}$
398 m	-	-	ν (Li-O)
375 m	-	-	ν (Co-O)

Table 4.14 FTIR band positions (cm^{-1}) and the possible assignment in three replications of $LiNiPO_4 \cdot H_2O$-dx using KBr pellet technique

Vibrational Band Positions (cm^{-1})			
Replication Numbers			Possible assignments
I	II	III	
3442 s	3442 s	3442 s	$\nu_3(B_2)$ H_2O
3337 m	3337 m	3337 m	ν_{OH}(HOD)
3168 s	3168 s	3160 s	$\nu_1(A_1)H_2O$
3038 s, sh	3038 s, sh	3038 s, sh	ν(MO-H)
2539 m	2539 m	2539 m	$\nu_3(B_2)D_2O$
2371 m	2371 m	2371 m	$\nu_1(A_1)D_2O$ or ν_{OD}(HOD)
2286 m	2286 m	2286 m	$\nu_1(A_1)D_2O$ or ν_{OD}(HOD)
1593 m	1593 m	1593 m	$\nu_2(A_1)H_2O$
1421 m	1421 m	1421 m	$\nu_2(A_1)$HOD
1075 vs	1075 vs	1075 vs	ν_3 $(F_2)PO_4^{3-}$
1018 vs	1018 vs	1018 vs	$\nu_3(F_2)PO_4^{3-}$
987 m	987 m	987 m	$\nu_1(A_1)PO_4^{3-}$
968 m, sh	967 m, sh	967 m, sh	$\nu_1(A_1)PO_4^{3-}$
943 s, sh	944 s, sh	943 m, sh	$\nu_{as}(A_1)$P-OH
886 s	886 s	886 s	$\nu_s(A_1)$P-OH
743 m	743 m	743 m	ρ_w (H_2O)
595 s	595 s	595 s	$\nu_4(F_2)PO_4^{3-}$
551 m, sh	549 m, sh	551 m, sh	$\nu_4(F_2)PO_4^{3-}$
480 m	481 m	482 w	$\nu_4(F_2)PO_4^{3-}$
397	397 m	397 m	ν (Li-O)
374	374 m	374 m	ν (Ni-O)

Table 4.15 FTIR band positions (cm^{-1}) and the possible assignment in three replications of $LiMnPO_4 \cdot H_2O$-dx using KBr pellet technique

Vibrational Band Positions (cm^{-1})			
Replication Numbers			Possible assignments
I	II	III	
3441 s	3440 s	3441 s	$\nu_3(B_2)$ H_2O
3314 s	3315 s	3317 s	ν_{OH}(HOD)
3195 s	3195 s	3195 s	$\nu_1(A_1)H_2O$
3105 s	3105 s	3105 s	ν(MO-H)
2542 m	2540 m	2542 m	$\nu_3(B_2)D_2O$
2448 w	-	-	$\nu_1(A_1)D_2O$ or ν_{OD}(HOD)
1638 m	1638 m	1638 m	$\nu_2(A_1)H_2O$
1302 s	1302 m	1302 m	$\nu_2(A_1)$HOD
1142 s, sh	1140 s, sh	1140 s, sh	$2\nu_4(F_2)PO_4^{3-}$
1120 s	1125 s	1123 s	$\nu_3(F_2)PO_4^{3-}$
1101 s	1101 s	1101 s	$\nu_3(F_2)PO_4^{3-}$
1066 vs	1064 vs	1066 vs	$\nu_3(F_2)PO_4^{3-}$
1023 s	1023vs	1023 s	$\nu_3(F_2)PO_4^{3-}$
984 vs	984 vs	986 vs	$\nu_1(A_1)PO_4^{3-}$
955 vs	955 vs	955 vs	$\nu_1(A_1)PO_4^{3-}$
745 m	743 w	745 w	ρ (H_2O)
584 s	581 s	580 s	$\nu_4(F_2)PO_4^{3-}$
563 m	563 m	563 m	$\nu_4(F_2)PO_4^{3-}$
534 s, sh	534 s, sh	534 s, sh	$\nu_4(F_2)PO_4^{3-}$
451 m	449 m	449 m	$\nu_2(E)PO_4^{3-}$
374 m	374 m	374 m	ν (M-O)

Table 4.16 FTIR band positions (cm^{-1}) and the possible assignment in three replications of $Li_2Zn(HPO_4)_2 \cdot H_2O$-dx using KBr pellet technique

Vibrational Band Positions (cm^{-1})			
Replication Numbers			Possible assignments
I	II	II	
3588 s	3587 s	3587 s	ν_{as}(H-OP)
3534 s	3536 s	3535 s	ν_s(H-OP)
3480 s, sh	3472 s, sh	3474 s, sh	$\nu_3(B_2)$ H_2O
3310 s, sh	3308 s, sh	3311 s, sh	$\nu_1(A_1)H_2O$
2572 m	2573 m	2573	$\nu_3(B_2)D_2O$
1609 m	1609 m	1609 m	$\nu_2(A_1)H_2O$
1410 m	1410 m	1410 m	$\nu_2(A_1)$HOD
1121 s, sh	1120 m, sh	1121 m, sh	$\nu_3(F_2)PO_4^{3-}$
1066 vs	1066 vs	1066 vs	$\nu_3(F_2)PO_4^{3-}$
1007 vs	1007 vs	1007 vs	$\nu_3(F_2)PO_4^{3-}$
987 vs	988 vs	989 vs	$\nu_1(A_1)PO_4^{3-}$
983 w, sh	982 w, sh	983 w, sh	$\nu_1(A_1)PO_4^{3-}$
948 s	948 s	947 s	$\nu_1(A_1)PO_4^{3-}$
631 s	630 s	629 s	$\nu_4(F_2)PO_4^{3-}$
614 m	613 m	614 m	$\nu_4(F_2)PO_4^{3-}$
575 m	574 m	574 m	$\nu_4(F_2)PO_4^{3-}$
561 m	560 m	561 m	$\rho(H_2O)$
507 m	507 m	506 m	$\rho(H_2O)$
471 m	473 m	471 m	$\nu_2(E)PO_4^{3-}$
414 m	414 m	414 m	$\nu_2(E)PO_4^{3-}$
400 m	399 m	399 m	ν (Li-O)
384 w	385 w	384 w	ν (Li-O)
374 w	374 w	374 w	ν (Zn-O)

4.8 FT Raman Spectra of Some Selected Hydrates

The FT Raman spectra of $LiMnPO_4.H_2O$, $LiMnPO_4.H_2O$-dx, $Li_2Zn(HPO_4)_2.H_2O$ and $Li_2Zn(HPO_4)_2.H_2O$-dx are shown in Figures 4.51, 4.52, 4.53 and 4.54 , respectively. In all spectra, the Vibrational bands appear in the 1200-500 cm^{-1} region corresponding to the stretching of phosphate anion. The frequencies of each species are the same as the FTIR spectra of each compound. However, some vibrational species are not observed in the FT Raman spectrum, which may be due to the selection rule. The band assignments are summarized in Table 4.17 for $LiMnPO_4.H_2O$, $LiMnPO_4.H_2O$-dx, $Li_2Zn(HPO_4)_2.H_2O$ and $Li_2Zn(HPO_4)_2.H_2O$-dx, respectively.

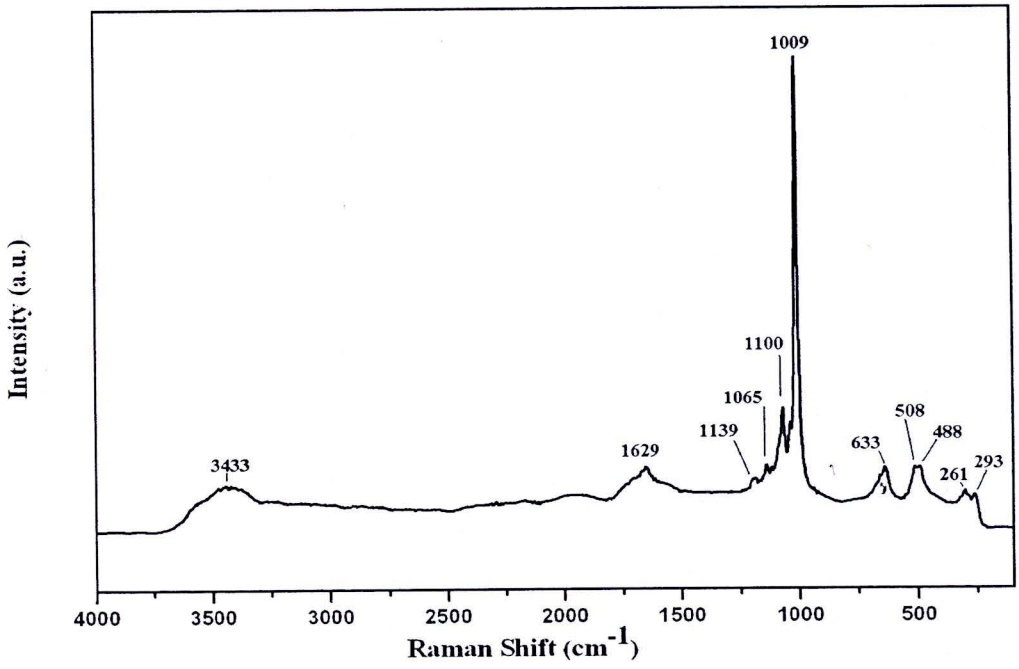

Figure 4.51 FT Raman spectrum of $LiMnPO_4.H_2O$ recorded on a Perkin Elmer Spectrum GX spectrophotometer in the region of 4000 – 250 cm^{-1} (64 scans)

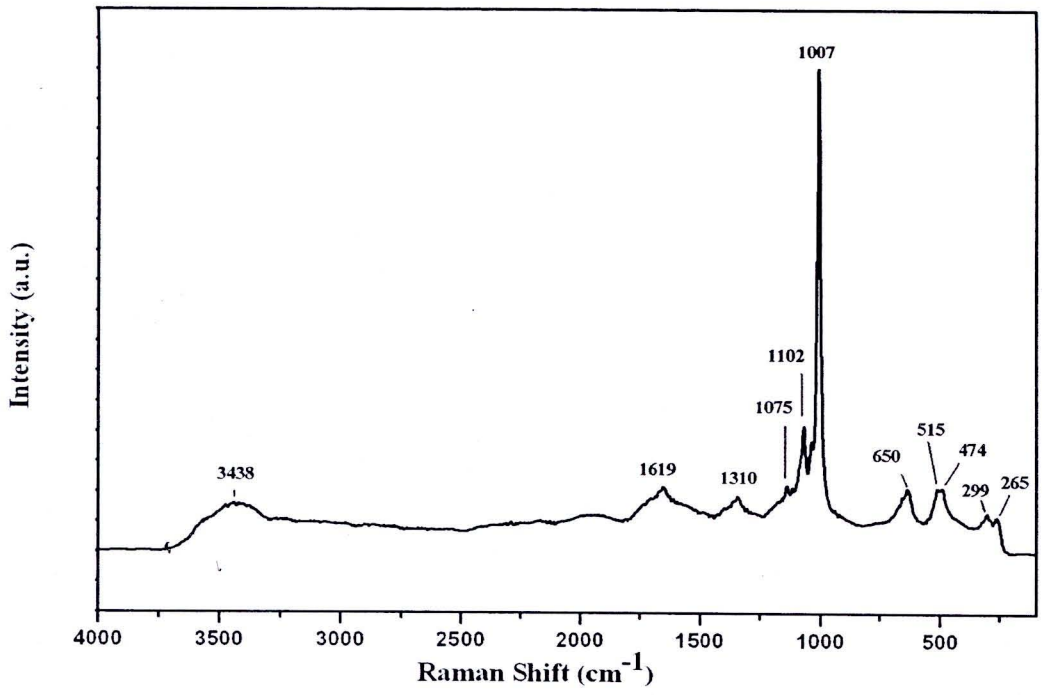

Figure 4.52 FT Raman spectrum of $LiMnPO_4.H_2O$-dx recorded on a Perkin Elmer Spectrum GX spectrophotometer in the region of 4000 – 250 cm^{-1} (64 scans)

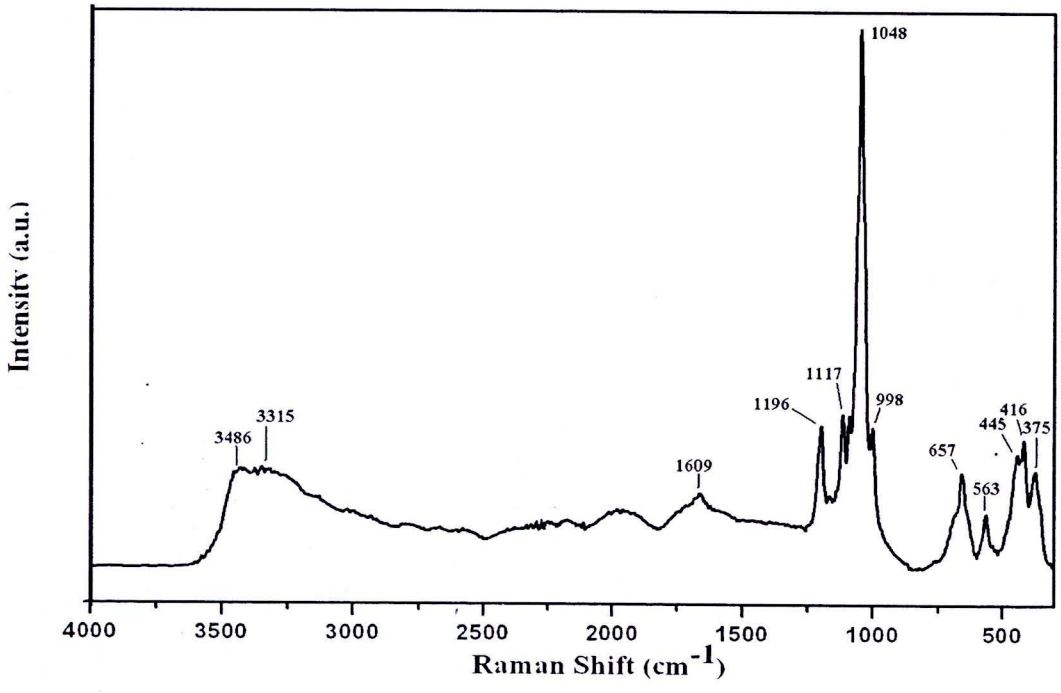

Figure 4.53 FT Raman spectrum of $Li_2Zn(HPO_4)_2.H_2O$ recorded on a Perkin Elmer Spectrum GX spectrophotometer in the region of 4000 – 250 cm^{-1} (64 scans)

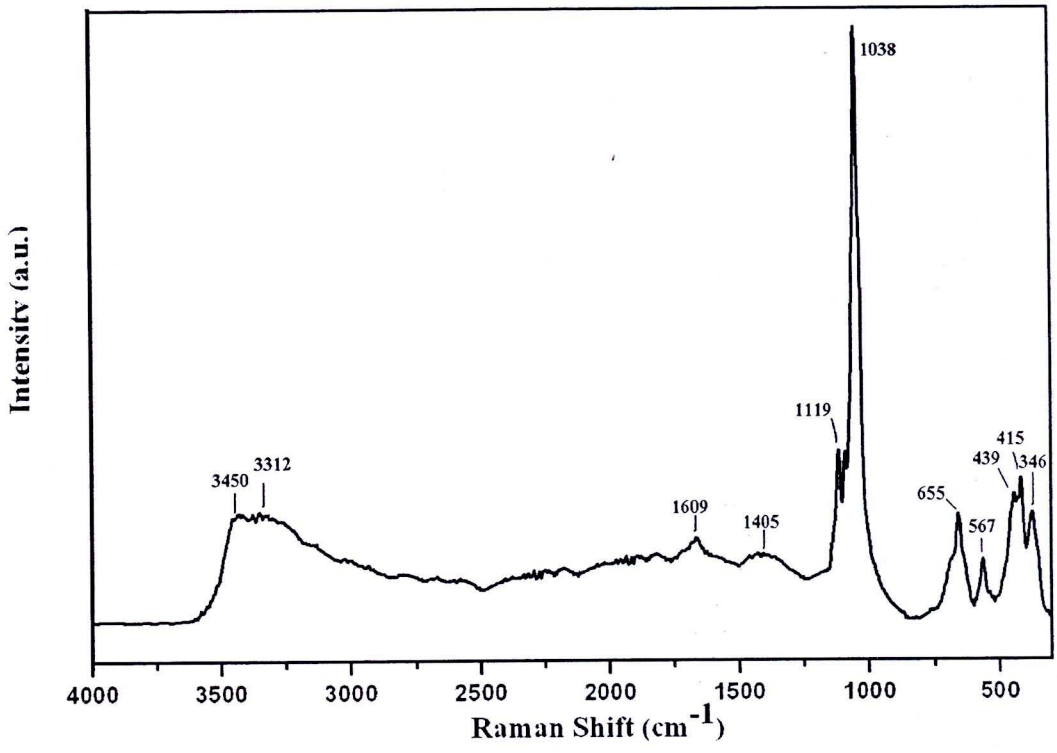

Figure 4.54 FT Raman spectrum of $Li_2Zn(HPO_4)_2.H_2O$-dx recorded on a Perkin Elmer Spectrum GX spectrophotometer in the region of 4000 – 250 cm^{-1} (64 scans)

Table 4.17 FTIR and FT Raman vibration frequencies (cm^{-1}) of $LiMnPO_4.H_2O$ and its deuterated analogue ($LiMnPO_4.H_2O$-dx)

Vibrational Band Position (cm^{-1})				Position assignment
$LiMnPO_4.H_2O$		$LiMnPO_4.H_2O$-dx		
FTIR	FT Raman	FTIR	FT Raman	
3410 s	3433 m	3441 s	3438 m	$\nu_3(B_2)$ H_2O
3115 s		3314 s		ν_{OH}(HOD)
		3195 s		$\nu_1(A_1)H_2O$
		3105 s		ν(MO-H)
1646 m	1629 m	1638 m	1619 m	$\nu_2(A_1)H_2O$
1609 s		1302 s	1310 m	$\nu_2(A_1)$HOD
		1142 s, sh		$2\nu_4(F_2)PO_4^{3-}$
1122 s	1139 s	1120 s		$\nu_3(F_2)PO_4^{3-}$
1067 vs	1065 s	1101 s	1075 s	$\nu_3(F_2)PO_4^{3-}$
1023 s	1100 s	1066 vs	1102 s	$\nu_3(F_2)PO_4^{3-}$
	1009 vs	1023 vs	1007 vs	$\nu_3(F_2)PO_4^{3-}$
984 vs		984 vs		$\nu_1(A_1)PO_4^{3-}$
953 vs		955 vs		$\nu_1(A_1)PO_4^{3-}$
792 m				ρ (H_2O)
743 m		745 m		ρ (H_2O)
587 s	633 s	584 s	650 s	$\nu_4(F_2)PO_4^{3-}$
568 s		563 m		$\nu_4(F_2)PO_4^{3-}$
520 s, sh	508 s	534 s, sh	515 s	$\nu_4(F_2)PO_4^{3-}$
473 w	488 s		474 s	$\nu_2(E)PO_4^{3-}$
445 m		451 m		$\nu_2(E)PO_4^{3-}$
397 w				ν (Li-O)
374 m		374 m		ν (Mn-O)
	293 s		299	External mode
	261 s		265	External mode

Table 4.18 FTIR and FT Raman vibration frequencies (cm^{-1}) of $Li_2Zn(HPO_4)_2.H_2O$ and its deuterated analogue ($Li_2Zn(HPO_4)2.H_2O$-dx)

Vibrational Band Position (cm^{-1})				Position assignment
$Li_2Zn(HPO_4)_2.H_2O$		$Li_2Zn(HPO_4)2.H_2O$-dx		
FTIR	FT Raman	FTIR	FT Raman	
3536 s		3588 s		ν_{as}(H-OP)
3481 s	3486 m	3534 s	3450 m	ν_s(H-OP)
3462 s, sh	3315 m	3480 s, sh	3312 m	$\nu_3(B_2)$ H_2O
3275 s, sh		3310 s, sh		$\nu_1(A_1)H_2O$
		2572 m		$\nu_3(B_2)D_2O$
1609 m	1609 s	1609 m	1609 s	$\nu_2(A_1)H_2O$
		1410 m	1405 m	$\nu_2(A_1)$HOD
1121 s, sh	1196 s	1121 s, sh	1119 s	$\nu_3(F_2)PO_4^{3-}$
1066 vs	1117 s	1066 vs		$\nu_3(F_2)PO_4^{3-}$
1007 vs	1048 vs	1007 vs	1038 vs	$\nu_3(F_2)PO_4^{3-}$
	998 m	987 vs		$\nu_1(A_1)PO_4^{3-}$
982 w, sh		983 w, sh		$\nu_1(A_1)PO_4^{3-}$
948 s		948 s		$\nu_1(A_1)PO_4^{3-}$
631 s	657 s	631 s	655 s	$\nu_4(F_2)PO_4^{3-}$
613 m		614 m		$\nu_4(F_2)PO_4^{3-}$
574 m	563 s	575 m	567 s	$\nu_4(F_2)PO_4^{3-}$
563 m		561 m		$\rho(H_2O)$
507 m		507 m		$\rho(H_2O)$
470 m	445 s	471 m		$\nu_2(E)PO_4^{3-}$
414 m	416	414 m	415 s	$\nu_2(E)PO_4^{3-}$
399 m		400 m		ν (Li-O)
385 w		384 w		ν (Li-O)
375 w		374 w		ν (Zn-O)
	375		346	External mode

4.9 Correlation Field Splitting Analysis

The assignments of vibrational spectra of water molecule and phosphate ion are important for the interpretation about the interaction between water molecule and their environments. The correlation field splitting was used to assign the vibrational bands.

The number of infrared – active and Raman – active modes of vibrations can be derived from the irreducible representations for (i) the point group of free ion or molecule, (ii) the site group symmetry and (iii) the unit cell group which is isomorphous with the factor group. The irreducible representations for each mode can be deduced.

4.9.1 Correlation Field Splitting Analysis of $ZnHPO_4.H_2O$ and $Co(H_2PO_4)_2.2H_2O$

$ZnHPO_4.H_2O$ and $Co(H_2PO_4)_2.2H_2O$ crystallize in the monoclinic system with space group C_{2h}, [7] with the site symmetry C_2 and Z=2. The correlation field splitting of PO_4^{3-} ion in this case is symbolized as T_d - C_2 - C_{2h} and shown in Table 4.19. The number of modes was suggested to be:

$$\Gamma_{Vib.} = 5A_g + 4B_g + 5A_u + 4B_u$$

The site symmetry of water molecule in this compound as previously mentioned, the number of internal modes are predicted by using correlation field splitting theory. The correlation field splittings of H_2O in $ZnHPO_4.H_2O$ and $Co(H_2PO_4)_2.2H_2O$ are symbolized as C_{2v}–C_s– C_{2h}^5 and shown in the Table 4.20. The number of modes was suggested to be :

Γ (vib,H_2O) = $2A_g + 1B_g + 2A_u + 1B_u$, under the selection rules of the C_s site group.

Table 4.19 T_d – C_s – C_{2h} correlation field splitting of phosphate ions (PO_4^{3-}) in $ZnHPO_4.H_2O$ and $Co(H_2PO_4)_2.2H_2O$.

Mode	Molecular Point Group	Site Group	Factor Group
	T_d	C_2	C_{2h}
ν_1	$A_1(1)$	A (5)	$A_g(5)$
ν_2	E(2)		$B_g(4)$
ν_3	F_2 (3)	B (4)	$A_u(5)$
ν_4	F_2 (3)		$B_u(4)$

Table 4.20 C_{2v}-C_s-C_{2h} correlation field splittings of H_2O in $ZnHPO_4.H_2O$ and $Co(H_2PO_4)_2.2H_2O$

Mode	Molecular Point Group	Site Group	Factor Group
	C_{2v}	C_s	C_{2h}
ν_1, ν_2	$A_1(2)$	A (2)	$A_g(2)$
			$B_g(1)$
ν_3	$B_2(1)$	B (1)	$A_u(2)$
			$B_u(1)$

4.9.2 Correlation Field Splitting Analysis of $LiFePO_4.3H_2O$, $LiCoPO_4.3H_2O$ $LiNiPO_4.H_2O$ and $LiMnPO_4.H_2O$

$LiFePO_4.3H_2O$, $LiCoPO_4.3H_2O$, $LiNiPO_4.H_2O$ and $LiMnPO_4.H_2O$ crystallize in the orthorhombic system with space group D_{2h}^{16}, $Z = Z' = 4$ and the site symmetry is C_s. The PO_4^{3-} ion and water molecule in $LiFePO_4.3H_2O$, $LiCoPO_4.3H_2O$ $LiNiPO_4.H_2O$ and $LiMnPO_4.H_2O$ will be considered. The free PO_4^{3-} ion belongs to T_d point group and locates on a C_s site symmetry for both hydrates. The correlation field splitting of PO_4^{3-} ion in these hydrates are symbolized as T_d-C_s-D_{2h}^{16} for the preservation of xy, xz and yz planes as shown in table 4.21-4.23, respectively. In the case of the correlation field splitting of H_2O in both hydrates are symbolized as C_{2v}-C_s-D_{2h} as shown in table 4.24-4.25, respectively. The number of modes was suggested to be :

Γ (vib,H_2O) = $3A_g + 3B_{3g} + 3B_{1u} + 3B2u$, under the selection rules of the C_s site group (yz plane preserved)

The Vibrational splitting in $LiFePO_4.3H_2O$, $LiCoPO_4.3H_2O$, $LiNiPO_4.H_2O$ and $LiMnPO_4.H_2O$ could be observed as a doubling bands for the doubly degenerate mode $\nu_2(E)$ and the triply degenerate $\nu_4(F_2)$, $\nu_3(F_2)$ modes. The number of vibrational modes of $LiFePO_4.3H_2O$, $LiCoPO_4.3H_2O$ $LiNiPO_4.H_2O$ and $LiMnPO_4.H_2O$ were calculated from (3N-6) x Z' = [3(5)-6 x 4] = 36 (since N represent the number of atoms of ion or molecule = 5 and Z' stands for the number of molecules in the Bravais or primitive cell = 4) of the PO_4^{3-} ion, the number of modes was suggest to be :

$\Gamma_{Vib.} = 6A_g + 6B_{1g} + 3B_{2g} + 3B_{3g} + 3A_u + 3B_{1u} + 6B_{2u} + 6B_{3u}$, under the selection rules of the C_s site group (xy plane preserved).

Table 4.21 $T_d - C_s - D_{2h}^{16}$ correlation field splitting of phosphate ions (PO_4^{3-}) in $LiFePO_4.3H_2O$, $LiCoPO_4.3H_2O$ $LiNiPO_4.H_2O$ and $LiMnPO_4.H_2O$ (xy plane preserved)

Mode	Molecular Point Group	Site Group	Factor Group
	T_d	C_s	D_{2h}^{16}
ν_1	$A_1(1)$		$A_g(6)$
			$B_{1g}(6)$
ν_2	$E(2)$	$A'(6)$	$B_{2g}(3)$
			$B_{3g}(3)$
ν_3	$F_2(3)$	$A''(3)$	$A_u(3)$
			$B_{1u}(3)$
ν_4	$F_2(3)$		$B_{2u}(6)$
			$B_{3u}(6)$

Table 4.22 $T_d - C_s - D_{2h}^{16}$ correlation field splitting of phosphate ions (PO_4^{3-}) in $LiFePO_4.3H_2O$, $LiCoPO_4.3H_2O$ $LiNiPO_4.H_2O$ and $LiMnPO_4.H_2O$ (zx plane preserved)

Mode	Molecular Point Group	Site Group	Factor Group
	T_d	C_s	D_{2h}^{16}
ν_1	$A_1(1)$		$A_g(6)$
			$B_{1g}(3)$
ν_2	E (2)	A′ (6)	$B_{2g}(6)$
			$B_{3g}(3)$
ν_3	F_2 (3)	A″ (3)	$A_u(3)$
			$B_{1u}(6)$
ν_4	F_2 (3)		$B_{2u}(3)$
			$B_{3u}(6)$

Table 4.23 $T_d - C_s - D_{2h}^{16}$ correlation field splitting of phosphate ions (PO_4^{3-}) in $LiFePO_4.3H_2O$, $LiCoPO_4.3H_2O$ $LiNiPO_4.H_2O$ and $LiMnPO_4.H_2O$ (yz plane preserved)

Mode	Molecular Point Group	Site Group	Factor Group
	T_d	C_s	D_{2h}^{16}
ν_1	$A_1(1)$		$A_g(6)$
			$B_{1g}(3)$
ν_2	$E(2)$	$A'(6)$	$B_{2g}(3)$
			$B_{3g}(6)$
ν_3	$F_2(3)$	$A''(3)$	$A_u(3)$
			$B_{1u}(6)$
ν_4	$F_2(3)$		$B_{2u}(6)$
			$B_{3u}(3)$

Table 4.24 C_{2v}-C_s-D_{2h}^{16} correlation field splitting of H_2O in $LiFePO_4.3H_2O$, $LiCoPO_4.3H_2O$, $LiNiPO_4.H_2O$ and $LiMnPO_4.H_2O$ (zx plane preserved)

Mode	Molecular Point Group	Site Group	Factor Group
	C_{2v}	C_s	D_{2h}^{16}
ν_1, ν_2	$A_1(2)$	$A'(2)$	$A_g(2)$, $B_{1g}(1)$, $B_{2g}(2)$, $B_{3g}(1)$
ν_3	$B_2(1)$	$A''(1)$	$A_u(1)$, $B_{1u}(2)$, $B_{2u}(1)$, $B_{3u}(2)$

Table 4.25 C_{2v}-C_s-D_{2h}^{16} correlation field splitting of H_2O in $LiFePO_4.3H_2O$, $LiCoPO_4.3H_2O$, $LiNiPO_4.H_2O$ and $LiMnPO_4.H_2O$ (yz plane preserved)

Mode	Molecular Point Group	Site Group	Factor Group
	C_{2v}	C_s	D_{2h}^{16}
ν_1, ν_2	$A_1(2)$	$A'(3)$	$A_g(3)$, $B_{3g}(3)$, $B_{1u}(3)$, $B_{2u}(3)$
ν_3	$B_2(1)$		

4.10 Calculation of $R_{O...O}$ Distance and Enthalpy of Hydrogen Bonding ($-\Delta H_H$)

The frequency shift of the uncouple ν_{OH}(HOD) leads to the estimation of $R_{O...O}$ distance and enthalpy of hydrogen bonding ($-\Delta H_H$) by using below equation [22, 44]

$$R_{O...O} = 3.764\ (Å) - 0.169\ (Å)\ \ln(\Delta\nu_{OH}/\ cm^{-1})\ (cm^{-1})$$

$$-\Delta H_H = 1.268 + 0.0418\ (\Delta\nu_{OH}(HOD)/\ cm^{-1}) \quad kJmol^{-1}OH$$

The calculation of $R_{O...O}$ distance and enthalpy of hydrogen bonding can be illustrated as following.

(i) The calculation of $R_{O...O}$ distance

For example $LiFePO_4.3H_2O$, the frequency shift of ν_{OH}(HOD) from sample I (see Figure 4.27) by using KBr pellet technique is 3382 cm^{-1}. The frequency shift $\Delta\nu_{OH}$(HOD) value is 3707-3382 = 325 cm^{-1}

Hence, $R_{O...O} = 3.764\ (Å) - 0.169\ (Å)\ \ln(\Delta\nu_{OH}/\ cm^{-1})$

$= 3.764\ (Å) - 0.169\ \ln(325)\ Å$

$= 3.764\ (Å) - 0.169 \times 5.784\ Å$

$R_{O...O} = 2.787\ Å$

(ii) The calculation of ($-\Delta H_H$)

From equation

$-\Delta H_H = 1.268 + 0.0418\ (\Delta\nu_{OH}(HOD)/\ cm^{-1})\ kJmol^{-1}OH$

$= 1.268 + 0.0418\ (325)\ kJmol^{-1}OH$

$= 14.853\ kJmol^{-1}OH$

The observed ν_{OH}(HOD), $\Delta\nu_{OH}$(HOD), $R_{O...O}$ distance, and $-\Delta H_H$ in three replications of $LiFePO_4.3H_2O$, $LiCoPO_4.H_2O$, $LiNiPO_4.H_2O$ and $LiMnPO_4.H_2O$ are shown in Table 4.26.

The $R_{O...O}$ distances in the range of 2.755-2.787 Å and $-\Delta H_H$ of these hydrates indicated that the strengths of hydrogen bonding are in the range of 14.853-17.440 kJ/mol OH by ranging in the sequence $LiMnPO_4.H_2O$ > $LiNiPO_4.H_2O$ > $LiCoPO_4.H_2O$ > $LiFePO_4.3H_2O$, respectively.

Table 4.26 The Observed ν_{OH}(HOD), $\Delta\nu_{OH}$(HOD), estimated of $R_{O...O}$ distance and enthalpy of hydrogen bonding ($-\Delta H_H$) of the synthesized hydrate

Hydrates	ν_{OH}(HOD) (cm^{-1})	$\Delta\nu_{OH}$(HOD) (cm^{-1})	$R_{O...O}$ distance (Å)	$-\Delta H_H$ ($kJmol^{-1}OH$)
$LiFePO_4.3H_2O$	3382	325	2.787	14.853
	3382	325	2.787	14.853
	3382	325	2.787	14.853
	mean	325	2.787	14.853
$LiCoPO_4.3H_2O$	3372	335	2.781	15.271
	3372	335	2.781	15.271
	3372	335	2.781	15.271
	mean	335	2.781	15.271
$LiNiPO_4.H_2O$	3337	370	2.765	16.734
	3337	370	2.765	16.734
	3337	370	2.765	16.734
	mean	370	2.765	16.734
$LiMnPO_4.H_2O$	3314	393	2.754	17.695
	3315	392	2.755	17.654
	3317	390	2.756	17.570
	mean	391.67	2.755	17.440

4.11 The Study on the Thermal Decomposition Kinetics

Decomposition of solids is the subjects of intensive kinetics studies. In many methods of kinetic estimation, isoconversional method is recommended as trustworthy way of obtaining reliable and consistent kinetic information. The aim of the kinetic studies from TA data is to find the most probable kinetic model which gives the best description of the studied compound and allows the calculation of reliable values for the kinetic parameters (activation energy E_a and pre-exponential factor A). The kinetic parameters E_a and A together with the reaction model are sometimes called the kinetic triplet. Model-free and model fitting approaches were used to investigate the kinetics under multiple-scan non-isothermal conditions. As one of the non-isothermal multiple-scan methods for studying of kinetics, isoconversion method is also called model-free method, because no kinetic model was set before the calculation of activation energy. Decomposition of crystalline hydrates is a solid-state process of the type: A(solid) → B(solid) + C (gas). The kinetics of such reactions is described by various equations taking into account the special features of their mechanisms. The activation energy can be calculated according to the iso-conversional methods. In kinetics study of $ZnHPO_4.H_2O$, $Co(H_2PO_4)_2.2H_2O$, $LiFePO_4.3H_2O$, $LiCoPO_4.3H_2O$, $LiNiPO_4.H_2O$, $LiMnPO_4.H_2O$ and $Li_2Zn(HPO_4)_2.H_2O$, Ozawa and Kissinger equations were used to determine the activation energy of the dehydration and decomposition reactions.

4.11.1 Thermal Decomposition Kinetics Study of $ZnHPO_4.H_2O$

The DSC curves for dehydration $ZnHPO_4.H_2O$ in nitrogen atmosphere at various heating rates (5, 10, 20, 30 and 40 °C min^{-1}) are shown in Figure 4.55. The curves show that the thermal decomposition of $ZnHPO_4.H_2O$ below 400°C occurs in two steps, which is related to the elimination of water of crystallization and decomposition of the sample. According to the isoconversional method, the basic data collected in Table 4.27 were used for the plot of ln β versus $1000/T_m$ (Ozawa) and ln (β/T_m^2) versus $1000/T_m$ (Kissinger). The activation energy E_a values can be calculated from the slopes of straight lines with best linear correlation

coefficient (r^2). Ozawa and Kissinger plots for the determination activation energies of $ZnHPO_4.H_2O$ are shown in Figures 4.56-4.59, respectively.

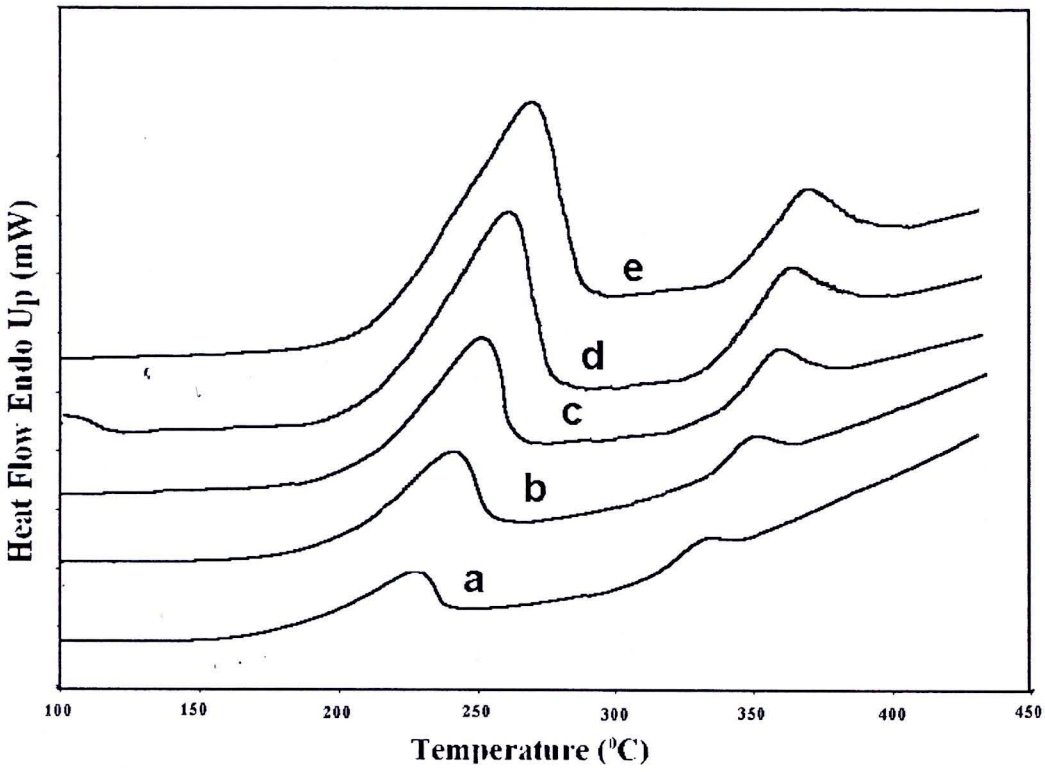

Figure 4.55 DSC curves of the synthesized $ZnHPO_4.H_2O$ at different heating rates: a = 5, b = 10, c = 20, d = 30 and e = 40 °C min^{-1} in N_2 atmosphere

Table 4.27 DSC data for Ozawa and Kissinger plots of $ZnHPO_4.H_2O$

β (°C min^{-1})	T_{m1} (K) (1^{st} step)	T_{m2} (K) (2^{nd} step)	$\ln \beta$	$\ln(\frac{\beta}{T_{m1}^2})$	$\ln(\frac{\beta}{T_{m2}^2})$
5	514.768	612.968	1.6094	-12.0115	-12.3607
10	520.508	619.818	2.3025	-11.6756	-12.0248
20	524.160	628.462	2.9957	-11.4264	-11.7893
30	530.018	634.952	3.4012	-11.3216	-11.6829
40	533.210	639.563	3.6888	-11..2525	-11.6162

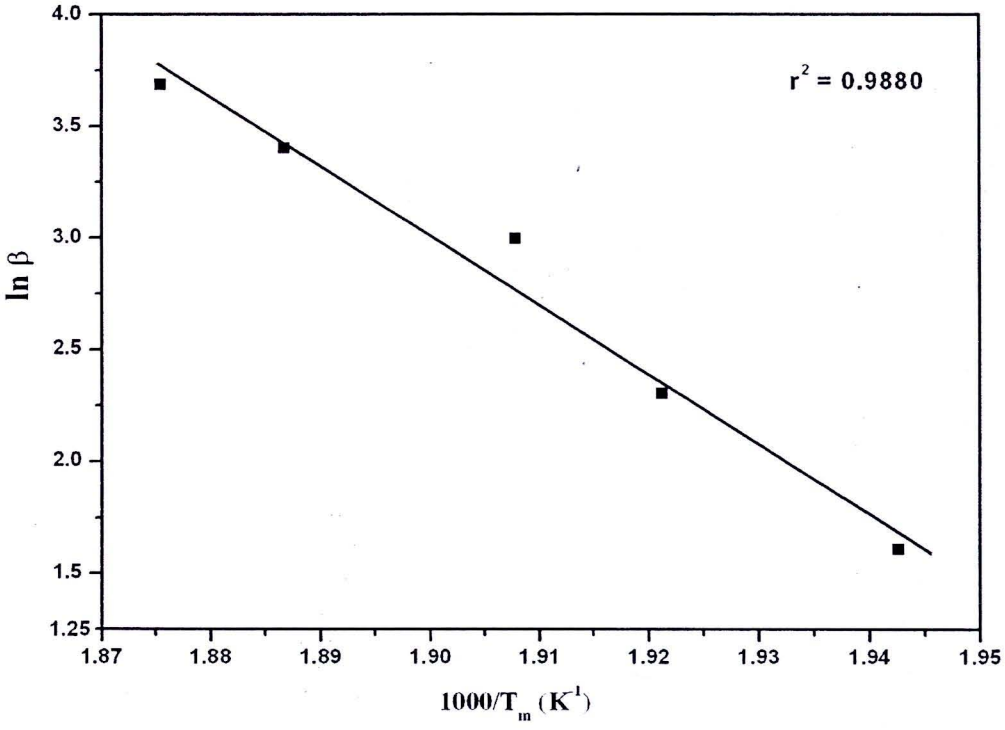

Figure 4.56 Ozawa plot for the first step of dehydration of $ZnHPO_4.H_2O$

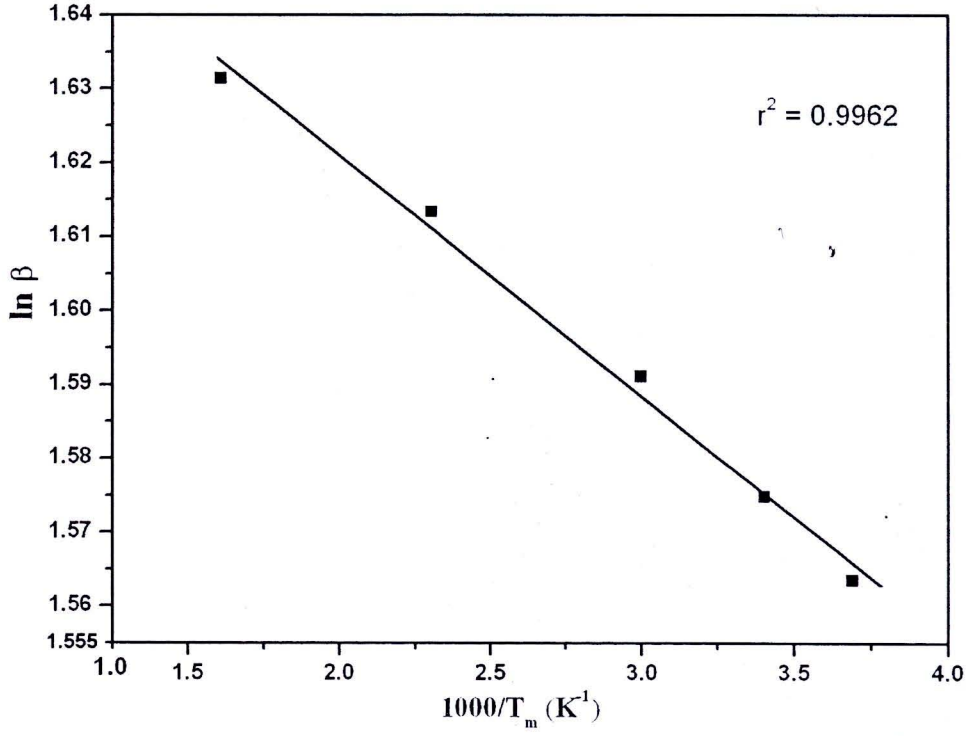

Figure 4.57 Ozawa plot for the second step of decomposition of $ZnHPO_4.H_2O$

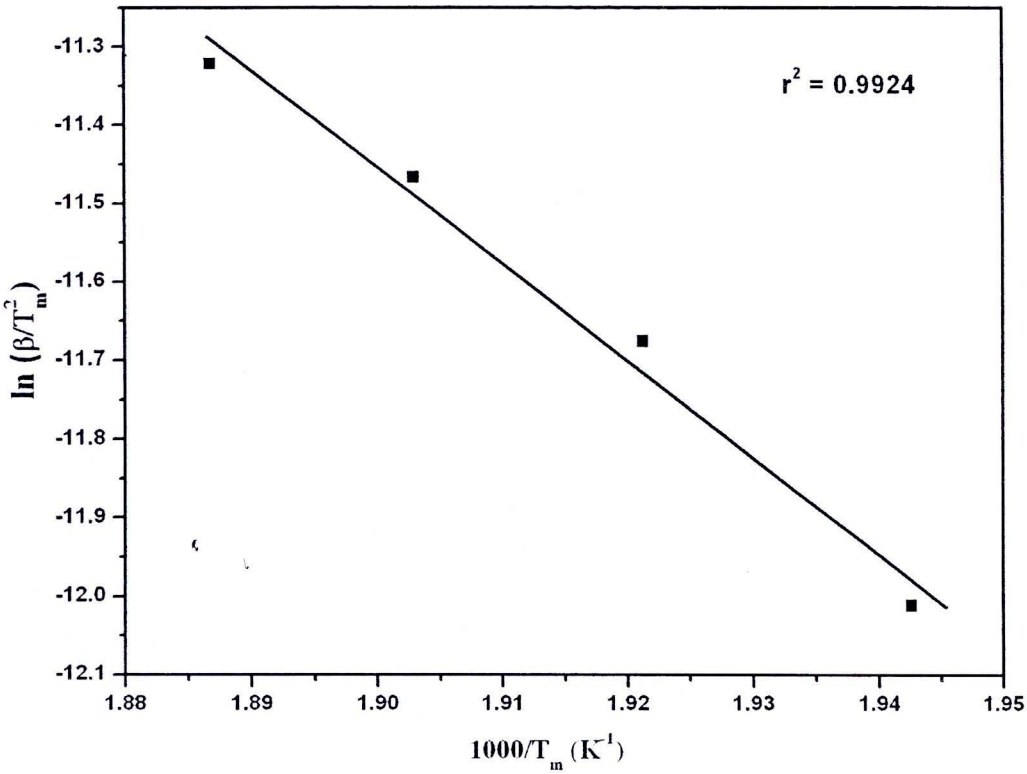

Figure 4.58 Kissinger plot for the first step of dehydration of $ZnHPO_4.H_2O$

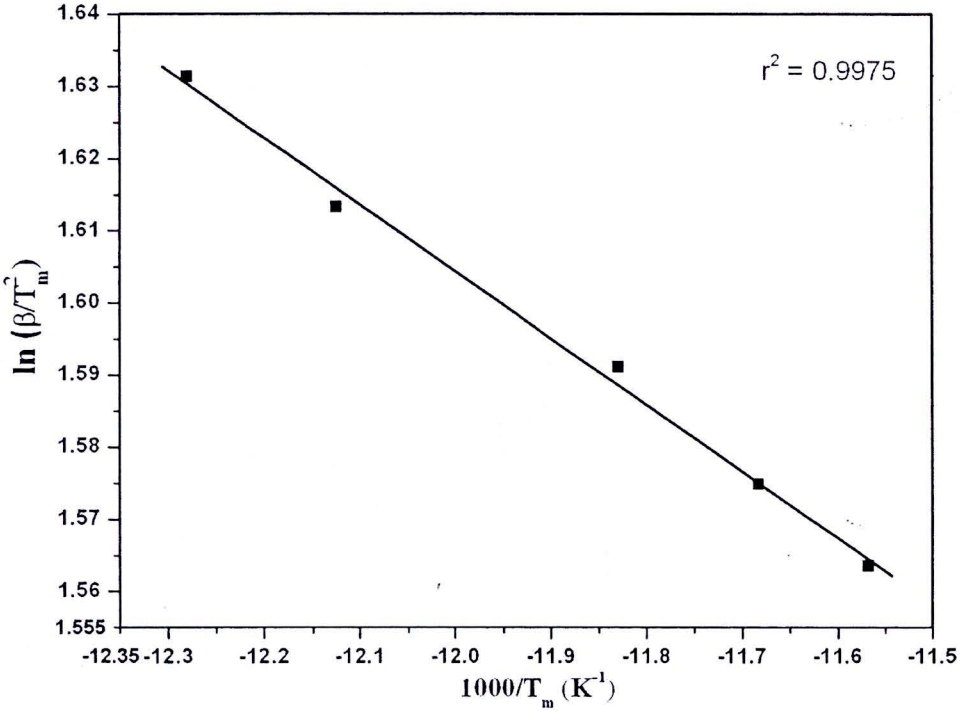

Figure 4.59 Kissinger plot for the second step of decomposition of $ZnHPO_4.H_2O$

From the slopes of both plots, ln β versus $1000/T_m$ (Ozawa, Figures 4.56, 4.57) and ln (β/T_m^2) versus $1000/T_m$ (Kissinger, Figures 4.58, 4.59), the activation energy values for all steps can be calculated and presented in Table 4.28.

Table 4.28 Activation energies E_a and correlation coefficient (r^2) calculated by Ozawa and Kissinger methods for the dehydration of $ZnHPO_4.H_2O$

Step	Ozawa method		Kissinger method	
	E_a (kJ mol^{-1})	r^2	E_a (kJ mol^{-1})	r^2
1st	258.7	0.9880	250.0	0.9924
2nd	252.6	0.9962	242.2	0.9975

4.11.2 Thermal Decomposition Kinetics Study of $Co(H_2PO_4).2H_2O$

The DSC curves for dehydration $Co(H_2PO_4)_2.2H_2O$ in nitrogen atmosphere at various heating rates (5, 10, 20, 30 and 40 °C min^{-1}) are shown in Figure 4.60. The curves showed that the thermal decomposition of below $Co(H_2PO_4)_2.2H_2O$ 400°C occurs in two steps, which is related to the elimination of water of crystallization and decomposition of sample. According to the isoconversional method, the basic data collected in Table 4.29 were used for the plot of ln β versus $1000/T_m$ (Ozawa) and ln (β/T_m^2) versus $1000/T_m$ (Kissinger). The activation energy E_a values can be calculated from the slopes of straight lines with better linear correlation coefficient (r^2). Ozawa and Kissinger plots for the determination activation energies of $Co(H_2PO_4)_2.2H_2O$ for both steps are shown in Figures 4.61-4.64, respectively.

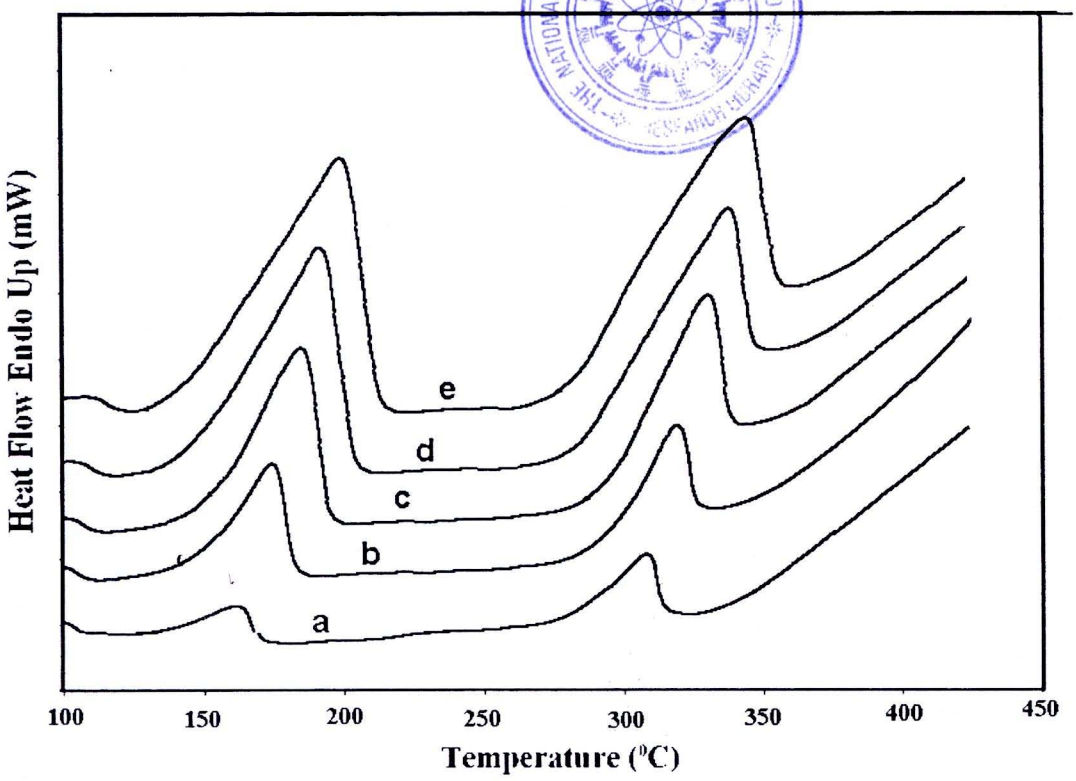

Figure 4.60 DSC curves of the synthesized $Co(H_2PO_4)_2.2H_2O$ at different heating rates: a = 5, b = 10, c = 20, d = 30 and e = 40 °C min^{-1} in N_2 atmosphere

Table 4.29 DSC data for Ozawa and Kissinger plots of $Co(H_2PO_4)_2.2H_2O$

β (°C min^{-1})	T_{m1} (K) (1st step)	T_{m2} (K) (2nd step)	$\ln \beta$	$\ln(\frac{\beta}{T_{m1}^2})$	$\ln(\frac{\beta}{T_{m2}^2})$
5	439.533	591.563	1.6094	-11.6955	-12.0301
10	446.741	601.819	2.3025	-11.3699	-11.9659
20	453.111	608.276	2.9957	-11.1350	-11.7240
30	461.583	614.931	3.4012	-11.0451	-11.6188
40	471.543	622.116	3.6888	-11.0067	-11.5609

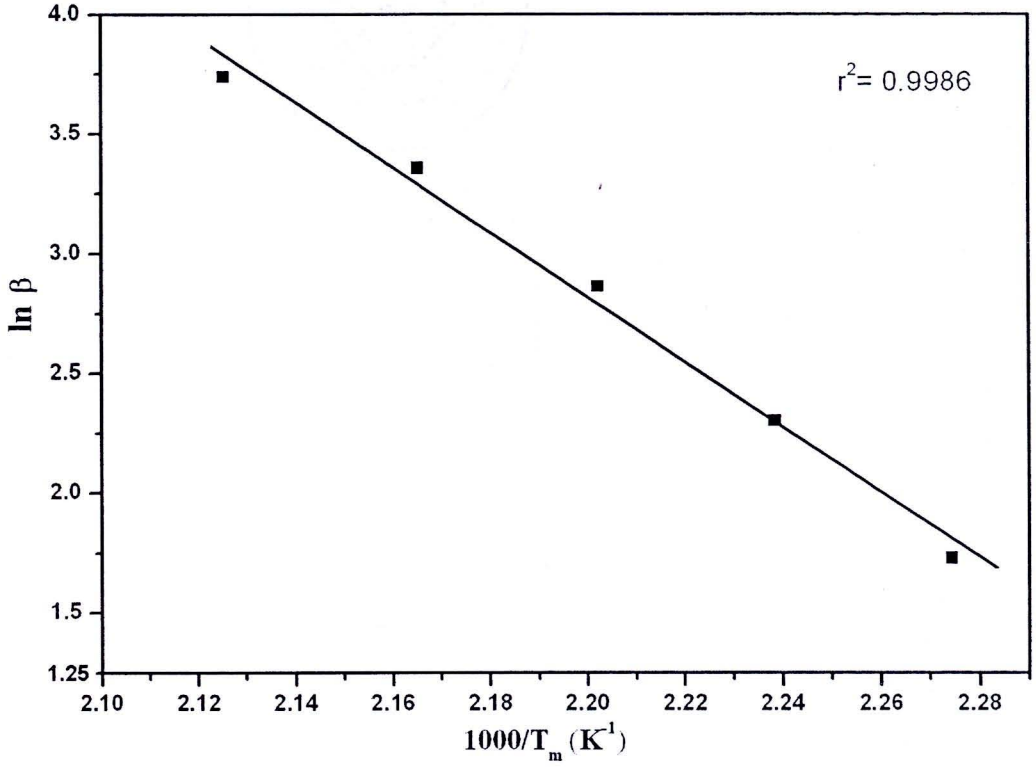

Figure 4.61 Ozawa plot for the first step of dehydration of $Co(H_2PO_4)_2.2H_2O$

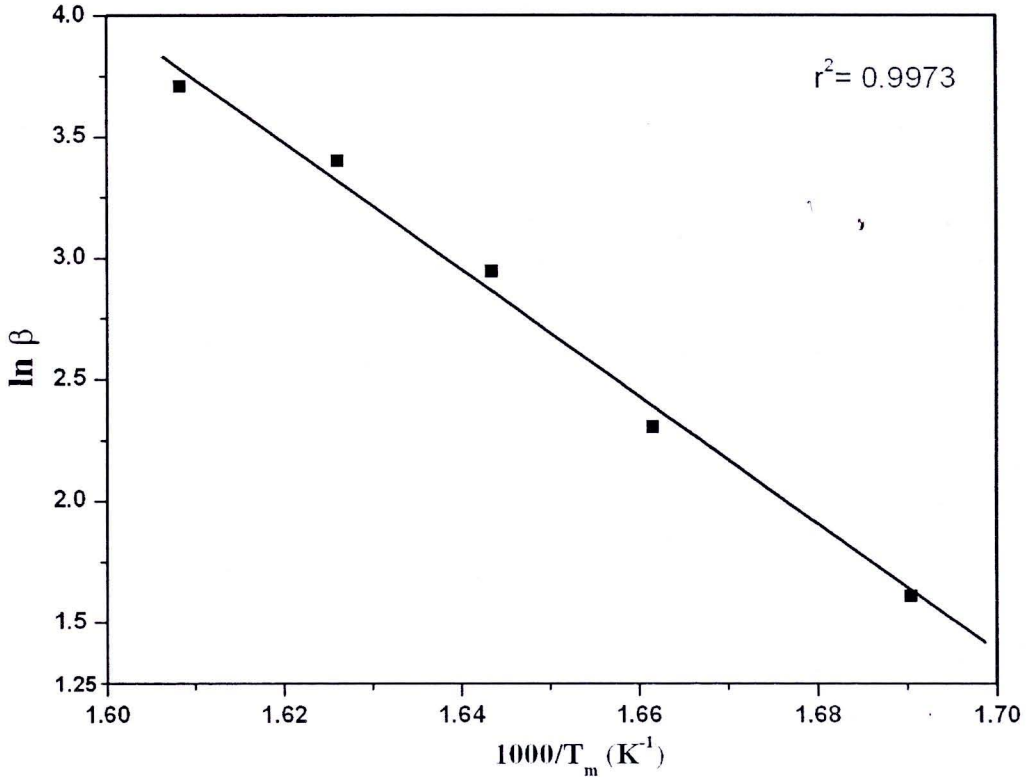

Figure 4.62 Ozawa plot for the second step of decomposition of $Co(H_2PO_4)_2.2H_2O$

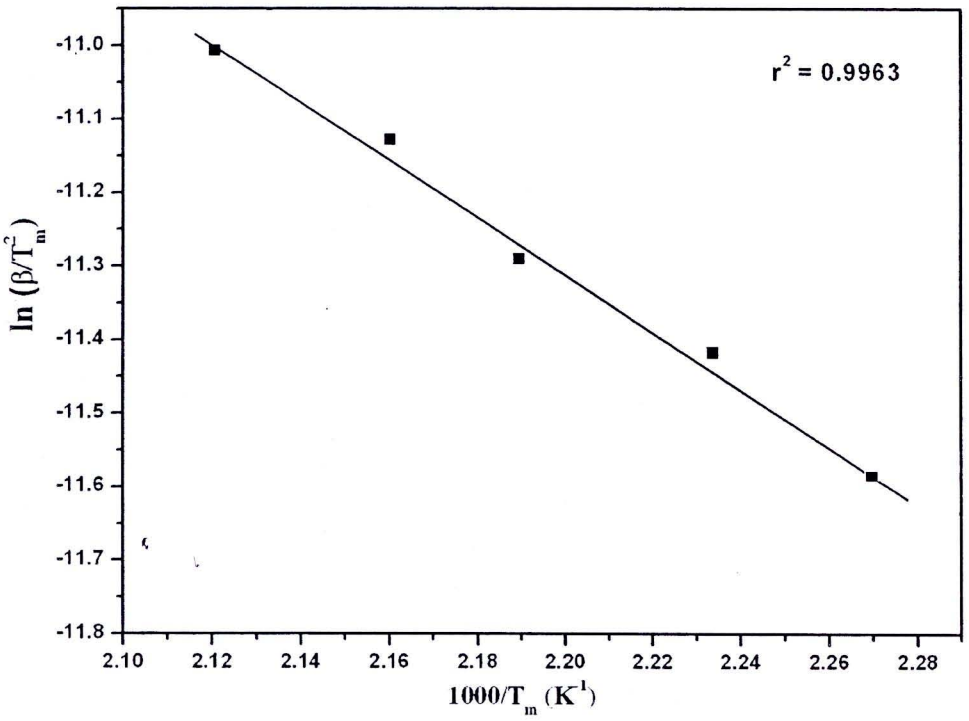

Figure 4.63 Kissinger plot for the first step of dehydration of $Co(H_2PO_4)_2.2H_2O$

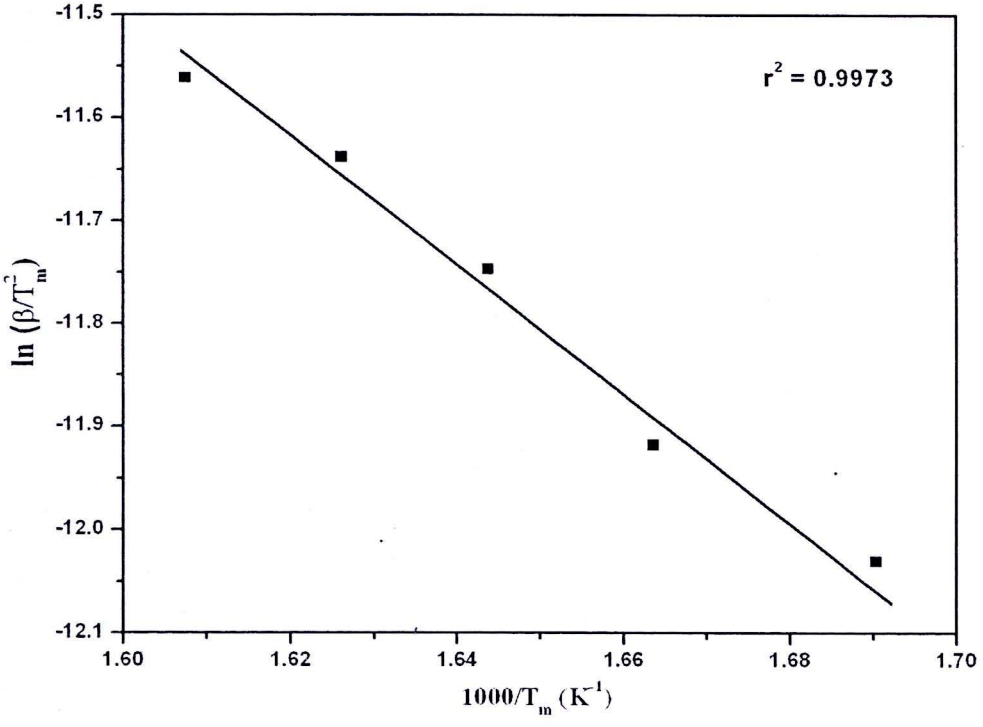

Figure 4.64 Kissinger plot for the second step of decomposition of $Co(H_2PO_4)_2.2H_2O$

From the slopes of both plots, ln β versus 1000/T_m (Ozawa, Figures 4.61, 4.62) and ln (β/T_m^2) versus 1000/T_m (Kissinger, Figures 4.63, 4.63), the activation energy values for all steps were calculated and are presented in Table 4.30.

Table 4.30 Activation energies E_a and correlation coefficient (r^2) calculated by Ozawa and Kissinger method for the dehydration of $Co(H_2PO_4)_2.2H_2O$

Step	Ozawa method		Kissinger method	
	E_a (kJ mol^{-1})	r^2	E_a (kJ mol^{-1})	r^2
1st	112.9	0.9986	104.5	0.9963
2nd	217.3	0.9973	207.7	0.9973

4.11.3 Thermal Decomposition Kinetics Study of $LiFePO_4.3H_2O$

The DSC curves for dehydration of $LiFePO_4.3H_2O$ in nitrogen atmosphere at various heating rate (5, 10, 20, 30 and 40 °C min^{-1}) are shown in Figure 4.65. The curves show that the thermal decomposition of $LiFePO_4.3H_2O$ below 400°C occurs in three steps, which is related to the elimination of water of crystallization in three steps: 104-140, 175-202.5 and 280-308 °C. According to isoconversional method, the basic data collected in Table 4.31 were used for the plot of ln β versus 1000/T_m (Ozawa) and ln (β/T_m^2) versus 1000/T_m (Kissinger). The activation energies E_a can be calculated from the slopes of straight lines with best linear correlation coefficient (r^2). Ozawa and Kissinger plot for the determination activation energies of $LiCoPO_4.3H_2O$ are shown in Figures 4.66-4.71, respectively.

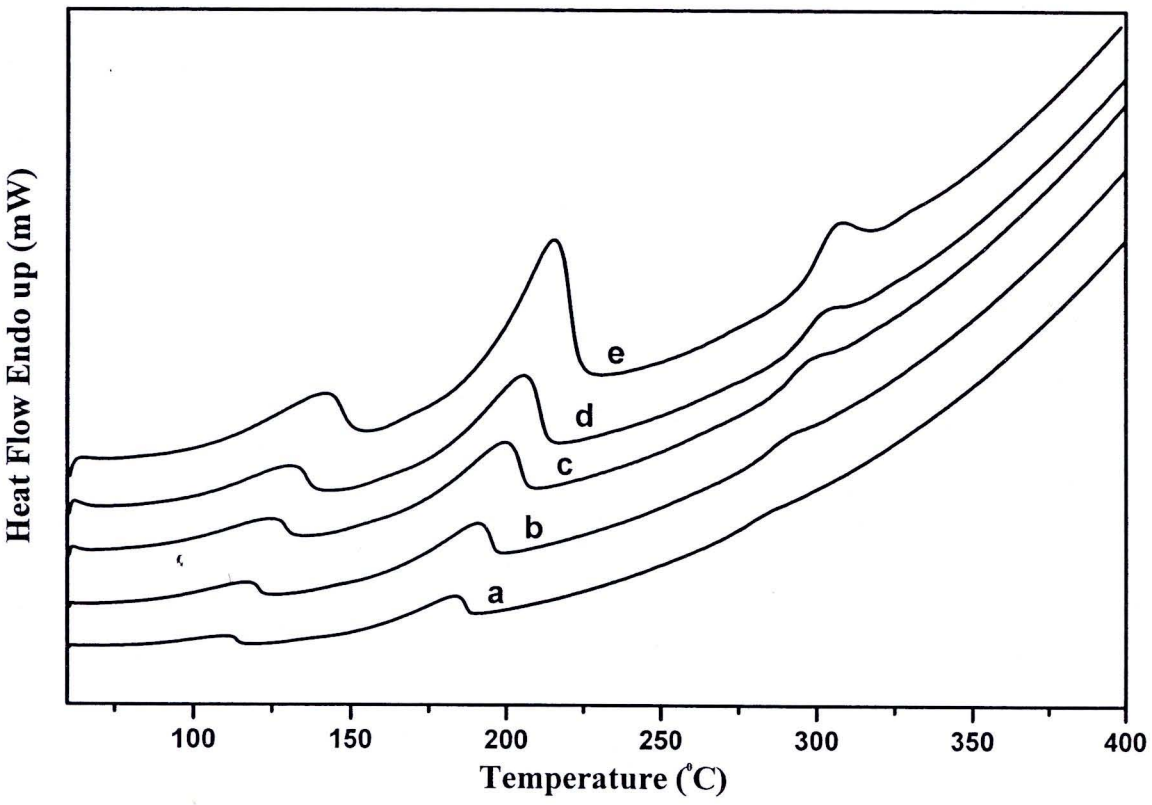

Figure 4.65 DSC curves of the synthesized $LiFePO_4.3H_2O$ at different heating rates: a = 5, b = 10, c = 20, d = 30 and e = 40 °C min^{-1} in N_2 atmosphere

Table 4.31 DSC data for Ozawa and Kissinger plots of $LiFePO_4.3H_2O$

β (°Cmin^{-1})	T_{m1} (K) (1^{st} step)	T_{m2} (K) (2^{nd} step)	T_{m3} (K) (3^{rd} step)	ln β	ln ($\frac{\beta}{T_{m1}^2}$)	ln ($\frac{\beta}{T_{m2}^2}$)	ln ($\frac{\beta}{T_{m3}^2}$)
5	382.309	455.974	557.191	1.6094	- 10.2830	- 10.6354	- 11.0363
10	389.211	463.462	563.978	2.3025	-9.6256	-9.9748	- 10.3674
20	397.002	472.407	570.543	2.9957	-8.9721	-9.3199	-9.6974
30	403.916	478.372	574.651	3.4012	-8.6012	-8.9395	-9.3063
40	410.171	488.294	579.926	3.6888	8.3442	8.6929	-9.0369

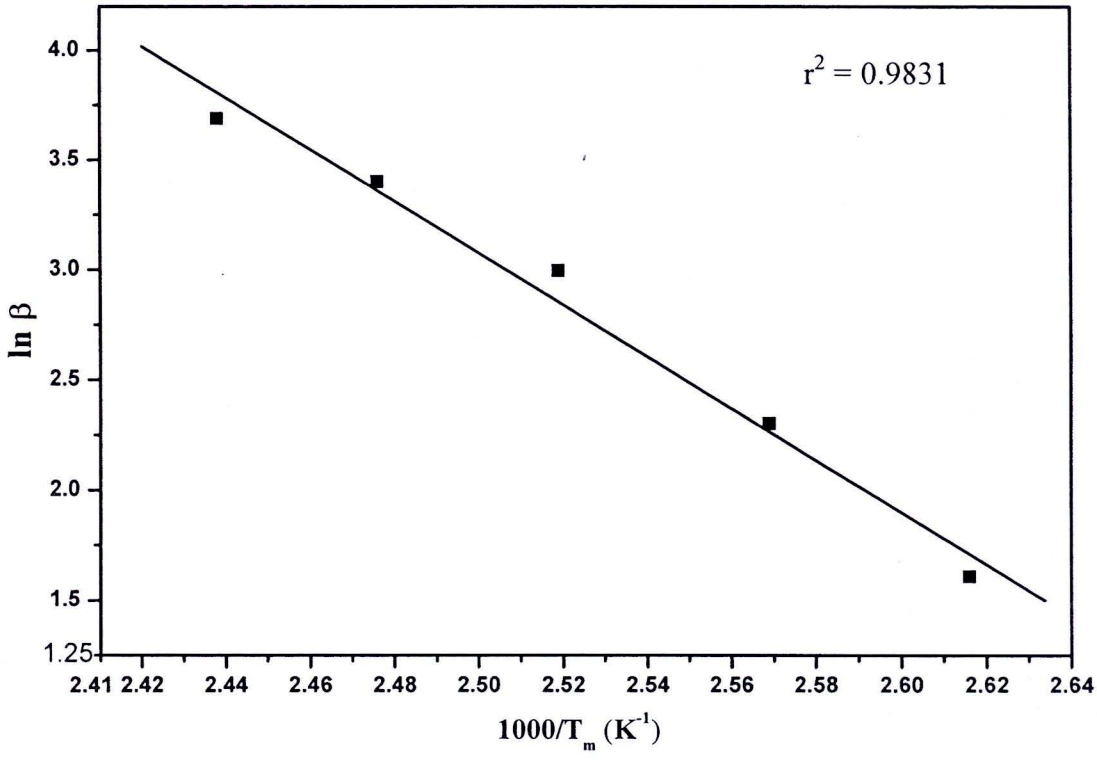

Figure 4.66 Ozawa plot for the first step of dehydration of $LiFePO_4.3H_2O$

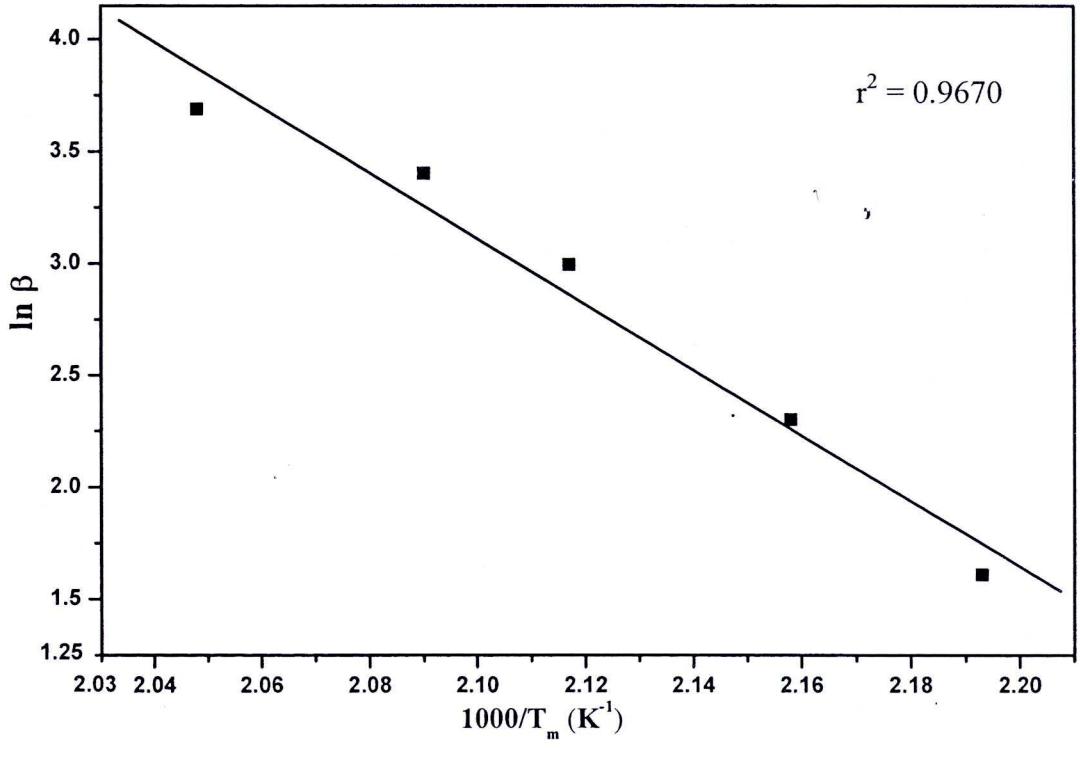

Figure 4.67 Ozawa plot for the second step of dehydration of $LiFePO_4.3H_2O$

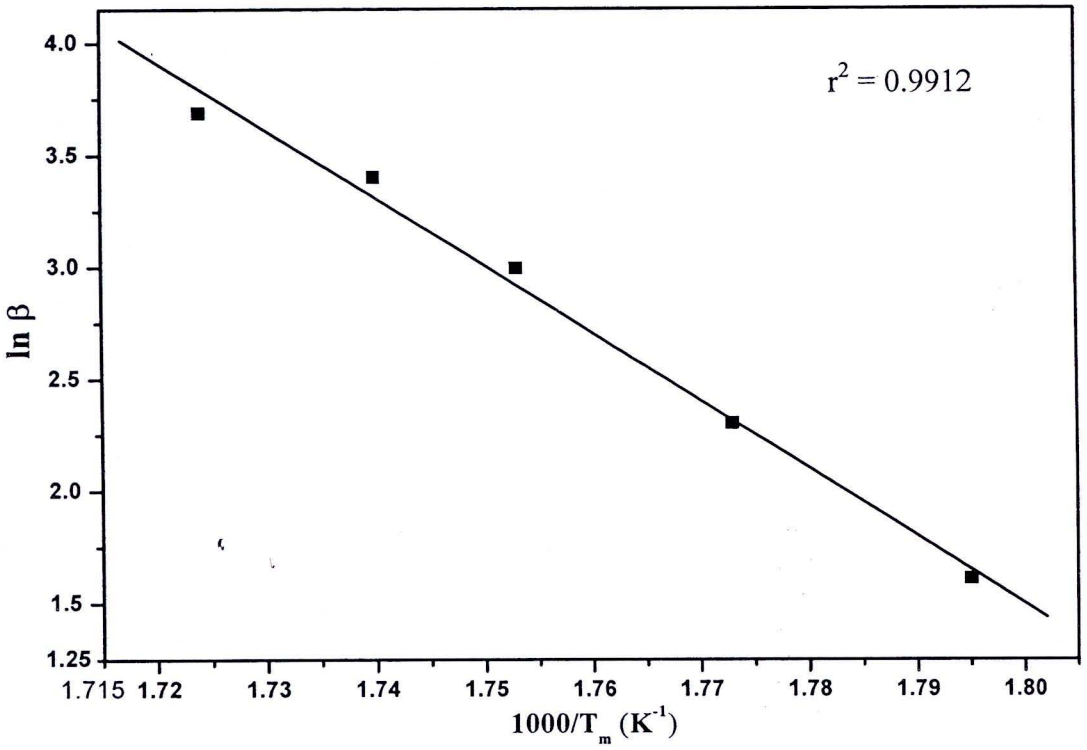

Figure 4.68 Ozawa plot for the third step of dehydration of $LiFePO_4.3H_2O$

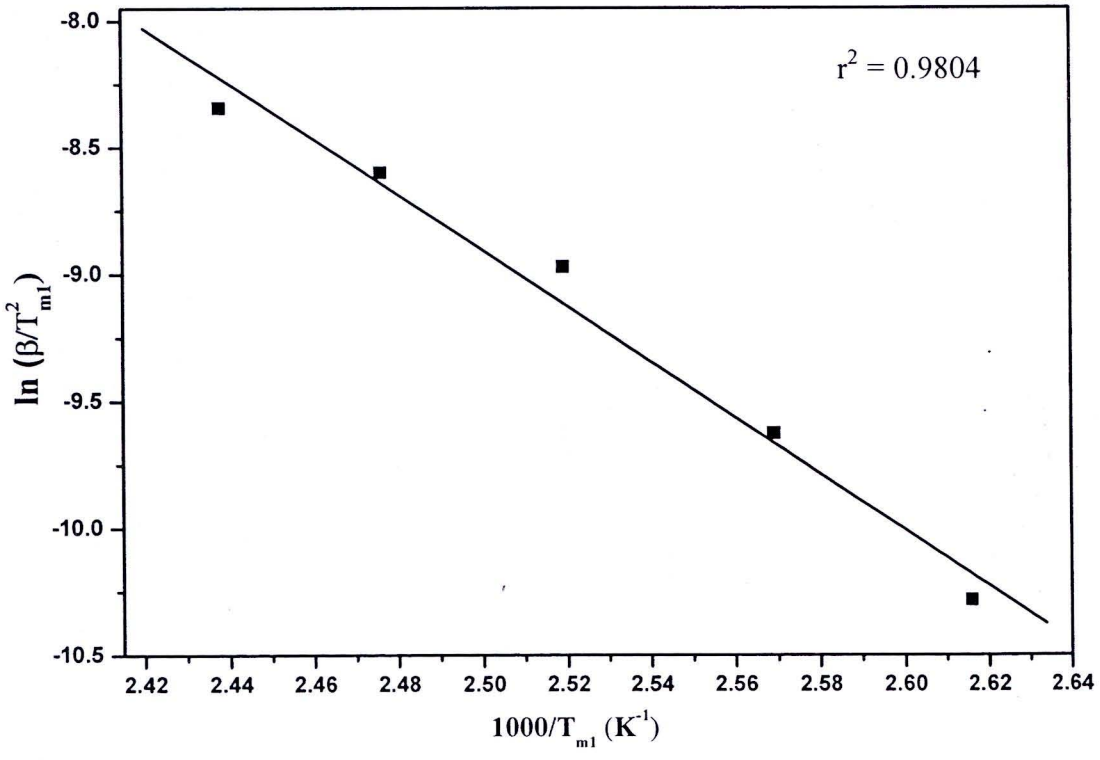

Figure 4.69 Kissinger plot for the first step of dehydration of $LiFePO_4.3H_2O$

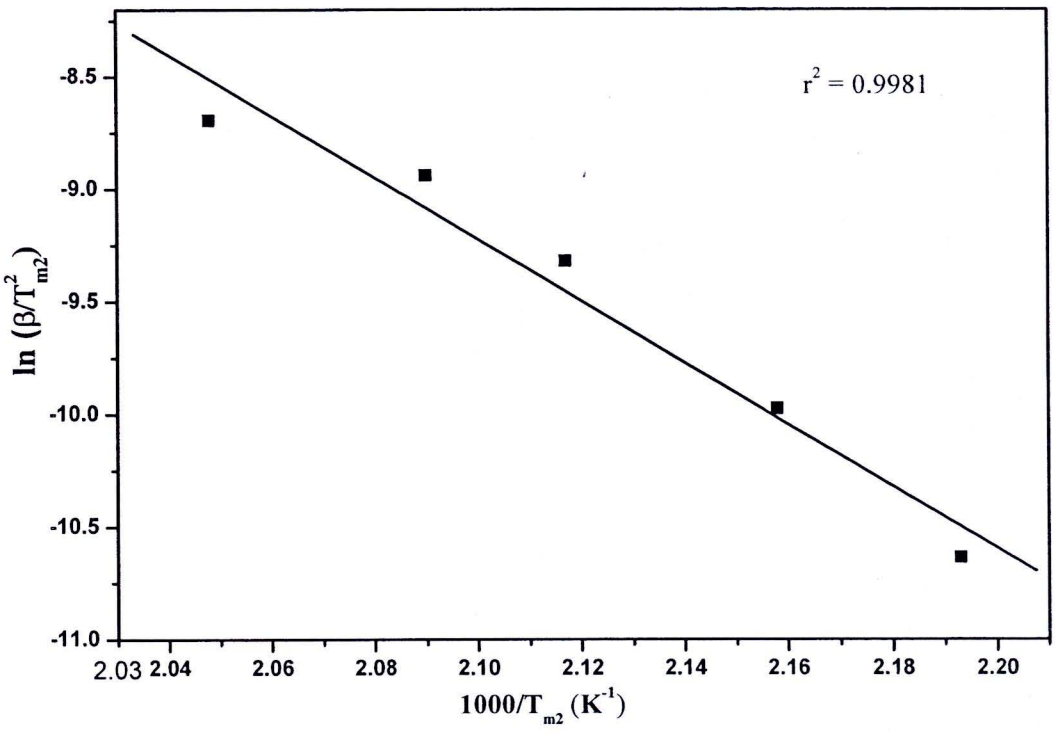

Figure 4.70 Kissinger plot for the second step of dehydration of $LiFePO_4.3H_2O$

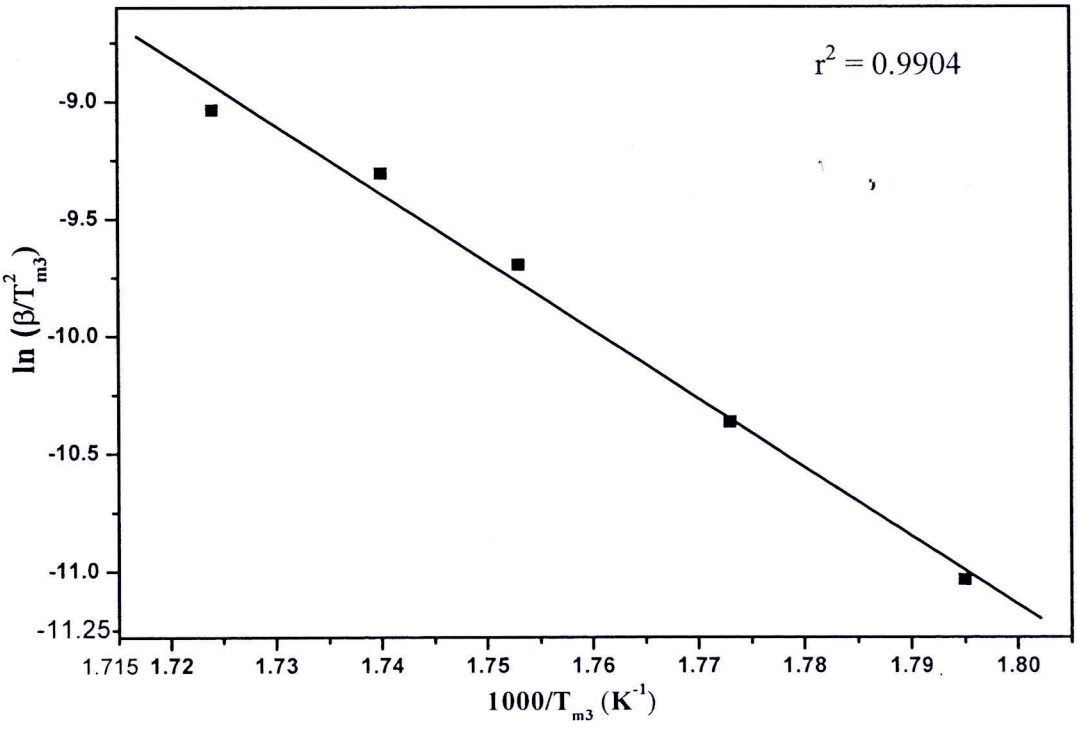

Figure 4.71 Kissinger for the third step of dehydration of $LiFePO_4.3H_2O$

From the slopes of both plots, ln β versus $1000/T_m$ (Ozawa, Figures 4.53-4.55) and ln (β/T_m^2) versus $1000/T_m$ (Kissinger, Figures 4.56-4.58), the activation energy values for all steps were calculated and are presented in Table 4.32.

Table 4.32 Activation energies E_a and correlation coefficient (r^2) calculated by Ozawa and Kissinger method for the dehydration of $LiFePO_4.3H_2O$

Step	Ozawa method		Kissinger method	
	E_a (kJ mol^{-1})	r^2	E_a (kJ mol^{-1})	r^2
1st	98.0	0.9831	91.4	0.9804
2nd	121.9	0.9670	114.1	0.9981
3rd	253.3	0.9912	243.8	0.9904

4.11.4 Thermal Decomposition Kinetics Study of $LiCoPO_4.3H_2O$

The DSC curves for dehydration of $LiCoPO_4.3H_2O$ in nitrogen atmosphere at various heating rates (5, 10, 20, 30 and 40 °C min^{-1}) are shown in Figure 4.72. The curves show three steps of thermal decomposition of $LiCoPO_4.3H_2O$ below 400°C, which is related to the elimination of water of crystallization with different strengths of hydrogen bondings. Three ranges of dehydration are 145-189, 193-202 and 212-218 °C. According to the isoconversional method, the basic data collected in Table 4.33 were used for the plot of ln β versus $1000/T_m$ (Ozawa) and ln (β/T_m^2) versus $1000/T_m$ (Kissinger). The activation energy E_a values can be calculated from the slopes of straight lines with the best linear correlation coefficient (r^2). Ozawa and Kissinger plots for the determination of activation energies of $LiCoPO_4.3H_2O$ are shown in Figures 4.73-4.78, respectively.

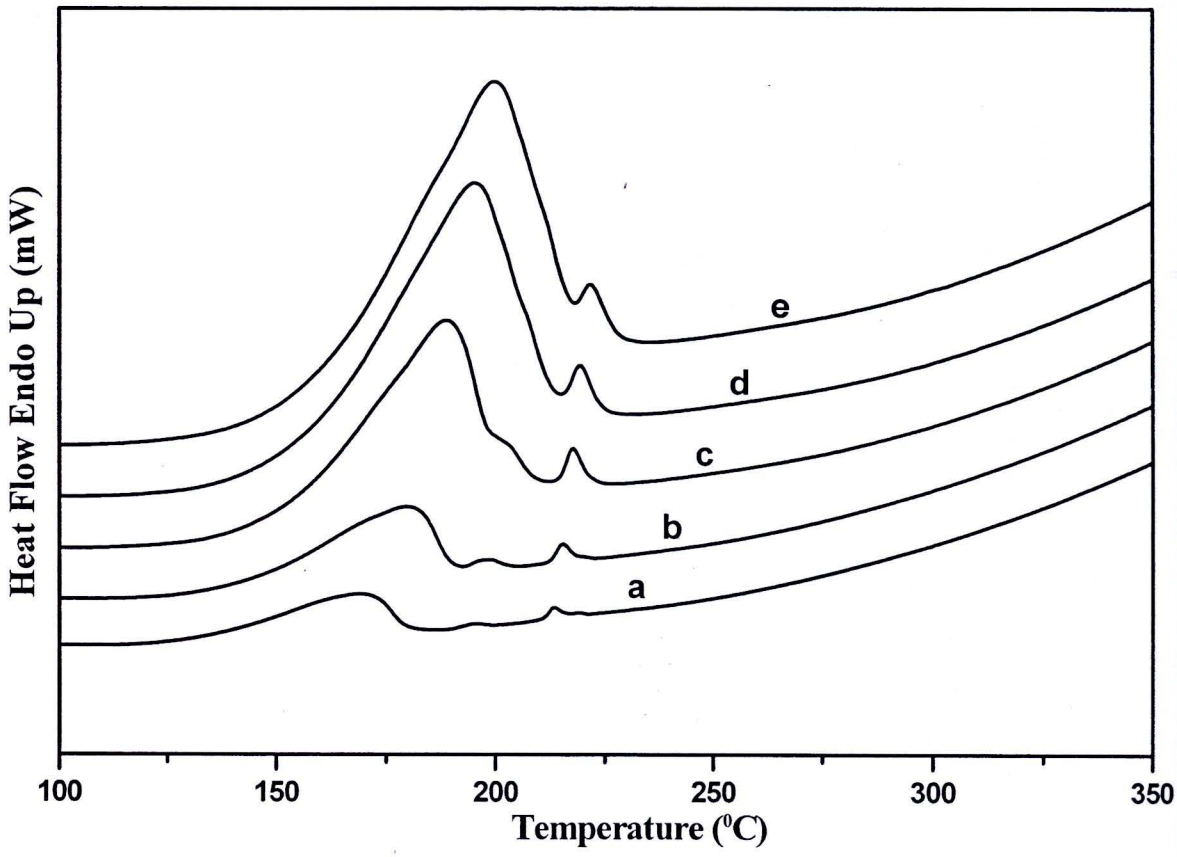

Figure 4.72 DSC curves of the synthesized $LiCoPO_4.3H_2O$ at different heating rates: a = 5, b = 10, c = 20, d = 30 and e = 40 °C min^{-1} in N_2 atmosphere

Table 4.33 DSC experimental data for Ozawa and Kissinger plots of $LiCoPO_4.3H_2O$

β (°C min^{-1})	T_{m1} (K) (1^{st} step)	T_{m2} (K) (2^{nd} step)	T_{m3} (K) (3^{rd} step)	ln β	$\ln(\frac{\beta}{T_{m1}^2})$	$\ln(\frac{\beta}{T_{m2}^2})$	$\ln(\frac{\beta}{T_{m3}^2})$
5	441.644	468.617	486.117	1.6094	-10.5715	10.6901	10.7634
10	452.399	471.673	488.747	2.3025	-9.9265	-	-
20	461.312	474.172	490.997	2.9957	-9.2724	10.0099	10.0811
30	468.289	-	492.737	3.4012	-8.8969	-9.3295	-9.3971
40	472.824	-	493.509	3.6888	-8.6285	-	-8.9987
						-	-8.7142

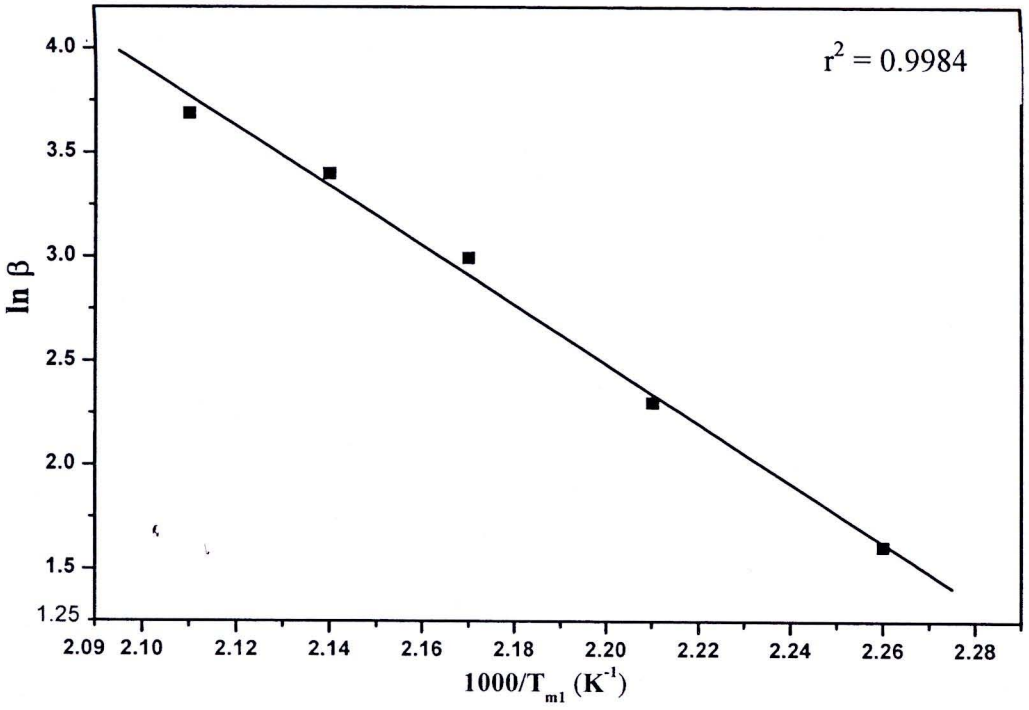

Figure 4.73 Ozawa plot for the first step of dehydration of $LiCoPO_4.3H_2O$

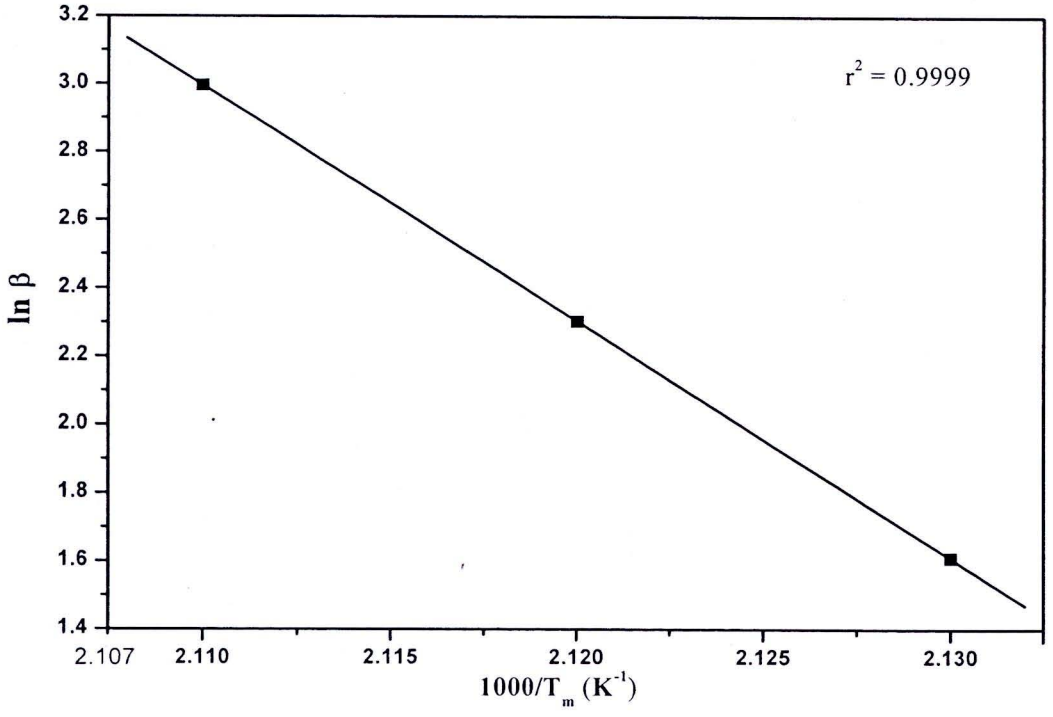

Figure 4.74 Ozawa plot the second step of dehydration of $LiCoPO_4.3H_2O$

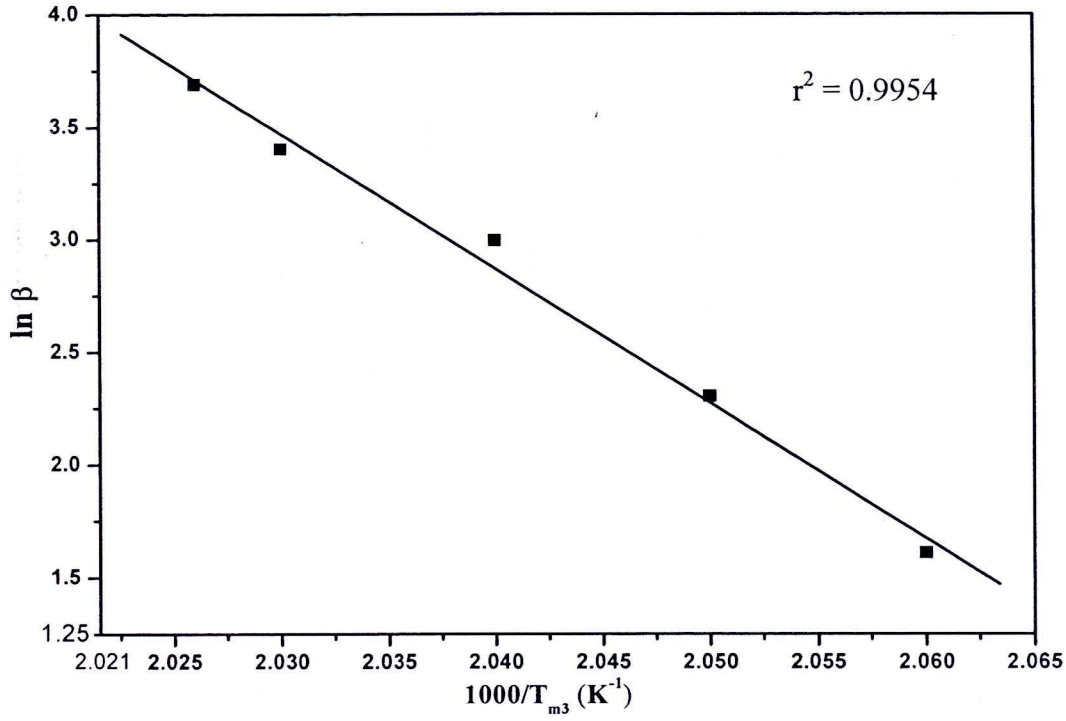

Figure 4.75 Ozawa plot for the third step of dehydration of $LiCoPO_4.3H_2O$

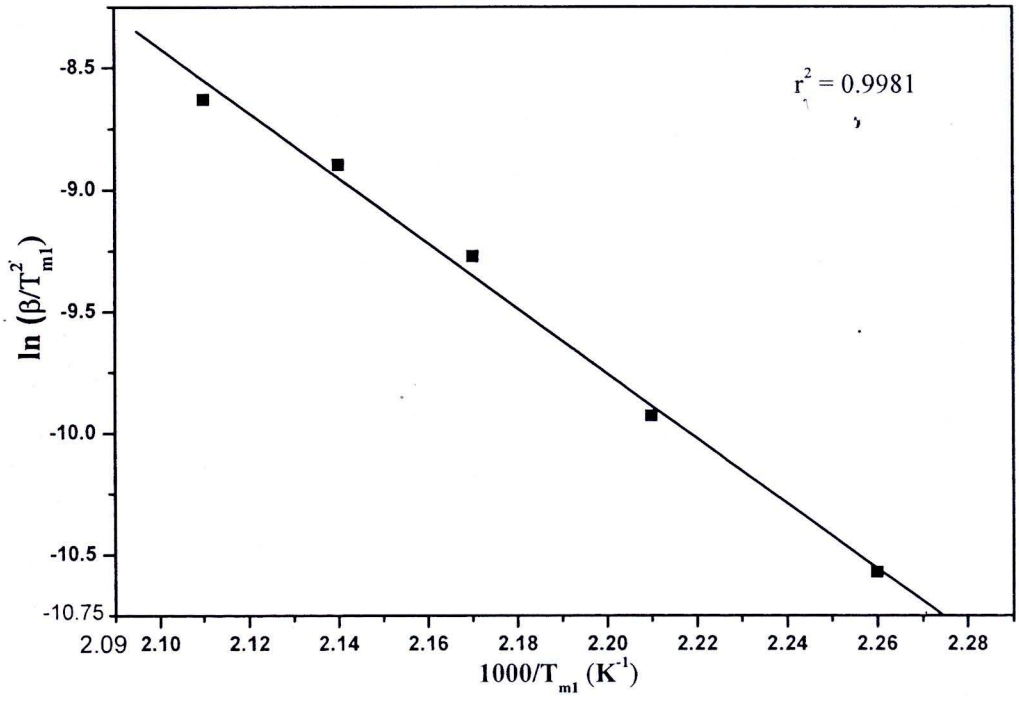

Figure 4.76 Kissinger plot for the first step of dehydration of $LiCoPO_4.3H_2O$

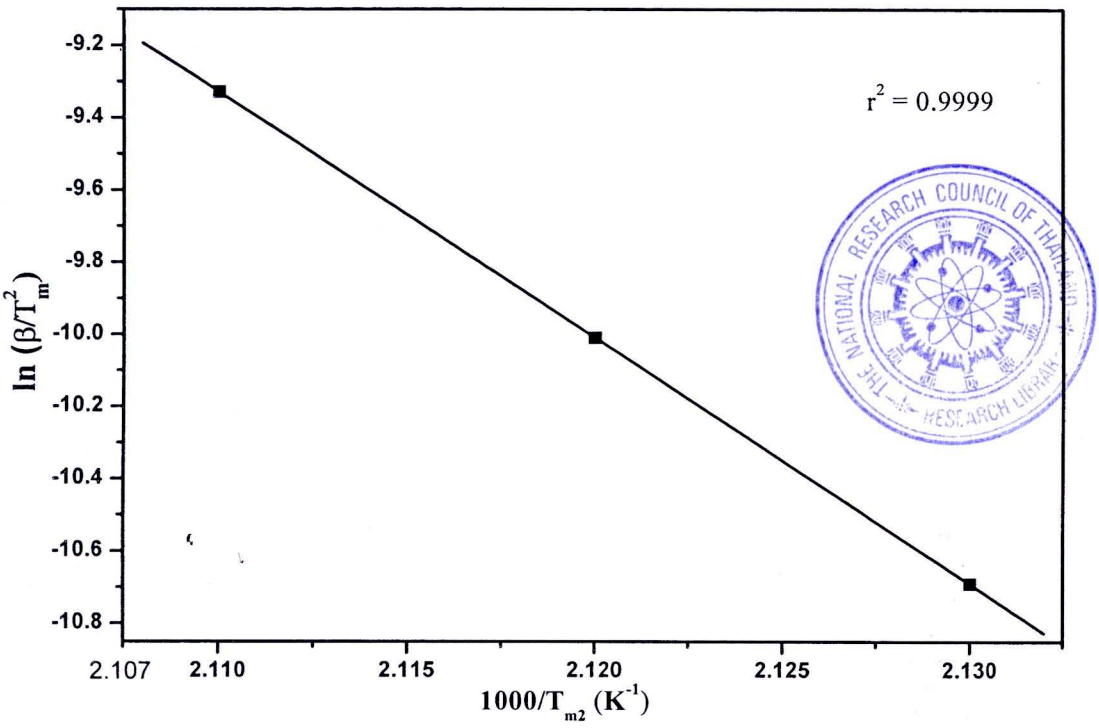

Figure 4.77 Kissinger plot for the second step of de hydration of $LiCoPO_4.3H_2O$

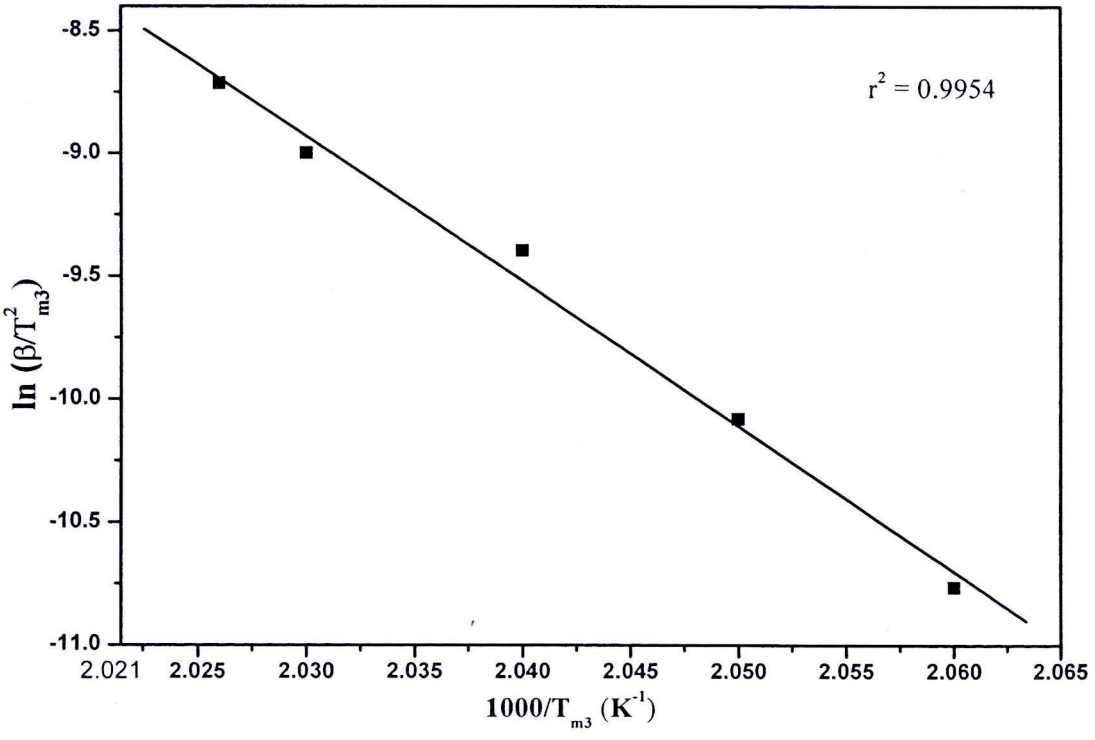

Figure 4.78 Kissinger plot for the third step of dehydration of $LiCoPO_4.3H_2O$

From the slopes of both plots, ln β versus $1000/T_m$ (Ozawa, Figures 4.73-4.75) and ln (β/T_m^2) versus $1000/T_m$ for (Kissinger, Figures 4.76-4.78), the activation energy values for the processes were calculated and are presented in Table 4.34.

Table 4.34 Activation energies E_a and correlation coefficient (r^2) calculated by Ozawa and Kissinger methods for the dehydration of $LiCoPO_4.3H_2O$

Step	Ozawa method		Kissinger method	
	E_a (kJ mol^{-1})	r^2	E_a (kJ mol^{-1})	r^2
1st	117.0	0.9984	109.4	0.9981
2nd	459.3	0.9999	450.8	0.9999
3rd	556.9	0.9954	548.8	0.9954

The activation energy values of the dehydration of $LiCoPO_4.3H_2O$ are in the range of 109-549 kJ mol^{-1} by using Ozawa method and close to the range of 117-557 kJ mol^{-1} obtained by the Kissinger method. The results show that the activation energy values from both methods are not significantly different for each step. Therefore, it can be concluded that each dehydration steps of $LiCoPO_4.3H_2O$ could be a simple dehydration reaction.

4.11.5 Thermal Decomposition Kinetics Study of $LiNiPO_4.H_2O$

DSC curves of the thermal decomposition of $LiNiPO_4.H_2O$ at five heating rates are shown in Figure 4.79. This Figure shows that $LiNiPO_4.H_2O$ decomposes in one step in the range of 191-237 °C. The basic data from Figure 4.79 are illustrated in Table 4.35. According to the previous mentioned equation, the plot of ln β versus $1000/T_m$ (Ozawa) and ln (β/T_m^2) versus $1000/T_m$ (Kissinger), the activation energies E_a can be calculated from the slopes of straight lines with best linear correlation coefficient (r^2). Ozawa and Kissinger plots for the determination activation energies of dehydration of $LiNiPO_4.H_2O$ are shown in Figures 4.80 and 4.81, respectively.

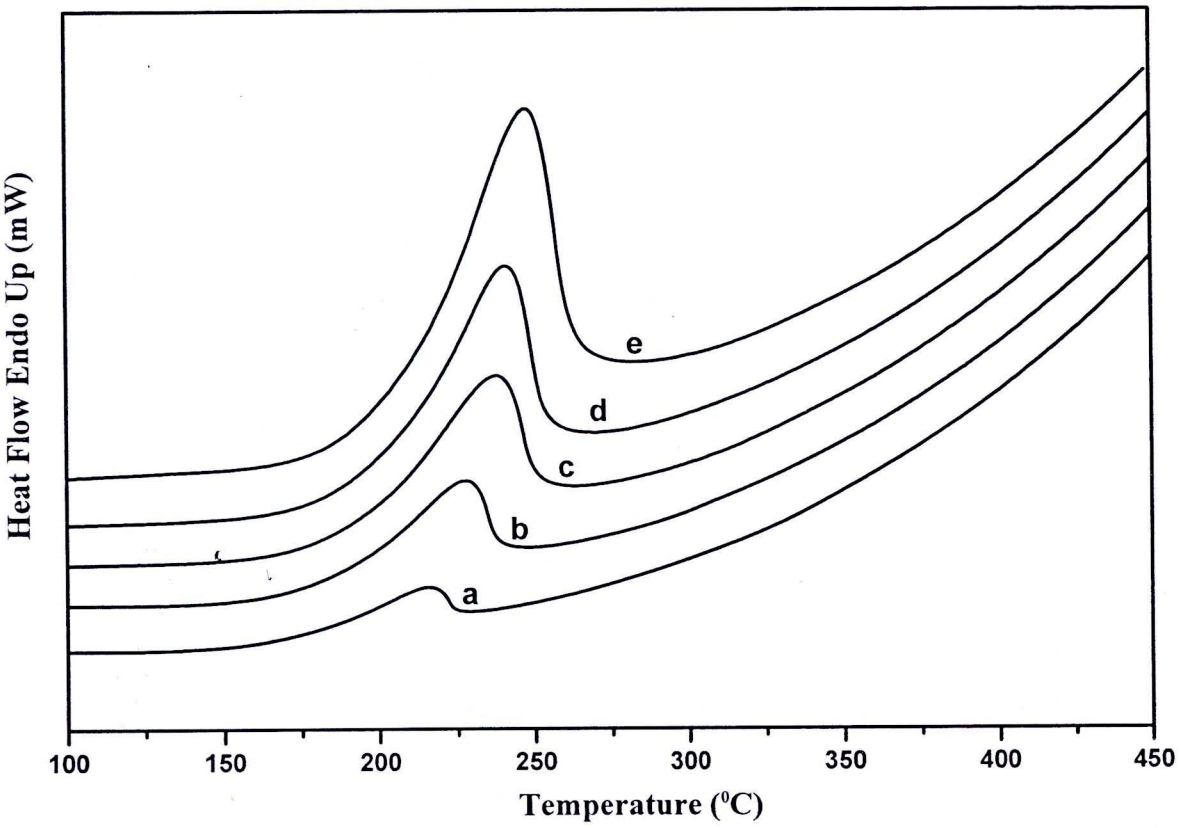

Figure 4.79 DSC curves of the synthesized $LiNiPO_4.H_2O$ at different heating rates: a = 5, b = 10, c = 20, d = 30 and e = 40 °C min^{-1} in N_2 atmosphere

Table 4.35 DSC data for Ozawa and Kissinger plot of $LiNiPO_4.H_2O$

β (°C min^{-1})	T_m (K)	$\ln \beta$	$\ln (\frac{\beta}{T_{m1}^2})$	$1000/T_m$ (K^{-1})
5	489.633	1.6094	-10.7778	2.0423
10	498.974	2.3025	-10.1225	2.0041
20	510.264	2.9957	-9.4741	1.9598
30	515.502	3.4012	-9.0891	1.9399
40	520.557	3.6888	-8.8205	1.9214

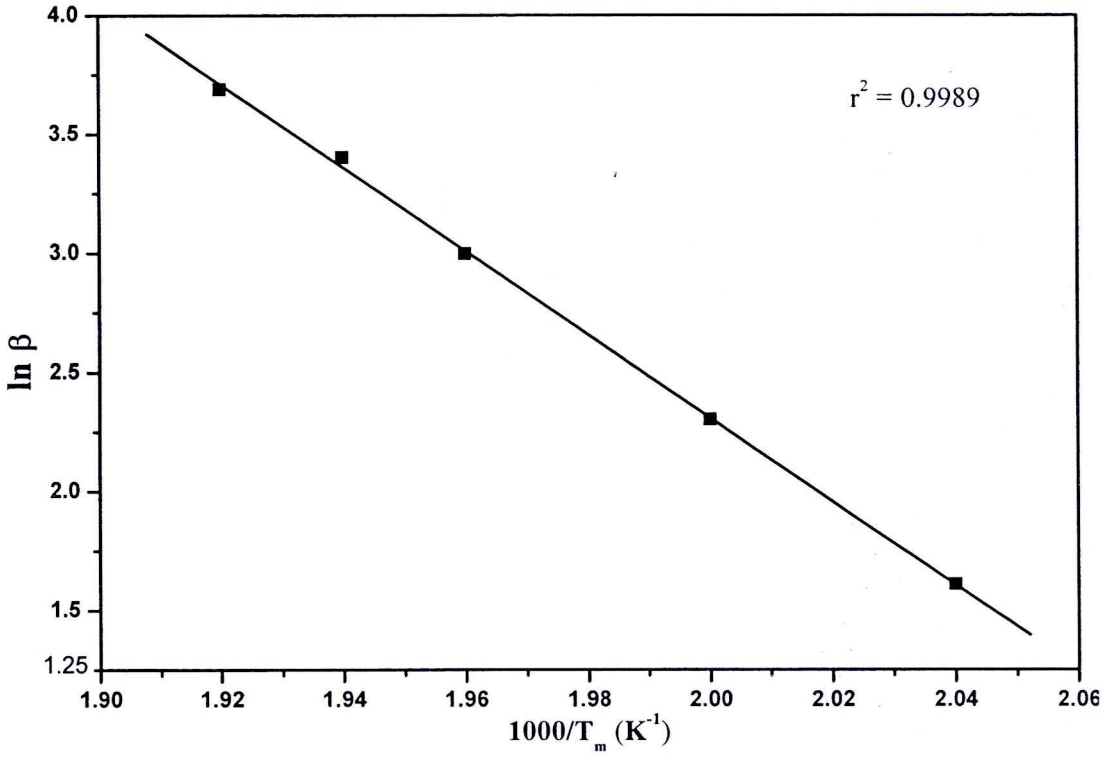

Figure 4.80 Ozawa plot of dehydration of $LiNiPO_4.H_2O$

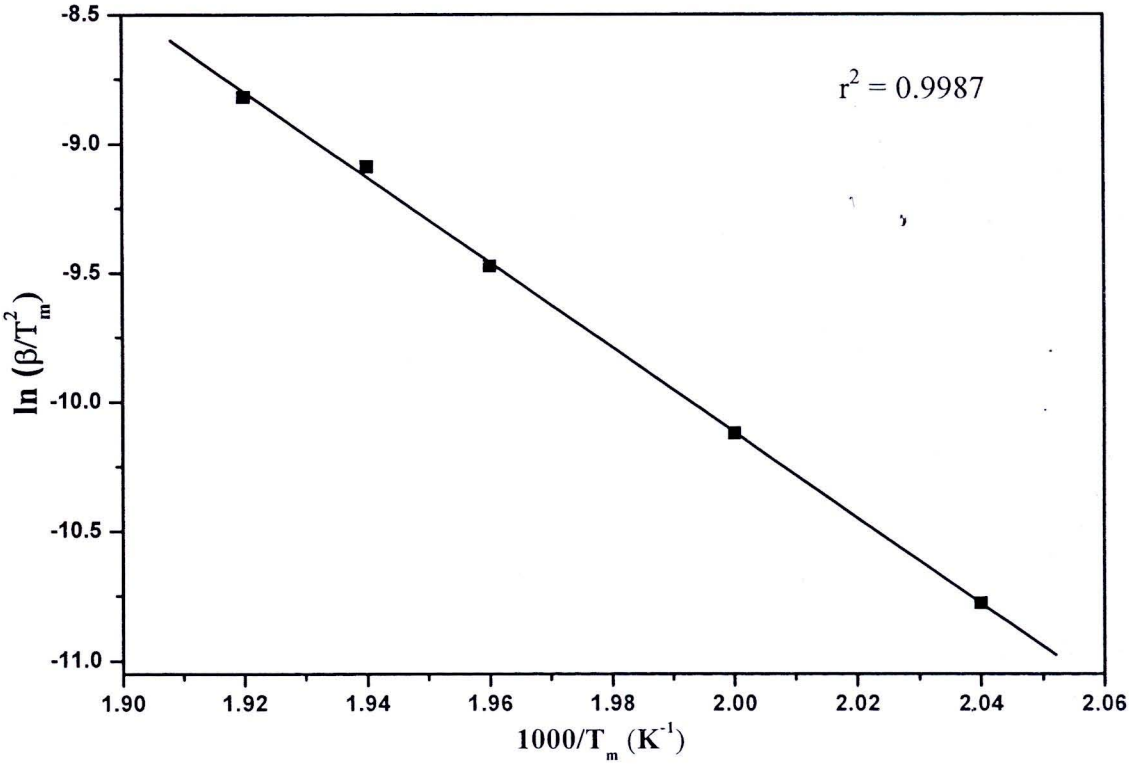

Figure 4.81 Kissinger plot of dehydration of $LiNiPO_4.H_2O$

From the slopes of both plots, of ln β versus 1000/T_m (Ozawa, Figure 4.80) and ln (β/T_m^2) versus 1000/T_m (Kissinger, Figure 4.81), the activation energy values for the dehydration process were calculated and are presented in Table 4.36.

Table 4.36 Activation energies E_a and correlation coefficient (r^2) calculated by Ozawa and Kissinger methods for the dehydration of $LiNiPO_4.H_2O$

Ozawa method		Kissinger method	
E_a (kJ mol^{-1})	r^2	E_a (kJ mol^{-1})	r^2
142.486	0.9989	134.090	0.9987

The results show that the activation energy values are not significantly different for both methods. Therefore, we draw a conclusion that the dehydration of $LiNiPO_4.H_2O$ could be a simple process.

4.11.6 Thermal Decomposition Kinetics Study of $LiMnPO_4.H_2O$

DSC curve of the thermal decomposition of $LiMnPO_4.H_2O$ at five heating rates are shown in Figure 4.82. According to this Figure, $LiMnPO_4.H_2O$ decomposes in one-step in the range of 181-210 °C. The basic data from Figure 4.82 are tabulated in Table 4.37. Similar to the previous treatment, the plot of ln β versus 1000/T_m (Ozawa) and ln (β/T_m^2) versus 1000/T_m (Kissinger), the activation energies E_a can be calculated from the slopes of straight lines with better linear correlation coefficient (r^2). Ozawa and Kissinger plot for the determination activation energies of dehydration of $LiMnPO_4.H_2O$ are shown in Figures 4.83 and 4.84, respectively.

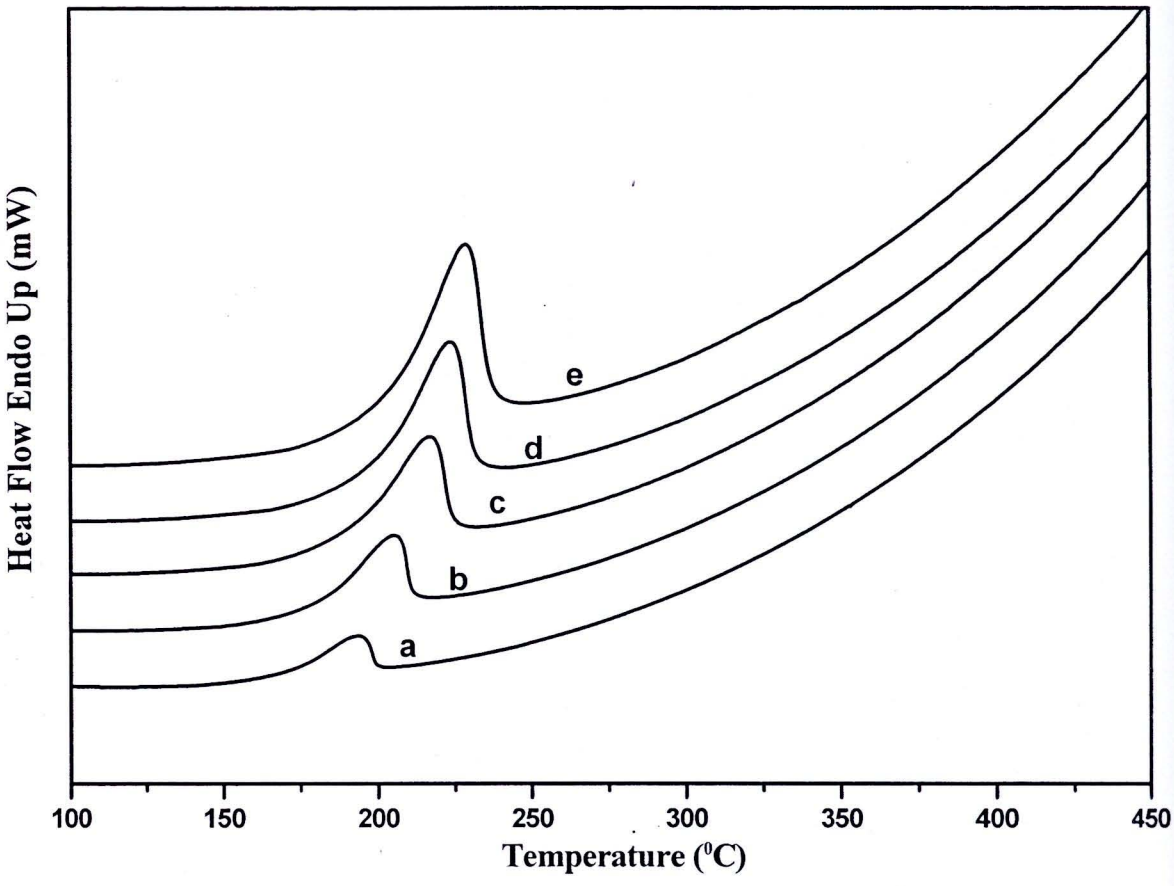

Figure 4.82 DSC curves of the synthesized $LiMnPO_4.H_2O$ at different heating rates: a = 5, b = 10, c = 20, d = 30 and e = 40 °C min^{-1} in N_2 atmosphere

Table 4.37 DSC data for Ozawa and Kissinger plot of $LiMnPO_4.H_2O$

β (°C min^{-1})	T_m (K)	ln β	$\ln(\frac{\beta}{T_{m1}^2})$	$1000/T_m$ (K^{-1})
5	466.533	1.6094	-10.6812	2.1435
10	478.204	2.3025	-10.0374	2.0912
20	489.839	2.9957	-9.3924	2.0415
30	496.454	3.4012	-9.0137	2.0143
40	501.704	3.6888	-8.7471	1.9932

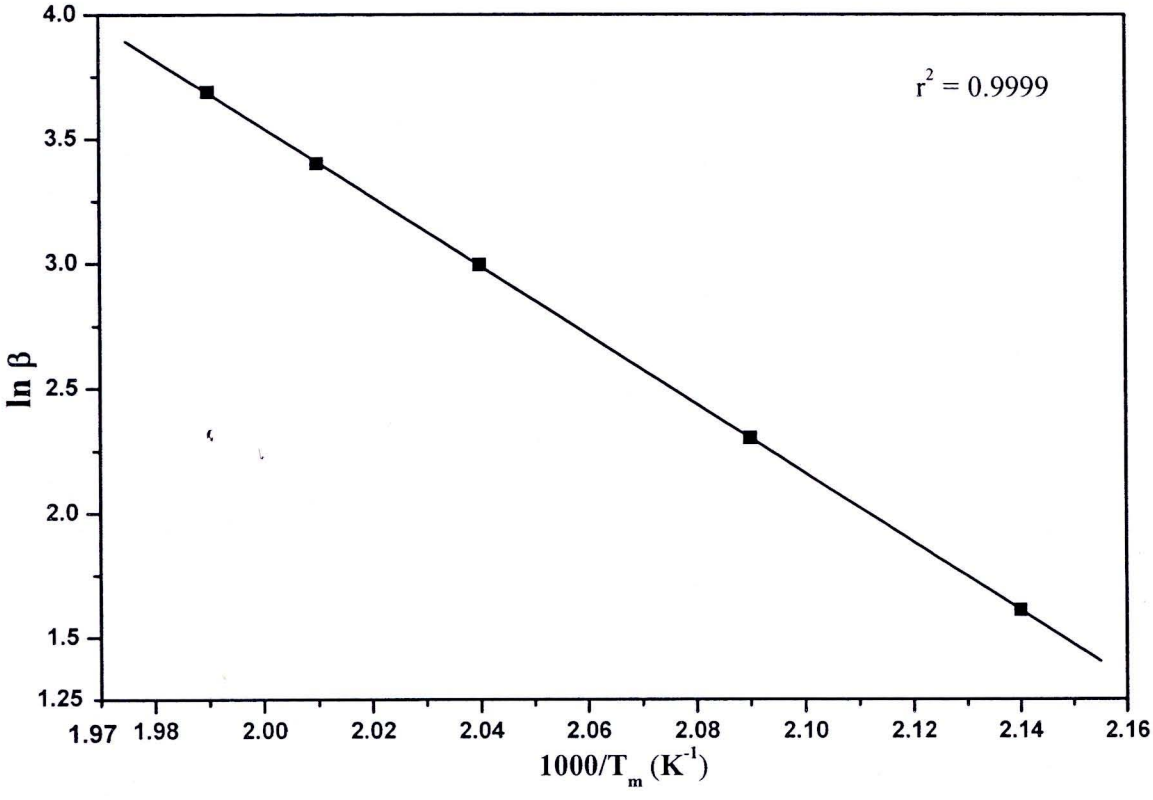

Figure 4.83 Ozawa plot of dehydration of $LiMnPO_4.H_2O$

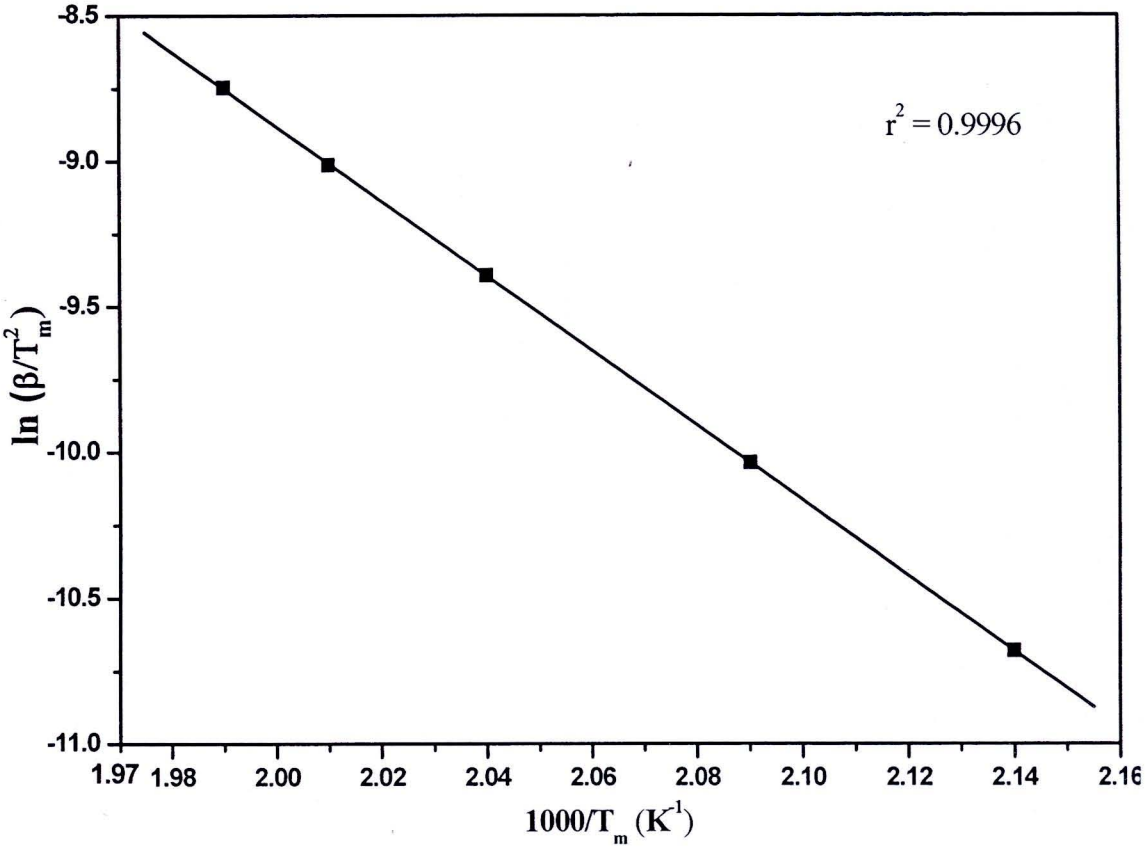

Figure 4.84 Kissinger plot of dehydration of $LiMnPO_4.H_2O$

From the slopes of both plots, ln β versus $1000/T_m$ (Ozawa, Figure 4.83) and ln (β/T_m^2) versus $1000/T_m$ (Kissinger, Figure 4.84), the activation energy values for the dehydration were calculated and are presented in Table 4.38.

Table 4.38 Activation energies E_a and correlation coefficient (r^2) calculated by Ozawa and Kissinger methods for the dehydration of $LiMnPO_4.H_2O$

Ozawa method		Kissinger method	
E_a (kJ mol^{-1})	r^2	E_a (kJ mol^{-1})	r^2
115.532	0.9999	107.492	0.9996

The results show that the activation energy values are not significantly different for the Ozawa and Kissinger methods. Therefore, the dehydration of $LiMnPO_4.H_2O$ can be interpreted to appear as a simple and single step process.

4.11.7 Thermal Decomposition Kinetics Study of $Li_2Zn(HPO_4)_2.H_2O$

DSC curves of the thermal decomposition of $Li_2Zn(HPO_4)_2.H_2O$ at five heating rates as shown in Figure 4.85 illustrate that this hydrate decomposes in two steps (161-194 and 278-302°C). The basic data from Figure 4.85 are illustrated in Table 4.39. The plots of ln β versus $1000/T_m$ (Ozawa) and ln (β/T_m^2) versus $1000/T_m$ (Kissinger) were carried out. The activation energies E_a can be calculated from the slopes of straight lines with best linear correlation coefficient (r^2). Ozawa and Kissinger plots for the determination activation energies of $Li_2Zn(HPO_4)_2.H_2O$ are shown in Figures 4.86-4.89, respectively.

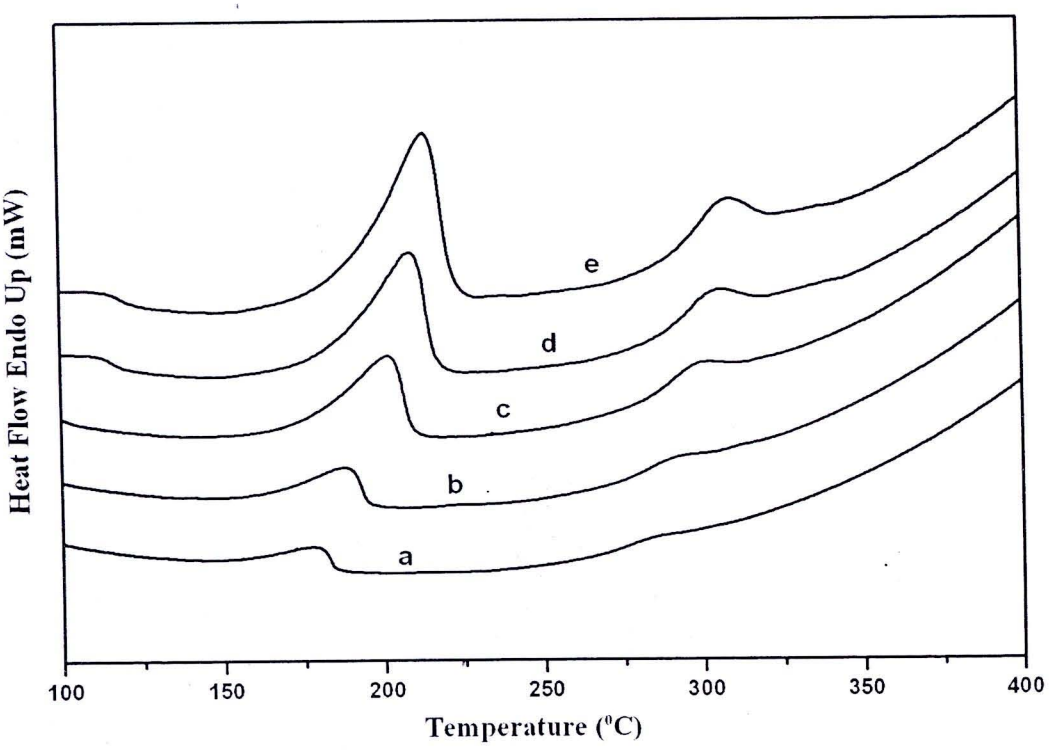

Figure 4.85 DSC curves of the synthesized $Li_2Zn(HPO_4)_2.H_2O$ at different heating rates: a = 5, b = 10, c = 20, d = 30 and e = 40 °C min^{-1} in N_2 atmosphere

Table 4.39 DSC data for Ozawa and Kissinger plot for the dehydration of $Li_2Zn(HPO_4)_2.H_2O$

β ($°C\ min^{-1}$)	T_{m1} (K) (1^{st} step)	T_{m2} (K) (2^{nd} step)	ln β	$\ln(\frac{\beta}{T_{m1}^2})$	$\ln(\frac{\beta}{T_{m2}^2})$
5	449.763	552.311	1.6094	-10.6080	-11.0187
10	460.632	560.493	2.3025	-9.9629	-10.3550
20	474.962	568.752	2.9957	-9.3307	-9.6912
30	481.550	574.214	3.4012	-8.9528	-9.3048
40	485.356	578.331	3.6888	-8.6808	-9.0314

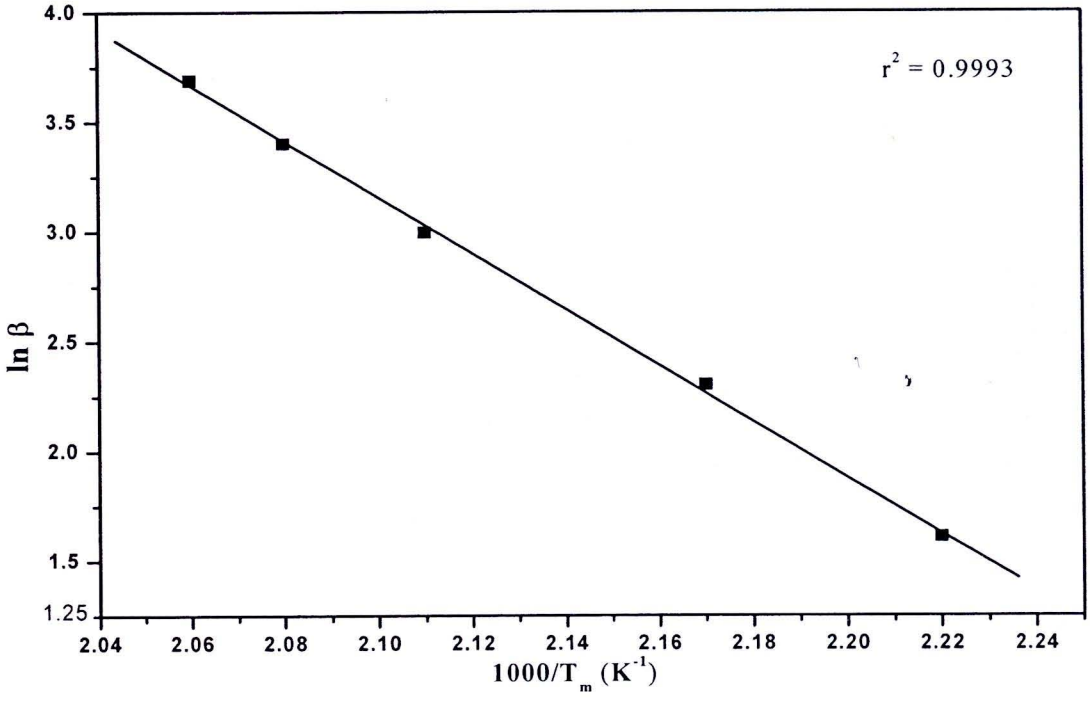

Figure 4.86 Ozawa plot the first step of dehydration of $Li_2Zn(HPO_4)_2.H_2O$

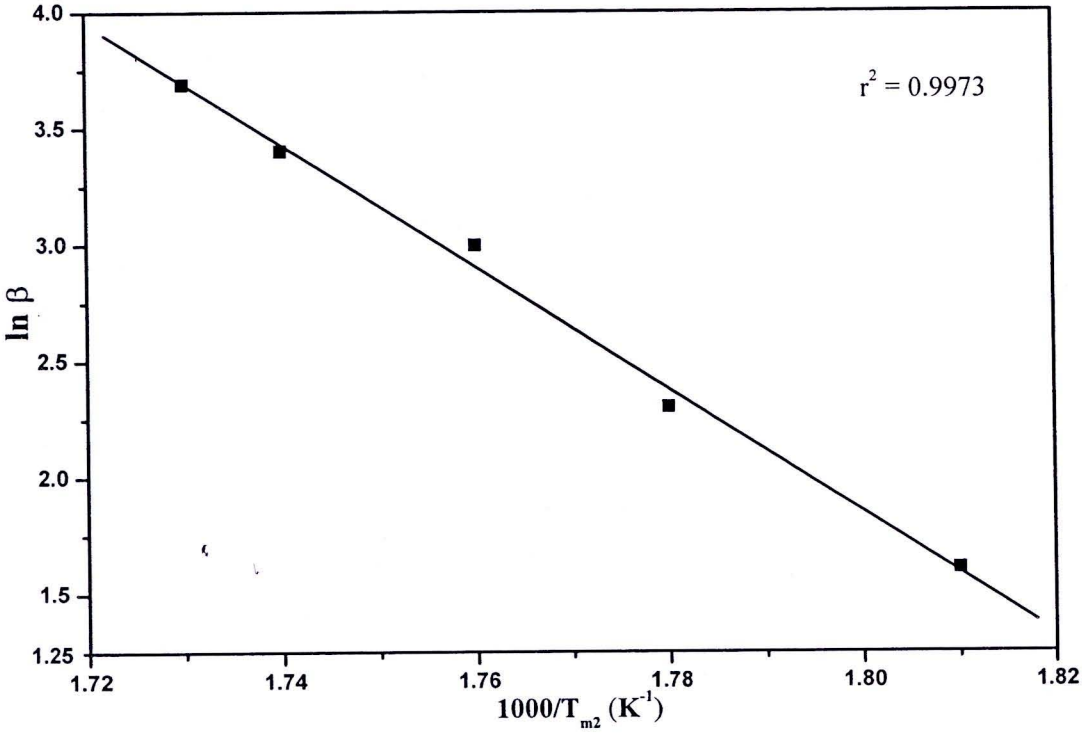

Figure 4.87 Ozawa plot for the second step of decomposition of $Li_2Zn(HPO_4)_2.H_2O$.

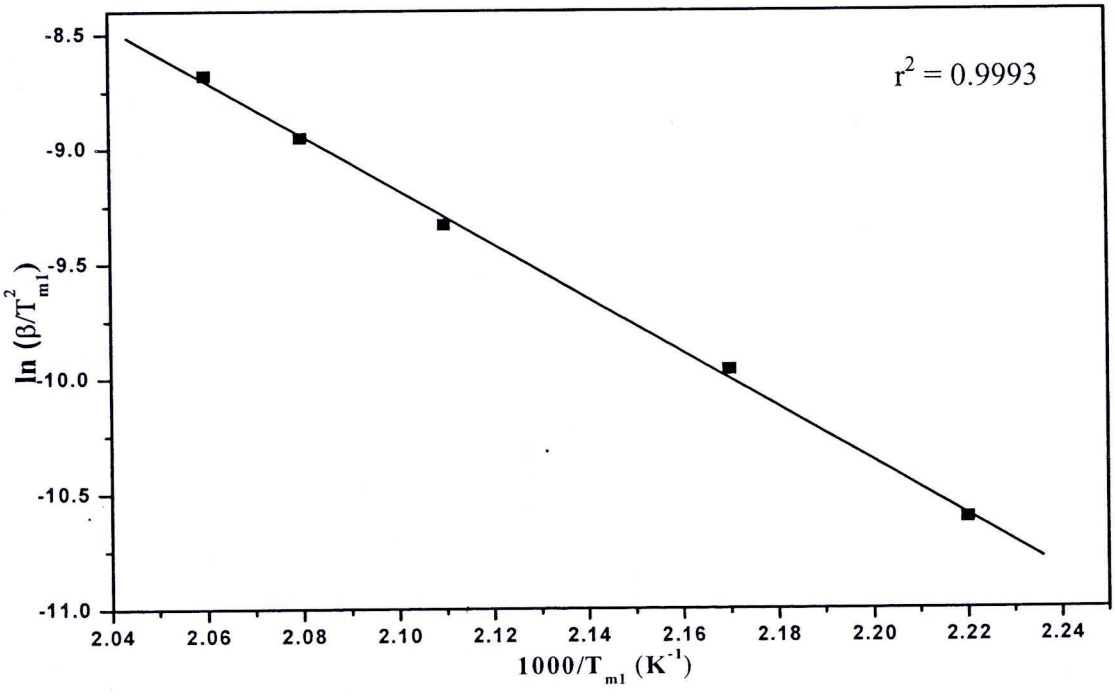

Figure 4.88 Kissinger plot for the first step of dehydration of $Li_2Zn(HPO_4)_2.H_2O$

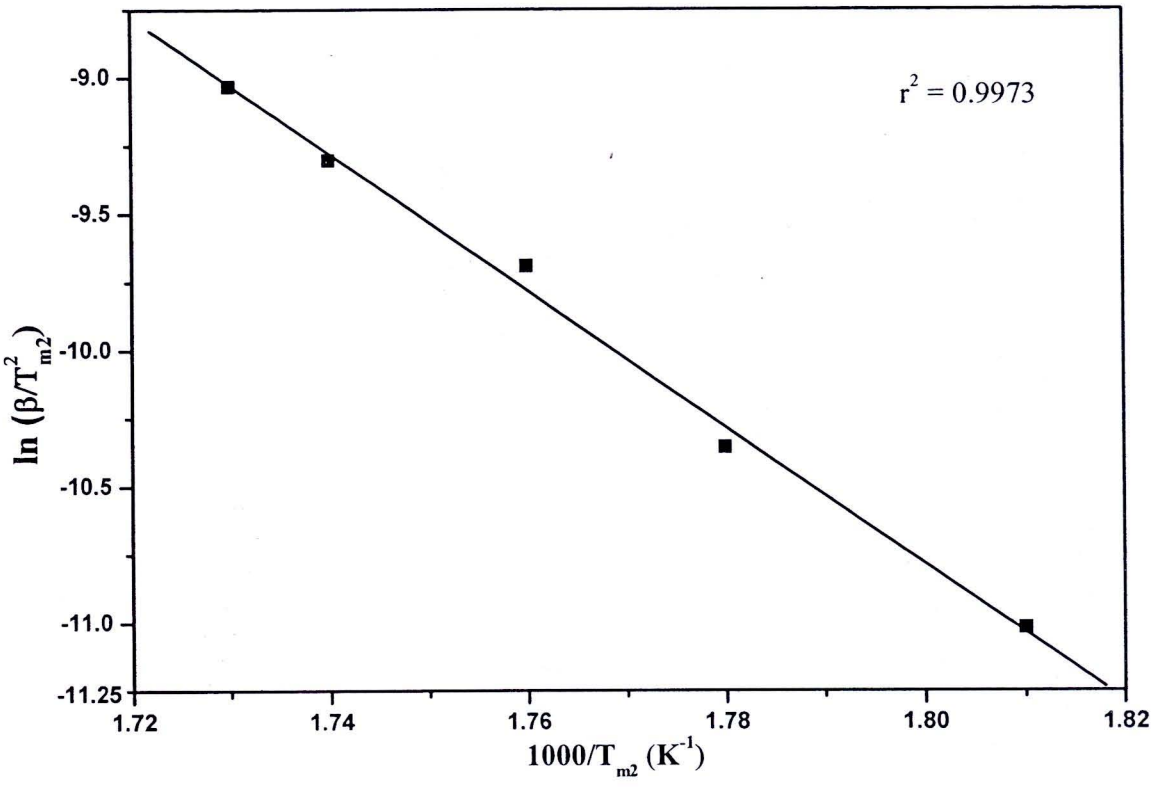

Figure 4.89 Kissinger plot for the second step $Li_2Zn(HPO_4)_2.H_2O$

From the slopes plots, ln β versus $1000/T_m$ (Ozawa, Figures 4.86, 4.87) and ln (β/T_m^2) versus $1000/T_m$ (Kissinger, Figures 4.88, 4.89), the activation energy values for the processes were calculated and are presented in Table 4.40.

Table 4.40 Activation energies E_a and correlation coefficient (r^2) calculated by Ozawa and Kissinger methods for the dehydration of $Li_2Zn(HPO_4)_2.H_2O$

step	Ozawa method		Kissinger method	
	E_a (kJ mol^{-1})	r^2	E_a (kJ mol^{-1})	r^2
1st	102.625	0.9993	94.839	0.9993
2nd	213.451	0.9973	204.046	0.9973

The activation energy values of the first dehydration step of $Li_2Zn(HPO_4)_2.H_2O$ were found to be about 103 and 95 kJ mol^{-1} by using Ozawa and Kissinger methods, respectively. The close values of the activation energy indicates that the first decomposition step of $Li_2Zn(HPO_4)_2.H_2O$ could be a simple dehydration process.

The activation energy values of second steps are 213 and 204 kJ mol^{-1} as found by Ozawa and Kissinger methods, respectively. The similar conclusion can be drawn that the second dehydration could also be the simple dehydration process.

4.11.6 Estimation of the Pre-Exponential Factor

The pre-exponential factor of $ZnHPO_4.H_2O$, $Co(H_2PO_4)_2.2H_2O$, $LiFePO_4.3H_2O$, $LiCoPO_4.3H_2O$, $LiNiPO_4.H_2O$, $LiMnPO_4.H_2O$ and $Li_2Zn(HPO_4)_2.H_2O$ can be calculated through the equation of the Ozawa. The pre-exponential factor values are tabulated Table 4.41

Table 4.41 The pre-exponential factor (A) of synthesized hydrates calculated by Ozawa and Kissinger methods

Synthesized samples	Ozawa			Kissinger		
	A (min^{-1})			A (min^{-1})		
	1st step	2nd step	3rd step	1st step	2nd step	3rd step
$ZnHPO_4.H_2O$	4.91×10^{17}	2.02×10^{19}	-	4.39×10^{17}	1.74×10^{19}	-
$Co(H_2PO_4)_2.2H_2O$	9.13×10^{12}	5.80×10^{12}	-	8.59×10^{12}	5.44×10^{12}	-
$LiFePO_4.3H_2O$	1.02×10^{13}	3.55×10^{13}	2.73×10^{23}	0.96×10^{13}	3.32×10^{13}	2.46×1
$LiCoPO_4.3H_2O$	2.28×10^{13}	1.92×10^{51}	9.57×10^{59}	1.98×10^{13}	1.62×10^{51}	9.23×1
$LiNiPO_4.H_2O$	5.36×10^{14}	-	-	4.49×10^{14}	-	-
$LiMnPO_4.H_2O$	3.15×10^{12}	-	-	2.49×10^{12}	-	-
$Li_2Zn(HPO_4)_2.H_2O$	2.32×10^{11}	6.24×10^{19}	-	1.96×10^{11}	5.86×10^{19}	-

4.12 Reversible Hydration of Selected Hydrates

4.12.1 Reversible hydration of $Li_2Zn(HPO_4)_2.H_2O$

The study of the dehydration and rehydration processes in this compound illustrated that the water molecules can be removed and rehydrated without disrupting the structure of the material, provided that the temperature is lower than 200 °C. The dehydration was investigated by heating the sample at 200 °C for 2 h, then the rehydration was carried out by exposing the dehydrated sample to water for 2 h at ambient temperature. The surface water was removed from the rehydrated sample by drying at 110 °C for 2 h. The dehydration and rehydration processes of the studied hydrate were confirmed by the FTIR spectra and the DSC curves. Indeed, the DSC

curve of the calcined sample at 200 °C (Figure 4.84b) does not show any endothermic peak at 187 °C which is the characteristic of the removal of water molecule as shown in Figure 4.85a, while the FTIR spectra show the significant decrease of ν_{OH} (H_2O) and $\nu_2(H_2O)$. The FTIR spectra (Figure 4.84c) and DSC curve (Figure 4.85b) of rehydration sample exhibit similar feature as those of the as-prepared sample.

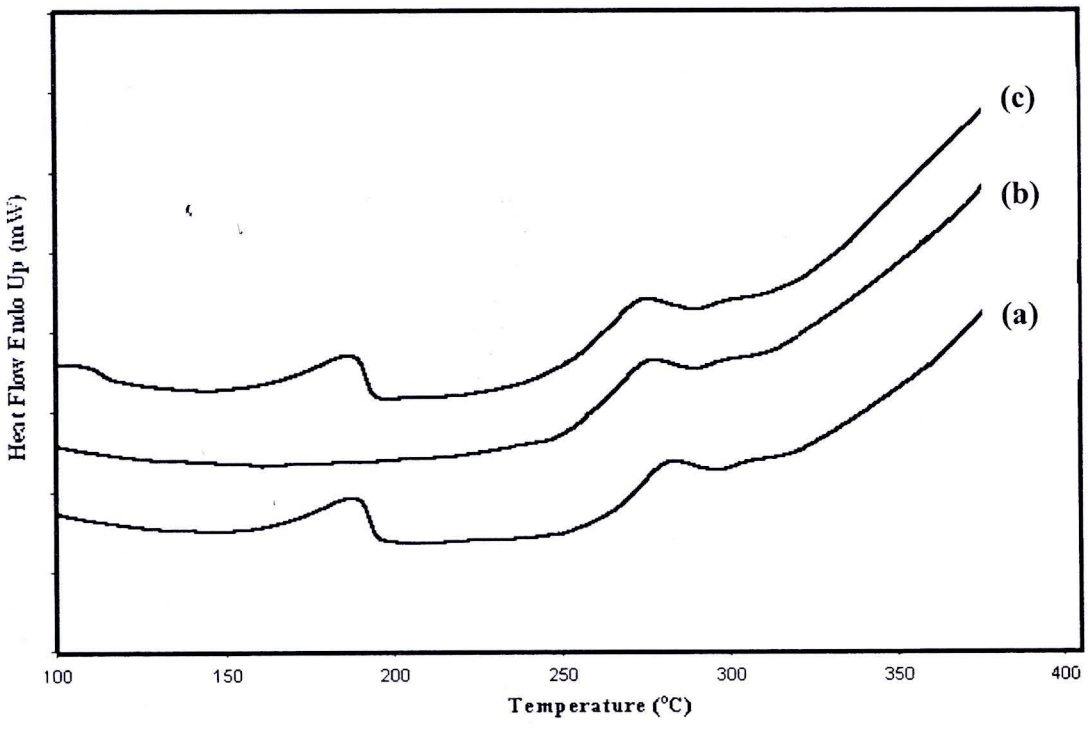

Figure 4.90 The DSC curves of: (a) the synthesized sample, (b) dehydration of sample and (c) the rehydration of sample

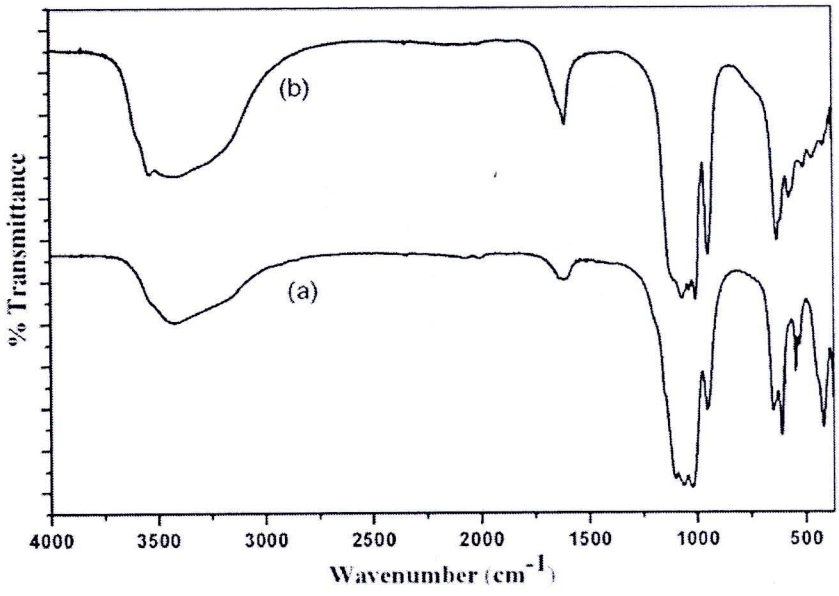

Figure 4.91 The FTIR spectra of: (a) the calcined product at 200 °C and (b) the dehydrated sample exposed to moisture at room temperature for 2 h

The water content of the rehydration sample was confirmed by using the Karl Fischer method and the mole ratio of salt:H_2O was found to be 1.00:1.13. The dehydration and rehydration processes of the synthesized sample showed that the water of crystallization can be removed and incorporated back to the structure under the condition of lower than 200 °C. The dehydration and rehydration processes of the synthesized compound are similar to the property of zeolite. Therefore, the synthesized compound can be an alternative material to replace zeolite in case of the acidity of material is required.